Numerical Methods for Transient Field-Circuit Coupled Simulations Based on the Finite Integration Technique and a Mixed Circuit Formulation

Vom Fachbereich Elektrotechnik und Informationstechnik
der Technischen Universität Darmstadt

zur Erlangung der Würde einer
Doktorin der Naturwissenschaften (Dr. rer. nat.)
genehmigte

Dissertation

von

diplomirovannij matematik i linguist/
Uljanovskij gosudarstvennyj universitet
(diplomierte Mathematikerin und Linguistin)

Galina Benderskaya
geboren am 07. Februar 1976 in Dimitrovgrad

Darmstadt 2007

Referent:	Prof. Dr.-Ing. Thomas Weiland
Korreferent:	Prof. Dr. Jens Lang
Tag der Einreichung:	06.12.2006
Tag der mündlichen Prüfung:	06.02.2007

D 17
Darmstädter Dissertation

To my father, Kuprienko Victor Anatolevich

Numerische Verfahren zu transienten Feld-Netzwerk gekoppelten Simulationen auf der Grundlage der Methode der Finiten Integration und einer eingebetteten Netzwerkformulierung

Kurzfassung der Arbeit

Das Ziel dieser Arbeit ist die Entwicklung und Implementierung von Zeitintegrationsverfahren höher Ordnung, mit denen die Rückwirkungen extern gekoppelter elektrischer Netzwerke bei der Berechnung langsam veränderlicher Magnetfelder simuliert werden können.

Im ersten Kapitel werden allgemeine Eigenschaften gekoppelter Probleme beschrieben, wobei ausdrücklich die Entwicklungsgeschichte der elektromagnetischen Feld-Netzwerk Kopplung einbezogen ist.

Im zweiten Kapitel werden die im Verlauf der Arbeit benötigten Grundlagen wie die Modellierung des Elektromagnetismus, quasistatische Felder, die Methode der Finiten Integration und die lineare Netzwerkanalyse betrachtet.

Das dritte Kapitel beleuchtet die externe Netzwerkbeschreibung und gibt einen kurzen Einblick in die Netzwerktopologie. Anschließend folgt die Entwicklung mathematischer Modelle für einen massiven Leiter und für eine gewickelte Spule im Zeitbereich. Die Kopplung externer elektrischer Netzwerke an elektromagnetische Felder, die mit massiven Leitern und/oder Spulen erzeugt werden, führt zu einem System differential-algebraischer Gleichungen vom Index 1.

Das vierte Kapitel geht näher auf die mathematischen Eigenschaften des entwickelten Feld-Netzwerk gekoppelten Systems ein. Zuerst werden die klassischen, so genannten "Theta"-Zeitintegrationsverfahren betrachtet. Die dargelegten numerischen Beispiele zeigen, wie sich diese Verfahren im Zusammenhang mit der Lösung gekoppelter Feld-Netzwerk Systeme verhalten und machen deutlich, dass manche klassischen Verfahren nicht stabil und daher unbrauchbar sind. Deswegen wird die gekoppelte Formulierung mit Zeitintegrationsmethoden höherer Ordnung, vorzugsweise mit impliziten Runge-Kutta Methoden, gelöst. Darüber hinaus werden in diesem Kapitel ebenfalls Zeitintegrationsmethoden für eine adaptive Zeitschrittsteuerung der entwickelten Formulierung präsentiert. Ein numerisches Beispiel am Ende dieses Kapitels demonstriert, wie die Auswahl verschiedener Normen als Maß für den lokalen Fehler den Zeitschrittsteuerungsprozess beeinflusst.

Für die Verbesserung der Effizienz einer Zeitschrittsteuerung bei der Integration differential-algebraischer Systeme vom Index 1 und sinusförmigem Lösungsverlauf wird im fünften Kapitel eine von der Standardlösung abweichende Technik vorgeschlagen. Der zweite Teil dieses Kapitels stellt ein sogenanntes "Envelope"- Zeitintegrationsverfahren vor. In Rahmen dieser Methode können etwaige schnelle und langsame Lösungskomponenten voneinander separiert werden, was insgesamt zu einer Beschleunigung des Zeitintegrationsprozesses führt. Für beide vorgeschlagenen Verfahren wurden jeweils repräsentative Testbeispiele simuliert.

Die Feld-Netzwerk gekoppelten Probleme mit schaltenden Elementen werden im Kapitel sechs betrachtet. Dort ist eine dreistufige Technik dargestellt, mit der sich

auch nichtlineare Bauteile in den Netzwerkzweigen effektiv simulieren lassen. Im Rahmen dieses Verfahrens werden die Schaltzeitpunkte sicher entdeckt und geeignete neue Anfangsbedingungen für die jeweils neue Topologie des Netzwerks berechnet. Diesem Kapitel sind ebenfalls zwei Simulationsbeispiele beigefügt.

Die Arbeit schließt mit einer kurzen Zusammenfassung.

Contents

Chapter 1

Introduction

1.1 Coupled Problems: Trends and Accomplishments

1.1.1 Introduction

In engineering applications, a coupled problem is defined as a dynamic problem that can be decomposed into physically heterogeneous parts that exhibit mutual interaction. Nowadays, coupled analysis envelopes a lot of engineering disciplines such as mechanics, fluiddynamics, acoustics, thermodynamics, electromagnetics, etc. In spite of the wide variety of coupled analyses, all coupled models can be classified into two main groups:

- coupled models arising from *multi-physical* coupling and
- coupled models arising from *methodological* coupling.

A coupling between an electromagnetic field and a thermal distribution occurring in electrical heating of fluids is a typical example of the multi-physical coupling. Here, the temperature distribution and, as a consequence, the electromagnetic material properties are governed by the fluid flow. Simultaneously, the electromagnetic power loss within the fluid influences the transient flow characteristics. The behavior of the electromagnetic field is governed by the Maxwell's equations, the fluid dynamics is ruled by the Navier-Stokes equations. Consequently, the considered coupled problem belongs to a class of multi-physical coupled problems [1]. The numerical simulation of these kinds of coupled problems employs different spatial discretization schemes and several requirements to the coupling interface have to be deduced [1].

A typical example for the second group of coupled analyses is the field-circuit electromagnetic interaction. Here, an electromagnetic device is connected to an external electrical circuit. The behavior of the electromagnetic field is described with the Maxwell's equations, the electrical circuit is ruled by the Kirchhoff's laws. Hybrid

disretization techniques are used for this type of coupled problems. In case of field-circuit coupled models, the spatial discretization is employed for the field part of a model, while the electrical circuit is described in terms of the lumped elements.

The proposed classification shows that the modelling of the coupled phenomena often involves distinct spatial subdomains with distinct sets of dependent variables. Consequently, neither subsystem can be solved independently of the other due to mutual interactions at the interface [2]. The interaction domains also have different dimensionality. The numerical simulation of the parts of coupled problems as separated items is pursued and refined within the requirements and laws of the corresponding disciplines.

1.1.2 Types of Coupled-Field Analysis

Independent of the type of coupled problem, there exist two major solution methods:

- *sequential method or weak coupling.* This method involves two or more sequential analyses of the individual subproblems. As a consequence, the two field quantities are coupled by propagating results from one analysis in another one;
- *direct method or strong coupling.* The implementation of this method presupposes just one analysis that uses a single system of equations containing all necessary degrees of freedom.

1.1.3 Coupled-Field Simulation Approaches

Mathematical models for coupled problems are usually governed by coupled partial differential equations in space and time. Some of these differential equations describe the material behavior and are called *constitutive equation*, while others capture fundamental *physical laws*.

A physical law is a scientific proposition based on empirical observations of physical behavior. Physical laws typically rely on the confirmation of hypotheses through repeated scientific experiments over many years. Among the important physical laws are *conservation laws* stating that a particular measurable property of an isolated system does not change as the system evolves. Conservation of *mass*, *energy* and *electrical charge* are just a few examples [3].

A constitutive equation is a relation between two physical quantities and does not follow directly from a physical law.

The spatial domain of coupled problems is discretized using e.g., the Finite Element Method, the Finite Difference Method, the Finite Integration Technique or the Boundary Element Method. It is also possible to exploit different discretization techniques on different physical parts. The spatial discretization leads to a system of ordinary differential equations (ODE) or differential-algebraic equations (DAE) in time. The time dependencies are resolved by a numerical integration technique. There exist three major approaches for the time integration of coupled systems:

- *Elimination.* One or more equations are eliminated by a particular technique, e.g., integral transforms or partial cutset/loop transformations in electrical circuit analysis. The remaining equations are treated by a simultaneous time integration scheme.

- *Simultaneous (or monolithic) integration.* Here, all equations of the coupled formulation are advanced simultaneously in time. It is also possible, however, that some of the equations will be eliminated from the system within each transient time step by means of e.g., Schur complement.

- *Partitioned integration.* According to this integration technique, the physically heterogeneous system parts are treated computationally as isolated items and, consequently, are advanced in time separately. Individual parts are linked using prediction, substitution and synchronization techniques to take the interaction effects into account.

The last two integration schemes are generally applicable, whereas the first one is restricted to particular linear problems. Within the scope of this work, a simultaneous integration of the field-circuit coupled electromagnetic problem is implemented.

1.2 Electromagnetic Field-Circuit Coupled Problems

In this part of the chapter, a brief history of the field-circuit electromagnetic coupling is given and the manuscript overview is presented.

1.2.1 History of the Field-Circuit Electromagnetic Coupling

This research item came into focus in the last thirty years. As a starting point, one can consider the work of A. Hannalla and D. Macdonald [4]. In this work, for the first time external circuit connections to conductors were taken into account directly. However, it was not yet realized at that time, that a combined field-circuit model should include, besides the usual one-component magnetic vector potential, a set of electric scalar potentials due to conductors. In 1981, two types of unknowns have been combined for the first time by Konrad who introduced the field-circuit coupled integrodifferential formulation in the frequency domain [5]. Thus, circuit constraints appeared to be included in the eddy current problem. However, the circuit description was not yet complete and the corresponding equations were limited to the known currents and voltages in the circuit branches. Later on, circuit loops were also taken into account [6],[7].

General techniques for dealing with arbitrary external circuit connections for 2-D eddy-current problems were proposed in [8] and [9]. The work of G. Bedrosian [10] drew a clear distinction between solid and stranded conductors supported by the corresponding mathematical treatment. A coupled three-dimensional field-circuit

formulation in frequency domain for the circuits with arbitrary topology was presented in [11]. The topological aspects of the coupling procedure were also fully highlighted in this work.

In the last fifteen years significant research was done in order to elaborate effective schemes for the numerical solution of the field-circuit coupled problems. Transient formulations are commonly solved using the standard θ-type time integration methods with constant time steps [12], [13], [14]. The usage of the Krylov subspace methods for the numerical solution of field-circuit coupled problems was proposed and analyzed in [11].

1.2.2 Manuscript Overview

The objective of this work is to propose effective and reliable higher order time integration schemes for electromagnetic field-circuit coupled problems. According to the classification criteria listed above, a strong coupling is implemented, i.e., field and circuit unknowns are treated together. The numerical integration process is implemented in a monolithic way.

The structure of the work is as follows: in the next chapter relevant fundamental concepts are discussed. First of all, the foundations of the electromagnetism are in the focus of consideration. Quasistatic field regimes and the conditions required for the appropriate field classification are elaborated. Secondly, a brief introduction to the applied method for spatial discretization, the Finite Integration Technique, is presented. Main principles and ideas of the method are listed. Finally, some elements of linear circuit analysis are discussed. These three sections of the second chapter can be considered as the foundation blocks for the field-circuit coupled analysis.

In the first part of the third chapter, the external circuit description and the network topology are considered. After that the basic types of the conductor models are discussed. Finally, a transient electromagnetic field-circuit coupled formulation is derived.

The fourth chapter starts with a numerical analysis of the derived formulation and considers the application of standard time integration schemes to this formulation using test examples. The subject of the final part of this chapter is the higher order integration methods, namely Runge-Kutta type methods, and their usage for the numerical integration of field-circuit transient formulations. Adaptive time integration schemes are then considered and their application to the coupled formulation is illustrated by a test problem.

In the first part of the fifth chapter, an efficient numerical technique for adaptive integration of problems with sinusoidal dynamics is developed. An envelope integration of electromagnetic problems based on the separation of slow and fast varying dynamics is presented in the second part of this chapter. All proposed numerical techniques are illustrated with appropriate numerical examples.

The subsequent sixth chapter covers important aspects of the numerical integration of field-circuit coupled problems with switching elements. A particular approach

allowing to use standard time integration schemes for DAE systems with discontinuities appearing in the system due to the presence of switching elements is given. Finally, two numerical examples are presented: a step-up converter with a conduction coil and a three-phase transformer coupled to a power electronic network.

The work is concluded with a short summary.

Chapter 2

Electromagnetic Field and Circuit Simulation

2.1 Introduction

The construction of field-circuit coupled electromagnetic models is based on the following constituents:

- classical electromagnetism,
- Finite Integration Technique as a method used for the spatial discretization of quasistatic formulations and
- linear circuit analysis.

The main ideas, postulates and principles of these subjects are briefly discussed in the present chapter.

2.2 Classical Electromagnetism

2.2.1 Basic Quantities, Universal Constants and Material Characteristics

Electromagnetic phenomena are described by four field equations postulated by J. C. Maxwell in 1873. Together with three medium-dependent equations they form the axiomatic basis of electromagnetism. Maxwell's equations establish the relations between five vector quantities and one scalar quantity, listed below in Tab. 2.1.

In addition to the field vector and scalar quantities presented in the table, there exist universal constants, that can be used to describe the properties of the free space (vacuum): *velocity of electromagnetic waves* in free space c_0; *permittivity* of

Electromagnetic Quantities		
Notation	**Definition**	**SI Units**
$\vec{E}$	electric field strength	[V/m]
$\vec{D}$	electric flux density	$[C/m^2] = [As/m^2]$
$\vec{H}$	magnetic field strength	[A/m]
$\vec{B}$	magnetic flux density	$[T] = [Vs/m^2]$
$\vec{J}$	electric current density	$[A/m^2]$
ρ	electric charge density	$[C/m^3]$

Table 2.1: Vector and scalar quantities essential for the classical electrodynamics.

free space, ε_0, and *permeability* of free space, μ_0. The velocity of light in free space was determined experimentally and equals

$$c_0 = 2.99792458 \cdot 10^8 \text{ m/s}. \tag{2.1}$$

The other two constants, ε_0 and μ_0, reflect electric and magnetic properties, respectively. In free space, ε_0 is the proportionality constant between the electric flux density $\vec{D}$ and the electric field intensity $\vec{E}$, i.e.,

$$\vec{D} = \varepsilon_0 \vec{E}, \tag{2.2}$$

and μ_0 is the proportionality constant between the magnetic flux density $\vec{B}$ and the magnetic field intensity $\vec{H}$, i.e.,

$$\vec{B} = \mu_0 \vec{H}. \tag{2.3}$$

The values of ε_0 and μ_0 are determined by the choice of the unit systems, and are therefore not independent. In the SI system, the permeability of free space is chosen to be

$$\mu_0 = 4\pi \cdot 10^{-7} \text{ H/m}. \tag{2.4}$$

With the values of c_0 and μ_0 fixed in relations (2.1) and (2.4), respectively, the value of the permittivity of free space is then derived from the relationship

$$c_0 = \frac{1}{\sqrt{\varepsilon_0 \mu_0}} \tag{2.5}$$

or

$$\varepsilon_0 = 8.854 \cdot 10^{-12} \text{ F/m}. \tag{2.6}$$

A dielectric or permeable medium may be polarised or magnetised by the incident electric or magnetic field. Then, the electric flux density $\vec{D}$ and the magnetic flux density $\vec{B}$ in the medium are functions of the *polarization* $\vec{P}$ and the *magnetization* $\vec{M}$, respectively:

$$\vec{D} = \varepsilon_0\vec{E} + \vec{P} \tag{2.7a}$$
$$\vec{B} = \mu_0\vec{H} + \mu_0\vec{M}. \tag{2.7b}$$

In linear polarized materials, the polarization can be expressed by $\vec{P} = \varepsilon_0\chi_e\vec{E}$, where χ_e is a *dielectric susceptibility*, whereas in linear magnetized media, the magnetization is given by $\vec{M} = \chi_m\vec{H}$, where χ_m is a *magnetic susceptibility*. Taking these relations into account, the following correlations can be derived:

$$\vec{D} = \varepsilon_0(1+\chi_e)\vec{E} = \varepsilon_0\varepsilon_r\vec{E} = \varepsilon\vec{E} \tag{2.8a}$$
$$\vec{B} = \mu_0(1+\chi_m)\vec{H} = \mu_0\mu_r\vec{H} = \mu\vec{H} \tag{2.8b}$$

containing the relative permittivity ε_r and the relative permeability μ_r [15].

The last field quantity to be determined is the electric current density $\vec{J}$, which is usually decomposed into

$$\vec{J} = \vec{J}_{\text{cond}} + \vec{J}_{\text{s}} + \vec{J}_{\text{conv}}, \tag{2.9}$$

where the first term represents the *conduction current density* and is expressed by Ohm's law

$$\vec{J}_{\text{cond}} = \sigma\vec{E} \tag{2.10}$$

with σ being a macroscopic constitutive parameter of the medium called the *conductivity*. Conduction currents in conductors and semiconductors are due to the drift motion of electrons and holes. The second item in (2.9) is the *source current density* which is independent of all field forces. If a charge density ρ flows with the velocity $\vec{v}$ through space free of matter a *convection current* $\vec{J}_{\text{conv}} = \rho\vec{v}$ is set up.

Equations (2.8) and (2.10) are *constitutive relations*. One distinguishes between linear and nonlinear materials, homogeneous and inhomogeneous materials, isotropic and anisotropic materials. For linear materials, the material parameters σ, ε, μ are independent of the fields $\vec{E}$ and $\vec{H}$; the material parameters of nonlinear media depend on the fields $\vec{E}$ and $\vec{H}$. For a *homogeneous* medium the material parameters are not dependent on the spatial coordinates. Conversely, the material parameters of inhomogeneous media are functions of the spatial coordinates. Isotropic and anisotropic materials are characterized by the absence or presence of a dependence of the material parameters upon the direction, respectively.

In this work, we only consider linear, homogenous and isotropic materials.

2.2.2 Maxwell's Equations

The set of Maxwell's equations in *differential form* reads:

$$\nabla \times \vec{\mathrm{E}} = -\frac{\partial \vec{\mathrm{B}}}{\partial t} \tag{2.11a}$$

$$\nabla \times \vec{\mathrm{H}} = \frac{\partial \vec{\mathrm{D}}}{\partial t} + \vec{\mathrm{J}} \tag{2.11b}$$

$$\nabla \cdot \vec{\mathrm{D}} = \rho \tag{2.11c}$$

$$\nabla \cdot \vec{\mathrm{B}} = 0. \tag{2.11d}$$

Equation (2.11a) is called *Faraday's law*, equation (2.11b) is *Ampère's (circulation) law*. Equation (2.11c) is referred to *Gauss's law* and equation (2.11d) signifies the *absence of magnetic charges*.

It is worthwhile to mention two other fundamental equations that go hand-in-hand with Maxwell's equations. The *continuity equation*

$$\nabla \cdot \vec{\mathrm{J}} = -\frac{\partial \rho}{\partial t} \tag{2.12}$$

expresses the conservation of electric charge. The *Lorentz force equation*

$$\vec{\mathrm{F}} = q\left(\vec{\mathrm{E}} + \vec{\mathrm{v}} \times \vec{\mathrm{B}}\right) \tag{2.13}$$

expresses the *electromagnetic force* acting on a charge q moving with the speed $\vec{\mathrm{v}}$ in an electromagnetic field. This equation represents a link between electromagnetics and mechanics.

Maxwell's equations (2.11) and the *constitutive relations* (2.8) and (2.10) explain and describe *all* macroscopic electromagnetic phenomena.

The differential representation of Maxwell's equations can be converted into its integral analogue. Stokes's theorem for any surface A bounded with a contour ∂A allows to rewrite equations (2.11a) and (2.11b) as:

$$\oint_{\partial A} \vec{\mathrm{E}} \cdot \mathrm{d}\vec{\mathrm{s}} = -\iint_{A} \frac{\partial \vec{\mathrm{B}}}{\partial t} \cdot \mathrm{d}\vec{\mathrm{A}} \tag{2.14a}$$

$$\oint_{\partial A} \vec{\mathrm{H}} \cdot \mathrm{d}\vec{\mathrm{s}} = \iint_{A} \left(\frac{\partial \vec{\mathrm{D}}}{\partial t} + \vec{\mathrm{J}}\right) \cdot \mathrm{d}\vec{\mathrm{A}}. \tag{2.14b}$$

Gauss's theorem[1] for any volume V enclosed by the boundary ∂V allows to transfer the last two equations of Maxwell's equations into their integral equivalents:

$$\oiint_{\partial V} \vec{\mathrm{D}} \cdot \mathrm{d}\vec{\mathrm{A}} = \iiint_{V} \rho \, \mathrm{dV} \tag{2.14c}$$

$$\oiint_{\partial V} \vec{\mathrm{B}} \cdot \mathrm{d}\vec{\mathrm{A}} = 0. \tag{2.14d}$$

[1] This theorem is also known as *divergence theorem*

In order to solve electromagnetic problems involving contiguous regions of different constitutive parameters, it is necessary to know the boundary conditions that the field vectors $\vec{\mathrm{E}}$, $\vec{\mathrm{H}}$, $\vec{\mathrm{D}}$ and $\vec{\mathrm{B}}$ must satisfy at the interfaces. To derive these conditions, consider an interface separating two different media 1 and 2 with constitutive parameters $(\sigma_1, \varepsilon_1, \mu_1)$ and $(\sigma_2, \varepsilon_2, \mu_2)$, respectively. The boundary conditions are obtained by applying the integral form of Maxwell's equations to a small region at the interface between two media and are as follows:

$$\mathrm{E_{2t}} = \mathrm{E_{1t}} \quad \text{or} \quad \vec{\mathrm{a}}_\mathrm{n} \times (\vec{\mathrm{E}}_2 - \vec{\mathrm{E}}_1) = 0 \tag{2.15a}$$

$$\mathrm{H_{2t}} - \mathrm{H_{1t}} = \mathrm{J_s} \quad \text{or} \quad \vec{\mathrm{a}}_\mathrm{n} \times (\vec{\mathrm{H}}_2 - \vec{\mathrm{H}}_1) = \vec{\mathrm{J}}_\mathrm{s} \tag{2.15b}$$

$$\mathrm{D_{2n}} - \mathrm{D_{1n}} = \rho_\mathrm{s} \quad \text{or} \quad \vec{\mathrm{a}}_\mathrm{n} \cdot (\vec{\mathrm{D}}_2 - \vec{\mathrm{D}}_1) = \rho_s \tag{2.15c}$$

$$\mathrm{B_{2n}} = \mathrm{B_{1n}} \quad \text{or} \quad \vec{\mathrm{a}}_\mathrm{n} \cdot (\vec{\mathrm{B}}_2 - \vec{\mathrm{B}}_1) = 0 \tag{2.15d}$$

where $\vec{\mathrm{a}}_\mathrm{n}$ is a normal vector pointing into medium 2, the subscripts 1 and 2 denote the fields in the regions 1 and 2, respectively, the subscripts t and n denote tangent and normal components of the fields, respectively. According to (2.15a) and (2.15d), the tangential component of $\vec{\mathrm{E}}$ and the normal component of $\vec{\mathrm{B}}$ are continuous functions across the interface. Equation (2.15b) states that the tangential component of $\vec{\mathrm{H}}$ is discontinuous across an interface where a surface current density $\vec{\mathrm{J}}_\mathrm{s}$ exists. The discontinuity in $\vec{\mathrm{D}}$ is determined by equation (2.15c) with ρ_s being a surface charge density [3], [16].

2.2.3 Potential Functions

In analyzing electromagnetic fields, it is often convenient to use auxiliary functions that simplify the process of finding analytical or numerical solutions of Maxwell's equations. Examples of such auxiliary functions are the *scalar electric potential* φ and the *vector magnetic potential* $\vec{\mathrm{A}}$.

The solenoidal nature of the $\vec{\mathrm{B}}$ field (eqn. 2.11d) allows to define a magnetic vector potential $\vec{\mathrm{A}}$ such that the magnetic flux density $\vec{\mathrm{B}}$ can exclusively be described by the curl of the potential:

$$\vec{\mathrm{B}} = \nabla \times \vec{\mathrm{A}}. \tag{2.16}$$

Substituting this into Faraday's law (2.11a) results in

$$\vec{\mathrm{E}} = -\nabla\varphi - \frac{\partial \vec{\mathrm{A}}}{\partial t} \tag{2.17}$$

where φ is a scalar electric potential.

Both potentials $\vec{\mathrm{A}}$ and φ defined in (2.16) and (2.17), respectively, are arbitrary in the sense that $\vec{\mathrm{B}}$ and $\vec{\mathrm{E}}$ are left unchanged if the gauge transformation

$$\vec{\mathrm{A}}' = \vec{\mathrm{A}} + \nabla\xi \tag{2.18a}$$

$$\varphi' = \varphi - \frac{\partial \xi}{\partial t} \tag{2.18b}$$

is applied where ξ is an arbitrary scalar function [17].

2.2.4 Classification of Electromagnetic Problems

The behavior of electromagnetic fields is governed by Maxwell's equations which represent a set of differential equations. According to the way how the time dependencies in these equations are treated, the following classification of electromagnetic problems can be derived:

1. *Static fields* are obtained by neglecting the time dependence in the electromagnetic field quantities $\vec{\mathrm{E}}$, $\vec{\mathrm{H}}$, $\vec{\mathrm{D}}$, $\vec{\mathrm{B}}$ and $\vec{\mathrm{J}}$. The static formulations can be further subdivided into electrostatic, magnetostatic and stationary current formulations.
2. *Fields in frequency domain* are considered if the time dependency is given by sinusoidal functions of a single angular frequency exclusively. In the frequency domain, one deals with a full set of Maxwell's equations which can be reduced in some cases to electro- and magnetoquasistatic formulations.
3. *Fields in time domain* are considered if the form of temporal dependency cannot be a priory specified. In this case, the variety of possible formulations is described by the full set of Maxwell's equations which can be reduced in some cases to electro- and magnetoquasistatic formulations.

Fig. 2.1 gives a graphical representation of the proposed classification.

2.2.5 Quasistatic Fields

Quasistatic approximations considered in *time domain* are in the focus of this treatise (Fig. 2.1). They are justified if the time rates of change are slow enough so that time delays due to the propagation of the electromagnetic waves can be neglected.

The *electroquasistatic* (EQS) approximations can be used when the influence of the magnetic induction can be neglected, i.e.,

$$\frac{\partial \vec{\mathrm{B}}}{\partial t} \simeq 0, \tag{2.19}$$

which leads to the following simplified system of Maxwell's equations:

$$\nabla \times \vec{\mathrm{E}} = 0 \tag{2.20a}$$

$$\nabla \times \vec{\mathrm{H}} = \frac{\partial \vec{\mathrm{D}}}{\partial t} + \vec{\mathrm{J}} \tag{2.20b}$$

$$\nabla \cdot \vec{\mathrm{D}} = \rho \tag{2.20c}$$

$$\nabla \cdot \vec{\mathrm{B}} = 0. \tag{2.20d}$$

In EQS approximations, (2.20a) requires that $\vec{\mathrm{E}}$ is essentially irrotational. With the given charge density ρ, equations (2.20a) and (2.20c) allow to determine the field $\vec{\mathrm{E}}$ uniquely. These equations express, therefore, the fundamental laws governing the electroquasistatic regime.

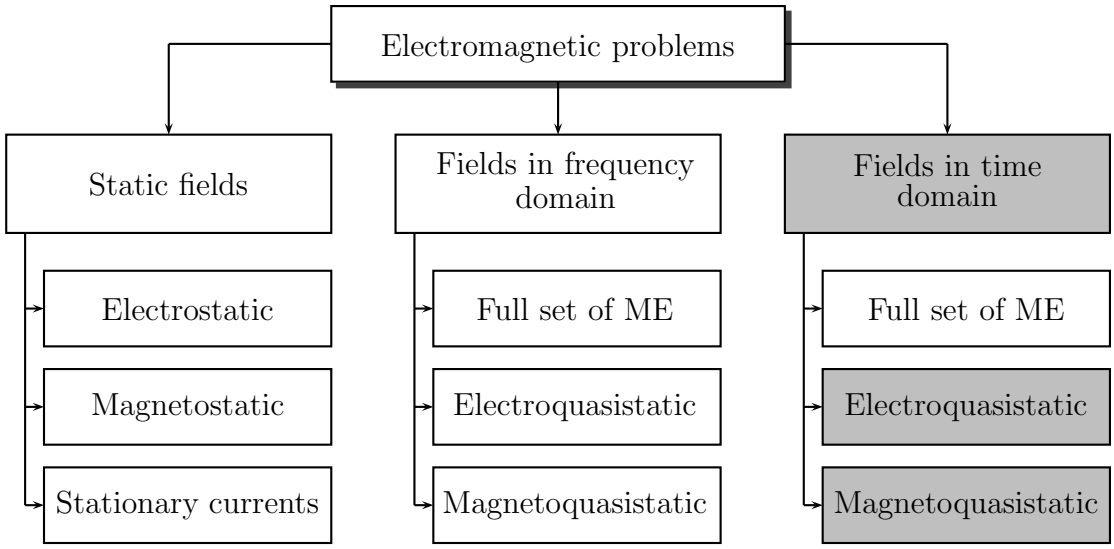

Figure 2.1: Mathematical classification of electromagnetic problems. (ME is an abbreviation for Maxwell's equations.)

The *magnetoquasistatic* (MQS) approximations can be used when the contribution of the displacement currents can be omitted with respect to the conduction currents, i.e.,

$$\max_{\vec{r}\in\mathbf{R}} \left| \frac{\partial \vec{\mathrm{D}}}{\partial t} \right| \ll \max_{\vec{r}\in\mathbf{R}} \left| \vec{\mathrm{J}} \right| . \tag{2.21}$$

The resulting set of equations then reads:

$$\nabla \times \vec{\mathrm{E}} = -\frac{\partial \vec{\mathrm{B}}}{\partial t} \tag{2.22a}$$

$$\nabla \times \vec{\mathrm{H}} = \vec{\mathrm{J}} \tag{2.22b}$$

$$\nabla \cdot \vec{\mathrm{D}} = \rho \tag{2.22c}$$

$$\nabla \cdot \vec{\mathrm{B}} = 0. \tag{2.22d}$$

In the MQS approximation, (2.22b) and (2.22d) are sufficient to determine field $\vec{\mathrm{H}}$ uniquely and, are, therefore, the fundamental laws governing the magnetoquasistatic regime.

Conditions for Fields to be Quasistatic

According to the argumentation given in [18], the decision whether a quasistatic field should be classified as electroquasistatic or magnetoquasistatic one can be made by simply following a rule of thumb. This rule is applied to a system consisting of "perfect conductors" and "perfect insulators". If together with the decrease of the frequency of the driving source up to the level where the fields become static, the magnetic field vanishes, then the field is electroquasistatic; if the electric field

vanishes, the field is magnetoquasistatic. In the praxis, however, the materials are not "perfect", i.e., the possibility to use this rule depends on understanding under which circumstances materials tend to behave as "perfect" conductors and insulators. Nevertheless, since many metals are very good conductors and gases, liquids and solids are very good insulators, the rule of thumb can be considered as a good intuitive approach.

To estimate the field magnitudes using the quasistatic laws, let ℓ be the typical length scale. Then the spatial derivatives that make up the curl and divergence operators are approximated by $1/\ell$ which means

$$\mathrm{E} = \frac{\rho\ell}{\varepsilon} \tag{2.23a}$$

for the electroquasistatic regime and

$$\mathrm{H} = \mathrm{J}\ell \tag{2.23b}$$

for the magnetoquasistatic regime. Here, E, H and J are used to describe the magnitudes of $\vec{\mathrm{E}}$, $\vec{\mathrm{H}}$ and $\vec{\mathrm{J}}$ [18].

In case of an electroquasistatic regime, a time varying charge causes a current which in turn induces a magnetic field. To estimate the magnitude of this induced field $\vec{\mathrm{H}}$, one can use Ampère's law. With the help of (2.23a) we obtain

$$\mathrm{H} = \frac{\varepsilon\mathrm{E}\ell}{\tau} = \frac{\ell^2\rho}{\tau} \tag{2.24a}$$

where τ is the characteristic time of an excitation.

For a magnetoquasistatic regime, a time varying current implies a time varying $\vec{\mathrm{H}}$ which on its turn induces an electric field according to Faraday's law. The magnitude of this field can be then approximated using (2.23b) as

$$\mathrm{E} = \frac{\mu\mathrm{H}\ell}{\tau} = \frac{\mu\mathrm{J}\ell^2}{\tau}. \tag{2.24b}$$

Having approximations (2.24) for the electro- and magnetoquasistatic regimes available, we can estimate the errors that are committed by ignoring the magnetic induction and displacement current terms in the respective EQS and MQS formulations. From the full set of Maxwell's equations the following expressions for the *curl* of the error fields are derived:

$$\frac{\mathrm{E}_{\mathrm{error}}}{\ell} = \frac{\mu\rho\ell^2}{\tau^2}\,, \tag{2.25a}$$

$$\frac{\mathrm{H}_{\mathrm{error}}}{\ell} = \frac{\varepsilon\mu J\ell^2}{\tau^2}\,. \tag{2.25b}$$

The ratio of the error fields to the quasistatic fields is estimated using (2.23) as

$$\frac{\mathrm{E}_{\mathrm{error}}}{\mathrm{E}} = \frac{\varepsilon\mu\ell^2}{\tau^2} \tag{2.26a}$$

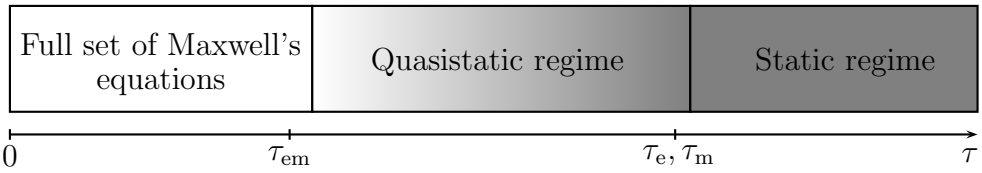

Figure 2.2: Range of characteristic times over which quasistatic approximation is valid. The transit time of an electromagnetic wave is τ_{em} while τ_{e} or τ_{m} is the time characterizing the dynamics of the quasistatic system.

for the electroqusistatic approximations and

$$\frac{\mathrm{H}_{\mathrm{error}}}{\mathrm{H}} \quad = \quad \frac{\varepsilon\mu\ell^2}{\tau^2} \tag{2.26b}$$

for the magnetoquasistatic approximations. For the quasistatic approximations to be justified, these error fields must be small compared to the quasistatic fields.

The last expressions show that whether (2.26a) is used to represent the electroquasistatic system, or (2.26b) is used for the magnetoquasistatic system, the condition on the spatial scale ℓ and characteristic time τ are exactly the same. Both electroquasistatic and magnetoquasistatic approximations are valid upon the conditions of sufficiently slow time variations and sufficiently small dimensions so that

$$\frac{\mu\varepsilon\ell^2}{\tau^2} \ll 1 \quad \Rightarrow \quad \sqrt{\mu\varepsilon}\,\ell = \frac{\ell}{c} =: \tau_{\mathrm{em}} \ll \tau \tag{2.27}$$

where $c = 1/\sqrt{\mu\varepsilon}$ and τ_{em} is the time required for an electromagnetic wave to propagate at the velocity c over the largest length ℓ of the system. Thus, any of the quasistatic approximations is valid if this time τ_{em} is much shorter compared to the characteristic constant of an excitation τ. The graphical representation of this requirement is give in Fig. 2.2. The intensity of the coloring illustrates an increase of the static properties. In Fig. 2.2, there are two other important time markers, namely, τ_{e} which is an *electroquasistatic charge relaxation time* and is defined as

$$\tau_{\mathrm{e}} \quad = \quad \frac{\varepsilon}{\sigma} \tag{2.28a}$$

and τ_{m} which is a *magnetoquasistatic magnetic (current) diffusion time* and is defined as

$$\tau_{\mathrm{m}} \quad = \quad \mu\sigma\ell^2. \tag{2.28b}$$

Both constants, τ_{e} and τ_{m}, are derived in [18]. The role of these constants in the definition of the quasistatic regimes is clarified in the subsequent discussion.

The decision which approximation can be used for a particular problem should be taken by considering the fields that would retain in the static case. This is, however, not always a simple task. One needs to elaborate more precise criteria allowing to distinguish between electro- and magnetoquasistatic, static and full dynamic regimes.

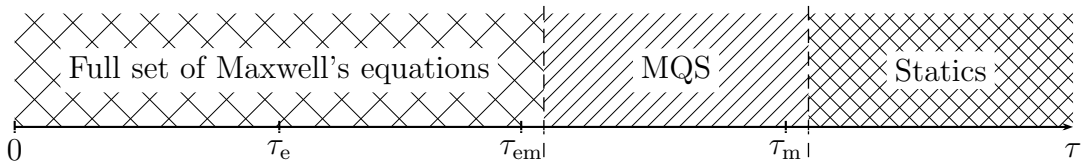

Figure 2.3: Ordering of the characteristic times in case $\tau_\mathrm{m} \gg \tau_\mathrm{e}$.

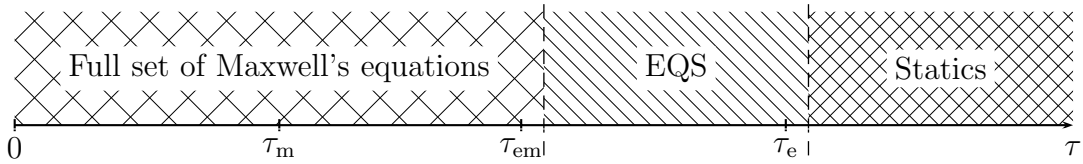

Figure 2.4: Ordering of the characteristic times in case $\tau_\mathrm{e} \gg \tau_\mathrm{m}$.

As a starting point of the derivation, we notice that

$$\tau_\mathrm{e}\,\tau_\mathrm{m} = \left(\sqrt{\varepsilon\mu}\ell\right)^2 = \tau_\mathrm{em}^2 \quad \Rightarrow \quad \tau_\mathrm{em} = \sqrt{\tau_\mathrm{e}\tau_\mathrm{m}}, \tag{2.29}$$

i.e., τ_em defines the geometric mean of the previously defined quantities τ_e and τ_m. Thus, the three time constants can be arranged in one of two orders. Either $\tau_\mathrm{m} > \tau_\mathrm{e}$ in which case the ordering of the times is as shown in Fig. 2.3, or the reverse situation is true and the order is as presented in Fig. 2.4.

While Fig. 2.3 and 2.4 allow to specify the time intervals in which magneto- or, respectively, electroquasistatic approximations are valid, they do not, however, reflect the dependence of the magnetoquasistatic diffusion time τ_m and the wave transit time τ_em on the length ℓ of the system. These dependencies can, however, also be taken into account if the electromagnetic phenomena are placed in a plane, in which one axis reflects the effect of the excitation time constant τ while the other one represents the length scale ℓ.

Normalization of the time constants to one characteristic time, here τ_em, leads to

$$\frac{\tau_\mathrm{em}}{\tau_\mathrm{em}} = 1 \tag{2.30a}$$

$$\frac{\tau_\mathrm{e}}{\tau_\mathrm{em}} = \frac{\varepsilon}{\sigma\ell\sqrt{\mu\varepsilon}} \quad \Rightarrow \quad \frac{\tau_\mathrm{e}}{\tau_\mathrm{em}} = \frac{\ell^*}{\ell} \tag{2.30b}$$

$$\frac{\tau_\mathrm{m}}{\tau_\mathrm{em}} = \frac{\mu\sigma\ell^2}{\ell\sqrt{\mu\varepsilon}} \quad \Rightarrow \quad \frac{\tau_\mathrm{m}}{\tau_\mathrm{em}} = \frac{\ell}{\ell^*} \tag{2.30c}$$

where

$$\ell^* = \frac{1}{\sigma}\sqrt{\varepsilon/\mu} = \frac{1}{\sigma\eta} \tag{2.31}$$

is a characteristic length and η denotes the intrinsic impedance of the medium. Introducing the notation

$$x := \log\left(\frac{\tau}{\tau_\mathrm{em}}\right) \tag{2.32}$$

$$y := \log\left(\frac{\ell}{\ell^*}\right) \tag{2.33}$$

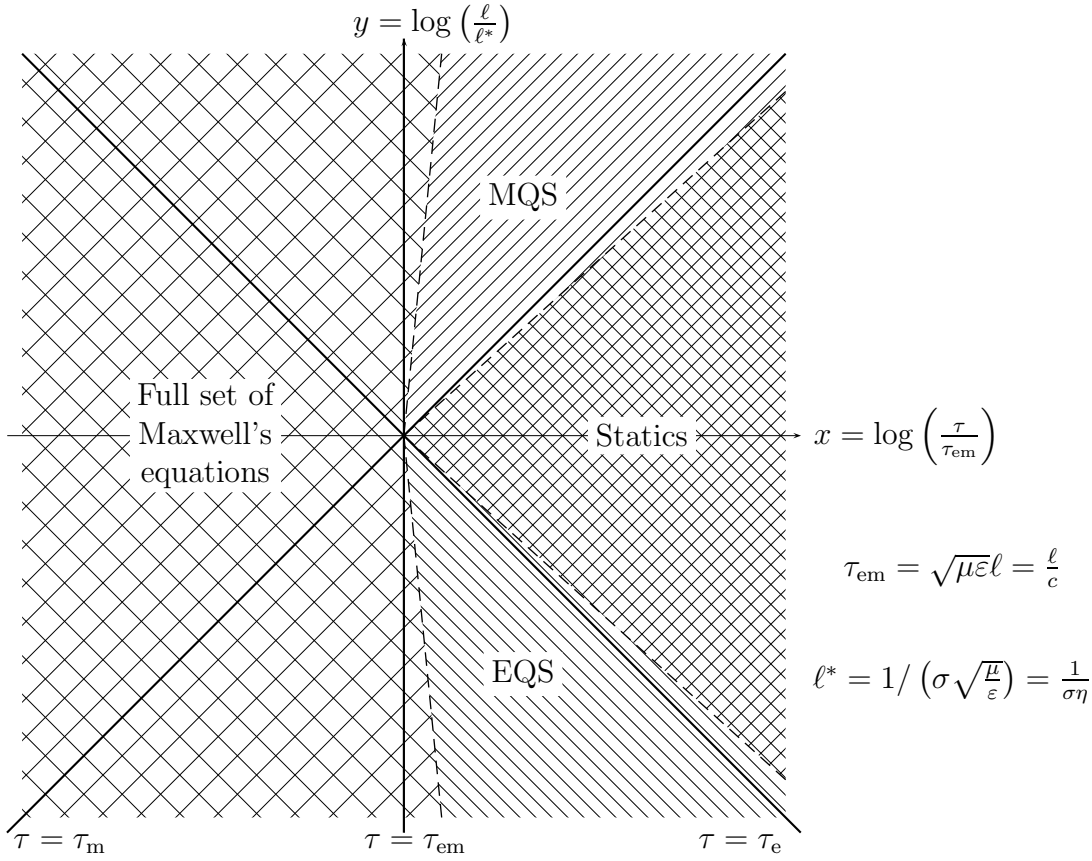

Figure 2.5: Graphical representation of the classical electromagnetic problems classification. Important characteristics are given by the model length ℓ, excitation time constant τ as well as by material properties σ, c and η.

the following characteristic curves are derived:

$$\tau = \tau_{\mathrm{em}} \quad \Rightarrow \quad \log\left(\frac{\tau}{\tau_{\mathrm{em}}}\right) = \log(1) \quad \Rightarrow \quad x = 0 \tag{2.34a}$$

$$\tau = \tau_{\mathrm{e}} \quad \Rightarrow \quad \log\left(\frac{\tau}{\tau_{\mathrm{em}}}\right) = \log\left(\frac{\ell^*}{\ell}\right) \quad \Rightarrow \quad y = -x \tag{2.34b}$$

$$\tau = \tau_{\mathrm{m}} \quad \Rightarrow \quad \log\left(\frac{\tau}{\tau_{\mathrm{em}}}\right) = \log\left(\frac{\ell}{\ell^*}\right) \quad \Rightarrow \quad y = x. \tag{2.34c}$$

The obtained characteristic curves combined with the asymptotic time boundaries illustrated in Fig. 2.3 and 2.4 allow to draw a two dimensional plot reflecting the placement of the approximation regimes depending on the characteristic time τ and length ℓ (see Fig. 2.5).

Diffusion Equations for Quasistatic Fields

Since in quasistatic approximations the effect of the wave propagation is no longer taken into account, the corresponding equations are called *diffusion equations*. They

can be deduced from systems (2.20) and (2.22) governing the electro- and magnetoqusistatic approximations, respectively, and using the already introduced potential functions φ and $\vec{\mathrm{A}}$:

$$\nabla \cdot \left(\frac{\partial}{\partial t}(\varepsilon \nabla \varphi) + \sigma \nabla \varphi \right) = 0 \tag{2.35a}$$

for electroquasistatic and

$$\sigma \frac{\partial \vec{\mathrm{A}}}{\partial t} + \nabla \times (\frac{1}{\mu} \nabla \times \vec{\mathrm{A}}) + \sigma \nabla \varphi = \vec{\mathrm{J}}_s \tag{2.35b}$$

for magnetoquasistatic regimes [19].

2.2.6 Examples

To complete the discussion, we consider three electromagnetic models all having a length of $\ell = 1$ m with a homogeneous filling of corn oil, water and copper, respectively. For all three media, $\mu = \mu_0$. The other material parameters, ε and σ, are given in Tab. 2.2. This table also contains the time intervals for the excitation time constant τ allowing to use one or the other approximation regime.

	Corn oil	Water	Copper
ε	$3.1\varepsilon_0$	$81\varepsilon_0$	$\approx \varepsilon_0$
σ [S/m]	5×10^{-11}	0.2	5.7×10^{7}
ℓ^* [m]	10^{8}	0.12	4.7×10^{-11}
$\log\left(\frac{\ell}{\ell^*}\right)$	-8	1	11
τ_{em}[s]	5.8×10^{-9}	3×10^{-8}	3×10^{-9}
Full set	$\tau < \tau_{\mathrm{em}}$	$\tau < \tau_{\mathrm{em}}$	$\tau < \tau_{\mathrm{em}}$
EQS	$\tau_{\mathrm{em}} < \tau < 5.8 \times 10^{-1}$ s	–	–
MQS	–	$\tau_{\mathrm{em}} < \tau < 3 \times 10^{-7}$ s	$\tau_{\mathrm{em}} < \tau < 3 \times 10^{2}$ s
Statics	$\tau > 5.8 \times 10^{-1}$ s	$\tau > 3 \times 10^{-7}$ s	$\tau > 3 \times 10^{2}$ s

Table 2.2: Different media and time ranges for the corresponding electromagnetic approximation regimes.

The two-dimensional plot of Fig. 2.5 can be used as a simple heuristic tool allowing to specify these time intervals. The main advantage in using this two dimensional graph is that one always avoids the computation of irrelevant time constants, e.g., τ_{m} for electroquasistatic regime or τ_{e} for magnetoquasistatic regime. Since the electric conductivity σ is a widely varying parameter, the values of ℓ^* also have a wide range of changes thus stipulating the choice of the approximation regime.

2.3 Finite Integration Technique

This part of the present treatise gives a survey on a spatial discretization method for solving Maxwell's equations in integral form. This numerical approach is called Finite Integration Technique (FIT) and was firstly developed and formulated in 1977 [20]. The primary objective of this development was the ability to numerically solve the complete set of Maxwell's equations in a general way. Over the years, the technique has been further developed by numerous contributions resulting so far in an extensive collection of discrete electromagnetic formulations.

By this technique, the space-continuous integral Maxwell's equations are transferred into their space-discrete analogue. The obtained matrix equations formulated for the quasistatic regimes discussed in the previous subsection are further used for the construction of field-circuit coupled formulations.

In the notation that follows, the simplest case of a three dimensional orthogonal Cartesian mesh is considered, however, the FIT theory is not only restricted to this particular type of meshes. The other types of orthogonal, e.g. cylindrical and spherical, and non-orthogonal meshes can also be considered in the frame of this approach [21], [22]. Consistent subgridding schemes have been developed in [23].

2.3.1 Cartesian Grid

The first step in the FIT discretization is the definition of the computational domain, which is a finite domain $\Omega \in \mathbb{R}^3$. The domain Ω is divided into a finite number of cells such that the intersection of two different cells is either empty or it is a two-dimensional polygon, a one-dimensional edge shared by both cells or a point [24]. To each edge of the cells an initial *orientation* is prescribed, so that the union of the oriented cells can be characterized as a *directed graph* [25]. The cell facets should also be supplied with an orientation.

For a brick-shaped region $\Omega \in \mathbb{R}^3$, the corresponding cell complex representing the hexahedral grid in Cartesian coordinates reads

$$\begin{aligned} G: \;=\; & \{V_{i,j,k} \in \mathbb{R}^3 |\; V_{i,j,k} = [x_i, x_{i+1}] \times [y_j, y_{j+1}] \times [z_k, z_{k+1}], \\ & i = 1, \cdots, I-1,\; j = 1, \cdots, J-1,\; k = 1, \cdots, K-1\} \end{aligned} \tag{2.36}$$

where I, J and K are the total numbers of grid lines in x, y and z directions, respectively. The total number of the grid points is then $N_p = I\,J\,K$. Three space indices i, j and k can be reduced to one canonical space index

$$n = 1 + (i-1)M_x + (j-1)M_y + (k-1)M_z \tag{2.37}$$

where $M_x = 1$, $M_y = I$, $M_z = I\,J$.

With respect to each *grid point* $P(n) = P_{i,j,k}$ one defines three *grid edges* $L_x(n) = L_x(i,j,k)$, $L_y(n) = L_y(i,j,k)$ and $L_z(n) = L_z(i,j,k)$, and three *grid facets* $A_x(n) = A_x(i,j,k)$, $A_y(n) = A_y(i,j,k)$ and $A_z(n) = A_z(i,j,k)$. Finally, one grid cell or *grid volume* $V_n = V_{i,j,k}$ is associated with the grid point $P(n) = P_{i,j,k}$. The graphical

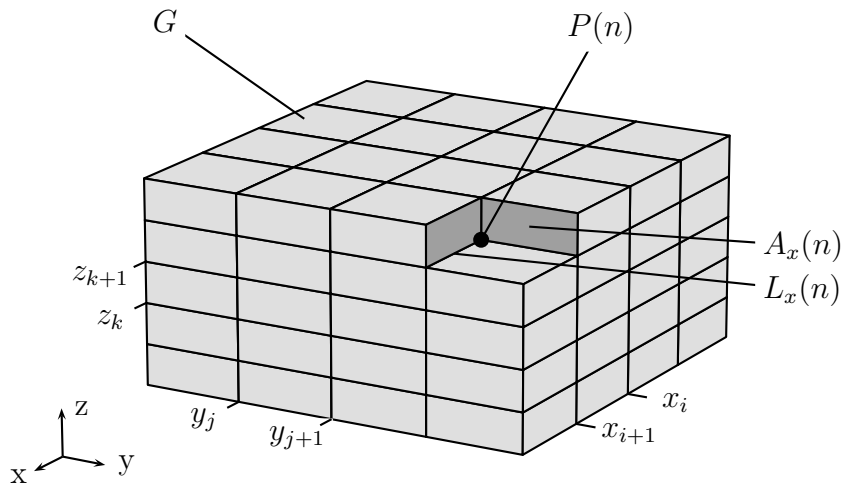

Figure 2.6: Computational domain Ω. The grid lines in x, y and z direction are enumerated with the indices i, j and k, respectively. With each point $P(n)$ of the grid domain G one can associate three grid lines, three grid facets and one grid cell.

illustration of the FIT computational domain Ω is presented in Fig. 2.6, where only one grid line, $L_x(n)$ and only one grid facet, $A_x(n)$, associated with the grid point $P(n)$ are given.

2.3.2 Maxwell's Grid Equations

The FIT state variables are the electrical grid voltages located on the grid edges (Fig. 2.7a), defined by

$$\widehat{\mathrm{e}}_{x,y,z}(n) = \int\limits_{L_{x,y,z}(n)} \vec{\mathrm{E}} \cdot \mathrm{d}\vec{\mathrm{s}} \tag{2.38}$$

and the magnetic grid fluxes allocated at the grid facets (Fig. 2.7b)

$$\widehat{\widehat{\mathrm{b}}}_{x,y,z}(n) = \int\limits_{A_{x,y,z}(n)} \vec{\mathrm{B}} \cdot \mathrm{d}\vec{\mathrm{A}}. \tag{2.39}$$

The introduction of the grid variables allocated at the grid edges and on the grid facets allows to consider the discretization of the equations (2.14a) and (2.14d), respectively, for any randomly chosen grid facet (Fig. 2.7a) and brick cell (Fig. 2.7b):

$$\widehat{\mathrm{e}}_x(n) + \widehat{\mathrm{e}}_y(n+M_x) - \widehat{\mathrm{e}}_x(n+M_y) - \widehat{\mathrm{e}}_y(n) = -\frac{\mathrm{d}}{\mathrm{d}t}\widehat{\widehat{\mathrm{b}}}_z(n)$$
$$-\widehat{\widehat{\mathrm{b}}}_x(n) - \widehat{\widehat{\mathrm{b}}}_y(n) - \widehat{\widehat{\mathrm{b}}}_z(n) + \widehat{\widehat{\mathrm{b}}}_x(n+M_x) + \widehat{\widehat{\mathrm{b}}}_y(n+M_y) + \widehat{\widehat{\mathrm{b}}}_z(n+M_z) = 0$$

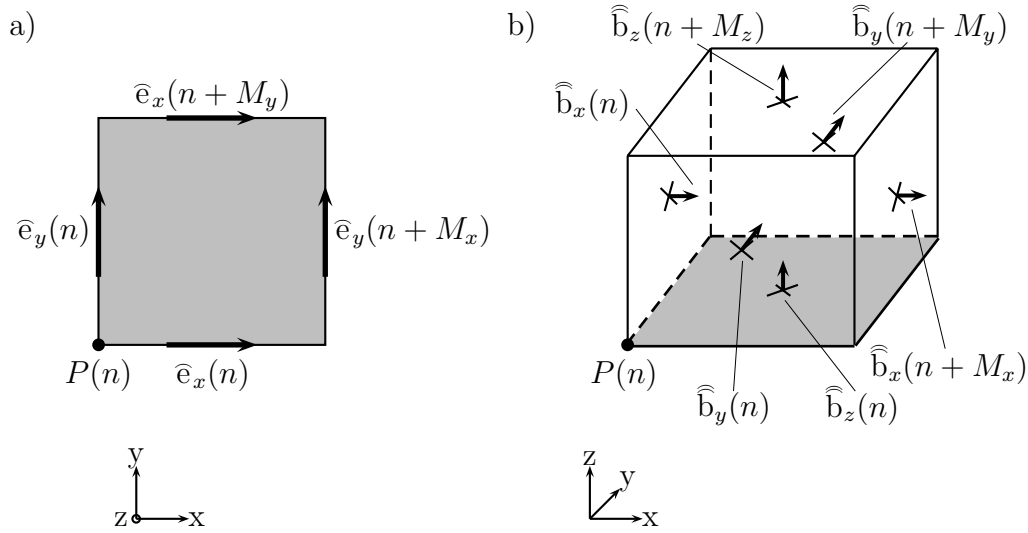

Figure 2.7: Allocation of the FIT degrees of freedom on the grid: a) randomly chosen grid facet and the grid voltages allocated at its edges; b) randomly chosen brick cell and the grid fluxes associated with its facets.

The same procedure can be repeated for each grid facet and each grid cell of the computational domain Ω leading to the following matrix equations:

$$\mathbf{C}\widehat{\mathbf{e}} = -\frac{\mathrm{d}}{\mathrm{d}t}\widehat{\widehat{\mathbf{b}}} \tag{2.40a}$$

$$\mathbf{S}\widehat{\widehat{\mathbf{b}}} = 0 \tag{2.40b}$$

which are the FIT discrete versions of the continuous integral equations (2.14a) and (2.14d), respectively. Vectors $\widehat{\mathbf{e}}$ and $\widehat{\widehat{\mathbf{b}}}$ contain the components of the grid voltages and grid fluxes, respectively, ordered in the way that we first collect all x, then all y and finally all z components:

$$\begin{aligned}\widehat{\mathbf{e}} &= (\widehat{\mathrm{e}}_x(1),\cdots,\widehat{\mathrm{e}}_x(N_p),\widehat{\mathrm{e}}_y(1),\cdots,\widehat{\mathrm{e}}_y(N_p),\widehat{\mathrm{e}}_z(1),\cdots,\widehat{\mathrm{e}}_z(N_p))^T\\ \widehat{\widehat{\mathbf{b}}} &= (\widehat{\widehat{\mathrm{b}}}_x(1),\cdots,\widehat{\widehat{\mathrm{b}}}_x(N_p),\widehat{\widehat{\mathrm{b}}}_y(1),\cdots,\widehat{\widehat{\mathrm{b}}}_y(N_p),\widehat{\widehat{\mathrm{b}}}_z(1),\cdots,\widehat{\widehat{\mathrm{b}}}_z(N_p))^T.\end{aligned}$$

The matrix $\mathbf{C}$ appearing in (2.40a) contains only information on the incidence relation of the cell edges and on their orientation, thus it only has matrix coefficients $\mathrm{c}_{i,j} \in \{-1,0,1\}$ [26]. It represents the *discrete curl* operator on the grid G and possesses a block structure:

$$\mathbf{C} = \begin{bmatrix} 0 & -P_z & P_y \\ P_z & 0 & -P_x \\ -P_y & P_x & 0 \end{bmatrix} \tag{2.41}$$

where the matrices P_x, P_y and P_z are the *discretized partial differential* operators defined by

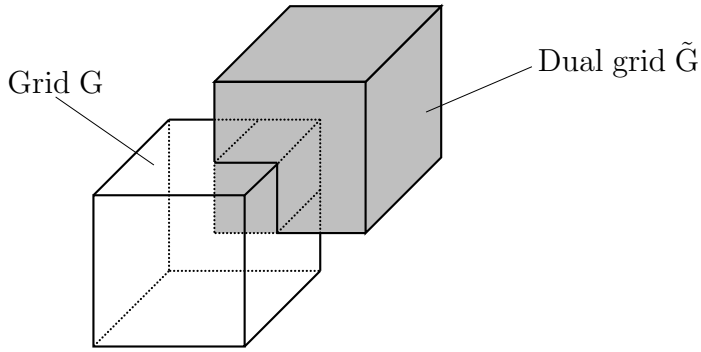

Figure 2.8: Spatial allocation of a primary cell and a dual cell of the grid doublet $\{G, \tilde{G}\}$ [26].

$$(P_x)_{pq} = \left\{ \begin{array}{ll} -1; & p = q \\ +1; & p = q + M_x \\ 0; & \text{else} \end{array} \right\} \begin{array}{l} p=1+(i-1)M_x+(j-1)M_y+(k-1)M_z, \\ 1\leq i\leq I-1,\ 1\leq j\leq J,\ 1\leq k\leq K \end{array} \tag{2.42a}$$

$$(P_y)_{pq} = \left\{ \begin{array}{ll} -1; & p = q \\ +1; & p = q + M_y \\ 0; & \text{else} \end{array} \right\} \begin{array}{l} p=1+(i-1)M_x+(j-1)M_y+(k-1)M_z, \\ 1\leq i\leq I,\ 1\leq j\leq J-1,\ 1\leq k\leq K \end{array} \tag{2.42b}$$

$$(P_z)_{pq} = \left\{ \begin{array}{ll} -1; & p = q \\ +1; & p = q + M_z \\ 0; & \text{else} \end{array} \right\} \begin{array}{l} p=1+(i-1)M_x+(j-1)M_y+(k-1)M_z. \\ 1\leq i\leq I,\ 1\leq j\leq J,\ 1\leq k\leq K-1 \end{array} \tag{2.42c}$$

The matrix $\mathbf{S}$ standing in the left hand side of equation (2.40b) gathers the information on the incidence relation and on the orientation of the facets of the brick cells, thus it has matrix coefficients $s_{i,j} \in \{-1, 0, 1\}$. It represents a *discrete divergence (source)* operator. Like the discrete curl operator $\mathbf{C}$, this matrix is also sub-structured and is composed of discrete partial differential operators [27]:

$$\mathbf{S} = [P_x; P_y; P_z]. \tag{2.43}$$

In order to discretize the two remaining Maxwell's equation, i.e., Ampére's law (2.14b) and Gauss's law (2.14c), the dual grid $\tilde{G}$ has to be introduced. For a Cartesian equidistant grid, it equals to the grid G shifted by half a cell length (Fig. 2.8). However, the definition of the dual FIT grid is much more general and, consequently, other orthogonal and non-orthogonal dual grids can be considered.

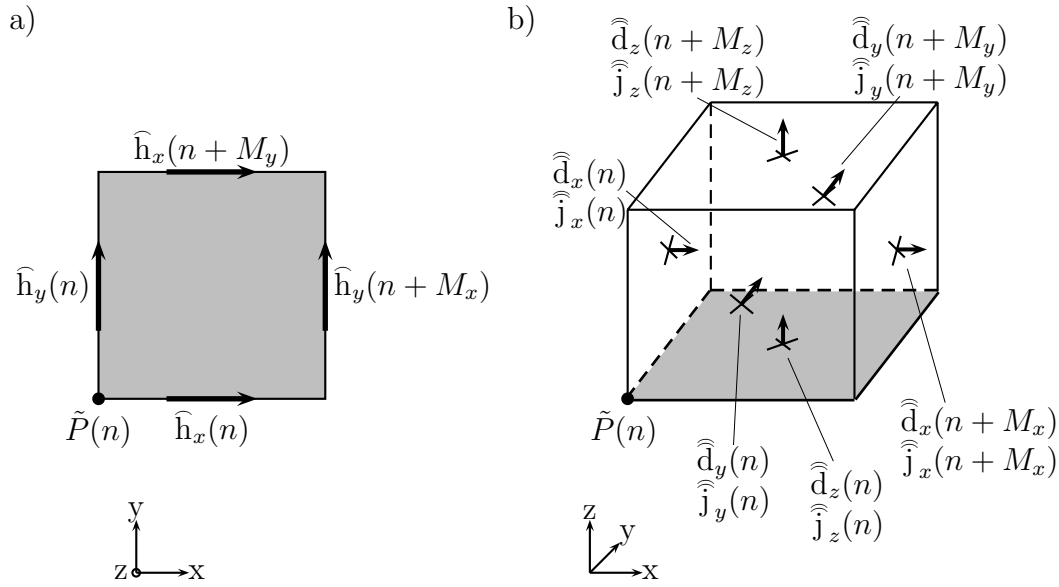

Figure 2.9: Allocation of the FIT degrees of freedom on the dual grid domain: a) randomly chosen dual grid facet and the grid voltages prescribed to its edges; b) randomly chosen brick cell of the dual grid and the grid fluxes and grid currents associated with its facets.

The introduction of the dual grid $\tilde{G}$ allows to specify another set of the FIT state variables, namely, the magnetic grid voltages allocated at the edges $\tilde{L}$ (Fig. 2.9a)

$$\widehat{\mathrm{h}}_{x,y,z}(n) = \int_{\tilde{L}_{x,y,z}(n)} \vec{\mathrm{H}} \cdot \mathrm{d}\vec{\mathrm{s}}, \tag{2.44}$$

the electrical grid fluxes allocated at the facets $\tilde{A}$ (Fig. 2.9b)

$$\widehat{\widehat{\mathrm{d}}}_{x,y,z}(n) = \int_{\tilde{A}_{x,y,z}(n)} \vec{\mathrm{D}} \cdot \mathrm{d}\vec{\mathrm{A}}, \tag{2.45}$$

and the electrical grid currents also allocated at the dual facets $\tilde{A}$ (Fig. 2.9b)

$$\widehat{\widehat{\mathrm{j}}}_{x,y,z}(n) = \int_{\tilde{A}_{x,y,z}(n)} \vec{\mathrm{J}} \cdot \mathrm{d}\vec{\mathrm{A}}. \tag{2.46}$$

The discretization of equations (2.14b) and (2.14c) is analogously to the above described procedure for the discretization of equations (2.14a) and (2.14d) with the only difference that the grid unknowns are allocated now at the dual grid elements. Combining these grid variables into the vectors

$$\begin{aligned}
\widehat{\mathbf{h}} &= (\widehat{\mathrm{h}}_x(1), \cdots, \widehat{\mathrm{h}}_x(N_p), \widehat{\mathrm{h}}_y(1), \cdots, \widehat{\mathrm{h}}_y(N_p), \widehat{\mathrm{h}}_z(1), \cdots, \widehat{\mathrm{h}}_z(N_p))^T \\
\widehat{\widehat{\mathbf{d}}} &= (\widehat{\widehat{\mathrm{d}}}_x(1), \cdots, \widehat{\widehat{\mathrm{d}}}_x(N_p), \widehat{\widehat{\mathrm{d}}}_y(1), \cdots, \widehat{\widehat{\mathrm{d}}}_y(N_p), \widehat{\widehat{\mathrm{d}}}_z(1), \cdots, \widehat{\widehat{\mathrm{d}}}_z(N_p))^T \\
\widehat{\widehat{\mathbf{j}}} &= (\widehat{\widehat{\mathrm{j}}}_x(1), \cdots, \widehat{\widehat{\mathrm{j}}}_x(N_p), \widehat{\widehat{\mathrm{j}}}_y(1), \cdots, \widehat{\widehat{\mathrm{j}}}_y(N_p), \widehat{\widehat{\mathrm{j}}}_z(1), \cdots, \widehat{\widehat{\mathrm{j}}}_z(N_p))^T
\end{aligned}$$

we come to the following matrix equations

$$\widetilde{\mathbf{C}}\widehat{\mathbf{h}} = \frac{\mathrm{d}}{\mathrm{d}t}\widehat{\widehat{\mathbf{d}}} + \widehat{\widehat{\mathbf{j}}} \tag{2.47a}$$

$$\widetilde{\mathbf{S}}\widehat{\widehat{\mathbf{d}}} = \mathbf{q} \tag{2.47b}$$

where $\widetilde{\mathbf{C}}$ is a discrete curl operator and $\widetilde{\mathbf{S}}$ is a discrete divergence operator of the dual grid. Vector $\mathbf{q}$ contains the discrete electrical charges. Equations (2.40) and (2.47) are called Maxwell's grid equations.

According to Poincaré's lemma, irrotational electromagnetic fields can be represented as gradient fields of scalar potentials. The FIT electric grid voltages are allocated at the cell edges and consequently can be represented as the difference of two nodal potential values. The discrete potential values ϕ_n are allocated at the grid mesh points $P_n \in G$ such that the relation $\phi_{n+1} - \phi_n = \widehat{\mathrm{e}}_k$ holds for every oriented edge $L_k \in G$ connecting nodes P_n and P_{n+1} [28].

When collecting these discrete potential values into a vector ϕ for the primary cell complex G, we come to the following grid relation

$$\widehat{\mathbf{e}} = -\mathbf{G}\phi \tag{2.48}$$

where the discrete *gradient* matrix $\mathbf{G}$ is the negative transpose of the dual discrete divergence operator [28].

The duality of the grid doublet $\{G, \tilde{G}\}$ results in the following topological properties:

$$\begin{aligned} &\mathbf{C} = \widetilde{\mathbf{C}}^T, \\ &\mathbf{C}\widetilde{\mathbf{S}}^T = 0, \quad \widetilde{\mathbf{C}}\mathbf{S}^T = 0 \\ &\mathbf{S}\mathbf{C} = 0, \quad \widetilde{\mathbf{S}}\widetilde{\mathbf{C}} = 0 \end{aligned} \tag{2.49}$$

that reflect the continuous relations

$$\begin{aligned} &\text{curl grad} \equiv 0, \\ &\text{div curl} \equiv 0. \end{aligned} \tag{2.50}$$

2.3.3 Discretization of the Material Relations

The discretization process described in the previous subsection does not meet any approximations since the Maxwell's equations have been directly applied to the grid.

The approximations in the method starts when the integral flux- and voltage state variables allocated at the two different grids are to be coupled to each other by the constitutive material relations, thus translating the continuous material equations into discrete ones.

An element $M_\varepsilon(n, n)$ of the discrete permittivity matrix $\mathbf{M}_\varepsilon$ (i.e. one entry on its main diagonal) is derived from the integration approximation of the ratio of the

electric flux density $\vec{\mathrm{D}}$ and the electric field strength $\vec{\mathrm{E}}$ on the grid doublet $\{G, \tilde{G}\}$ as follows:

$$\begin{aligned}\frac{\int\limits_{\tilde{A}_n} \vec{\mathrm{D}} \cdot \mathrm{d}\vec{\mathrm{A}}}{\int\limits_{L_n} \vec{\mathrm{E}} \cdot \mathrm{d}\vec{\mathrm{s}}} &= \frac{\int\limits_{\tilde{A}_n} \varepsilon(n)|\vec{\mathrm{E}}_n|\mathrm{dA} + \mathcal{O}(h^{k+2})}{\int\limits_{L_n} |\vec{\mathrm{E}}_n|\mathrm{ds} + \mathcal{O}(h^{k+1})} = \frac{\bar{\varepsilon}(n)\int\limits_{\tilde{A}_n} \mathrm{dA}}{\int\limits_{L_n} \mathrm{ds}} + \mathcal{O}(h^{k+1}) \\ &\approx \frac{\bar{\varepsilon}(n)|\tilde{A}_n|}{|L_n|} =: M_\varepsilon(n,n) = \frac{\hat{\bar{\mathrm{d}}}_n}{\hat{\mathrm{e}}_n} \end{aligned} \tag{2.51}$$

where $\bar{\varepsilon}(n)$ is an averaged permittivity, h is the maximum length from the primary grid edge lengths and $|\vec{\mathrm{E}}_n|$ is the sample value of the electric field strength $\vec{\mathrm{E}}$ at the center of the grid edge L_n.

The upper index k in (2.51) signifies the convergence order of the FIT approximation. For a staircase discretization, the convergence order is $1 < k < 2$ [29]. An equidistant grid spanned over a computational domain discretized with a homogeneous material allows to achieve the convergence order of 2.

An element $M_\sigma(n,n)$ of the discrete conductivity matrix $\mathbf{M}_\sigma$ obtained by the integration approximation of the ratio of the conduction current density $\vec{\mathrm{J}}_{\mathrm{cond}}$ and the electric field strength is defined as follows:

$$\begin{aligned}\frac{\int\limits_{\tilde{A}_n} \vec{\mathrm{J}}_{\mathrm{cond}} \cdot \mathrm{d}\vec{\mathrm{A}}}{\int\limits_{L_n} \vec{\mathrm{E}} \cdot \mathrm{d}\vec{\mathrm{s}}} &= \frac{\int\limits_{\tilde{A}_n} \sigma(n)|\vec{\mathrm{E}}_n|\mathrm{dA} + \mathcal{O}(h^{k+2})}{\int\limits_{L_n} |\vec{\mathrm{E}}_n|\mathrm{ds} + \mathcal{O}(h^{k+1})} = \frac{\bar{\sigma}(n)\int\limits_{\tilde{A}_n} \mathrm{dA}}{\int\limits_{L_n} \mathrm{ds}} + \mathcal{O}(h^{k+1}) \\ &\approx \frac{\bar{\sigma}(n)|\tilde{A}_n|}{|L_n|} =: M_\sigma(n,n) = \frac{\hat{\bar{\mathrm{j}}}_n}{\hat{\mathrm{e}}_n} \end{aligned} \tag{2.52}$$

with the averaged conductivity $\bar{\sigma}(n)$.

Finally, an element $M_{\mu^{-1}}(n,n)$ of the discrete inverse permeability matrix $\mathbf{M}_{\mu^{-1}}$ is obtained by the integration approximation of the ratio of the magnetic field strength $\vec{\mathrm{H}}$ and the magnetic flux density $\vec{\mathrm{B}}$:

$$\begin{aligned}\frac{\int\limits_{\tilde{L}_n} \vec{\mathrm{H}} \cdot \mathrm{d}\vec{\mathrm{s}}}{\int\limits_{A_n} \vec{\mathrm{B}} \cdot \mathrm{d}\vec{\mathrm{A}}} &= \frac{\int\limits_{\tilde{L}_n} \mu^{-1}(n)|\vec{\mathrm{B}}_n|\mathrm{ds} + \mathcal{O}(h^{k+1})}{\int\limits_{A_n} |\vec{\mathrm{B}}_n|\mathrm{dA} + \mathcal{O}(h^{k+2})} = \frac{\bar{\mu}^{-1}(n)\int\limits_{\tilde{L}_n} \mathrm{ds}}{\int\limits_{A_n} \mathrm{dA}} + \mathcal{O}(h^{k+2}) \\ &\approx \frac{\bar{\mu}^{-1}(n)|\tilde{L}_n|}{|A_n|} =: M_{\mu^{-1}}(n,n) = \frac{\hat{\mathrm{h}}_n}{\hat{\bar{\mathrm{b}}}_n} \end{aligned} \tag{2.53}$$

where $\bar{\mu}^{-1}(n)$ is an inverse averaged permeability and $|\vec{\mathrm{B}}_n|$ is the sample value of the magnetic flux density $\vec{\mathrm{B}}$ at the center of the grid facet A_n.

The material matrices $\mathbf{M}_\varepsilon$, $\mathbf{M}_\sigma$ and $\mathbf{M}_{\mu^{-1}}$ are composed from the entries $M_\varepsilon(n,n)$, $M_\sigma(n,n)$ and $M_{\mu^{-1}}(n,n)$, respectively. They are diagonal matrices in case of isotropic materials and the mutually orthogonal grids since there exist a bijection mapping

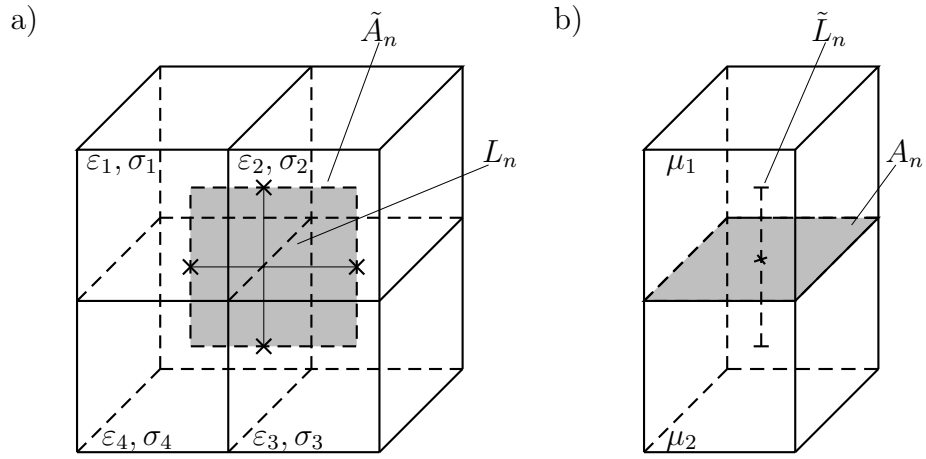

Figure 2.10: Construction of the discrete material matrices: a) the permittivity and the conductivity are averaged over a dual facet $\tilde{A}_n$ containing in the four adjacent primal cells having a common edge L_n; b) the inverse permeability is averaged over a dual edge $\tilde{L}_n$ penetrating two adjacent primal cells having a common facet A_n.

between the grid fluxes and grid voltages. In case of non-orthogonal grids, band structured matrices result. The construction of the material matrices is also possible for anisotropic materials and for materials changing their properties with respect to frequency [29], [30].

The averaged permittivity and conductivity parameters appearing in formula (2.51) and (2.52), respectively, are defined by the averaging process over the dual grid facet $\tilde{A}_n$ contained in the four adjacent primary cells having a common edge L_n (Fig. 2.10a):

$$\begin{aligned}\bar{\varepsilon}_u(n) := \frac{\int\limits_{\tilde{A}_n} \varepsilon(n)\mathrm{dA}}{\int\limits_{\tilde{A}_n} \mathrm{dA}} &= \frac{1}{4\tilde{A}_u(n)}(\varepsilon_u(n-M_v-M_w)A_u(n-M_v-M_w) \\ &+ \varepsilon_u(n-M_w)A_u(n-M_w) \\ &+ \varepsilon_u(n)A_u(n) \\ &+ \varepsilon_u(n-M_v)A_u(n-M_v)), \end{aligned} \tag{2.54}$$

$$\begin{aligned}\bar{\sigma}_u(n) := \frac{\int\limits_{\tilde{A}_n} \sigma(n)\mathrm{dA}}{\int\limits_{\tilde{A}_n} \mathrm{dA}} &= \frac{1}{4\tilde{A}_u(n)}(\sigma_u(n-M_v-M_w)A_u(n-M_v-M_w) \\ &+ \sigma_u(n-M_w)A_u(n-M_w) \\ &+ \sigma_u(n)A_u(n) \\ &+ \sigma_u(n-M_v)A_u(n-M_v)) \end{aligned} \tag{2.55}$$

where $A_u(n - M_v - M_w)$, $A_u(n - M_w)$, $A_u(n)$, $A_u(n - M_v)$ are the areas of primal facets of the four adjacent primal cells having a common edge L_n and containing a dual facet $\tilde{A}_n$, $u = \{x, y, z\}$, $v = \{y, z, x\}$, $w = \{z, x, y\}$.

For the inverse permeability, the averaging process is applied over the dual edge $\tilde{L}_n$ penetrating two adjacent primary cells having a common facet A_n (Fig. 2.10b):

$$\bar{\mu}^{-1}(n) := \frac{\int\limits_{\tilde{L}_n} (1/\mu)\mathrm{ds}}{\int\limits_{\tilde{L}_n} \mathrm{ds}} = \frac{\frac{L_u(n)}{2\mu(n)} + \frac{L_u(n-M_u)}{2\mu(n-M_u)}}{\tilde{L}_u(n)} \tag{2.56}$$

where $\frac{L_u(n)}{2}$ and $\frac{L_u(n-M_u)}{2}$ are the lengths of the two dual edge parts in each primary cell and $u = \{x, y, z\}$.

The averaged material parameters in all three directions (x, y, z) can be collected into the matrices $\mathbf{D}_{\bar{\varepsilon}}$, $\mathbf{D}_{\bar{\sigma}}$ and $\mathbf{D}_{\bar{\mu}^{-1}}$, respectively. The material matrices then read:

$$\mathbf{M}_{\varepsilon} = \tilde{\mathbf{D}}_A \mathbf{D}_{\bar{\varepsilon}} \mathbf{D}_S^{-1} \tag{2.57a}$$
$$\mathbf{M}_{\sigma} = \tilde{\mathbf{D}}_A \mathbf{D}_{\bar{\sigma}} \mathbf{D}_S^{-1} \tag{2.57b}$$
$$\mathbf{M}_{\mu^{-1}} = \tilde{\mathbf{D}}_S \mathbf{D}_{\bar{\mu}^{-1}} \mathbf{D}_A^{-1} \tag{2.57c}$$

where $\mathbf{D}_A$ and $\tilde{\mathbf{D}}_A$ are the diagonal matrices containing the cross-sections of the primary and dual facets, respectively; $\mathbf{D}_S$ and $\tilde{\mathbf{D}}_S$ are the diagonal matrices of the primary and dual edge lengths, respectively.

Finally, on the grid doublet $\{G, \tilde{G}\}$ the discrete material equations are formulated as:

$$\widehat{\widetilde{\mathbf{d}}} = \mathbf{M}_{\varepsilon} \widehat{\mathbf{e}} \tag{2.58a}$$
$$\widehat{\widetilde{\mathbf{j}}} = \mathbf{M}_{\sigma} \widehat{\mathbf{e}} + \widehat{\widetilde{\mathbf{j}}}_{\mathrm{s}} + \widehat{\widetilde{\mathbf{j}}}_{\mathrm{conv}} \tag{2.58b}$$
$$\widehat{\mathbf{h}} = \mathbf{M}_{\mu^{-1}} \widehat{\widetilde{\mathbf{b}}}. \tag{2.58c}$$

where $\widehat{\widetilde{\mathbf{j}}}_{\mathrm{s}}$ and $\widehat{\widetilde{\mathbf{j}}}_{\mathrm{conv}}$ are grid source and convection currents, respectively, located at at the facets of the dual grid.

2.3.4 Quasistatic Formulations Discretized by the FIT

To derive an electroquasistatic FIT formulation one uses the grid potentials introduced earlier as

$$\widehat{\mathbf{e}} = -\mathbf{G}\phi.$$

With the help of this notation, the continuous electroquasistatic formulation (2.35a) is transferred into its discrete FIT analog [31]

$$-\widetilde{\mathbf{S}}\mathbf{M}_{\varepsilon}\mathbf{G}\frac{\mathrm{d}\phi}{\mathrm{d}t} - \widetilde{\mathbf{S}}\mathbf{M}_{\sigma}\mathbf{G}\phi = 0 \tag{2.59}$$

where the conductivity matrix $\mathbf{M}_\sigma$ may be a function of the electric field intensity, i.e., $\mathbf{M}_\sigma = \mathbf{M}_\sigma(\mathbf{G}\phi)$. System (2.59) represents a stiff system of ordinary differential equations whose solution is unequivocally defined if at least one grid potential is supplied with a prescribed value. Since the determination of the grid potentials usually takes place on the boundaries of the computational domain, they are referred to as *boundary conditions* (BCs).

Magnetoquasistatic FIT formulation [31] which is in the focus of the present treatise starts with the introduction of the magnetic vector potential (MVP) $\widehat{\mathbf{a}}$ defined by $\mathbf{C}\widehat{\mathbf{a}} = \widehat{\widehat{\mathbf{b}}}$. Then the electric grid voltages are:

$$\widehat{\mathbf{e}} = -\frac{\mathrm{d}}{\mathrm{d}t}\widehat{\mathbf{a}} \,. \tag{2.60}$$

In terms of these primary variables, a magnetoquasistatic formulation for slowly varying transient fields can be formulated as a system of first order differential equations

$$\widetilde{\mathbf{C}}\mathbf{M}_{\mu^{-1}}\mathbf{C}\widehat{\mathbf{a}}(t) + \mathbf{M}_\sigma \frac{\mathrm{d}}{\mathrm{d}t}\widehat{\mathbf{a}}(t) = \widehat{\widehat{\mathbf{j}}}_s(t) \tag{2.61}$$

subjected to a consistent initial solution vector $\widehat{\mathbf{a}}_0 := \widehat{\mathbf{a}}(t_0)$. The specified right-hand-side vector $\widehat{\widehat{\mathbf{j}}}_s(t)$ should be a divergence-free, i.e., $\widetilde{\mathbf{S}}\widehat{\widehat{\mathbf{j}}}_s(t) = 0$ has to be fulfilled.

The diagonal conductivity matrix is singular if non-conductive areas are present in the computational domain. Consequently, an index 1 differential-algebraic system of equations of form (2.61) has to be solved. Note additionally that in case of the whole absence of the conductive materials in the computational domain, equation (2.61) reduces to a magnetostatic vector potential formulation [31]:

$$\widetilde{\mathbf{C}}\mathbf{M}_{\mu^{-1}}\mathbf{C}\widehat{\mathbf{a}} = \widehat{\widehat{\mathbf{j}}}_s. \tag{2.62}$$

2.3.5 Boundary Conditions

A boundary condition (BC) is used to specify the field behavior on the surfaces of the design model. Each of the surfaces can have its own unique BC assigned or multiply adjoining surfaces can share the same BCs. In practical applications, it is also possible that the constrained surfaces are not necessarily located at the geometrical borders of the computational domain, as can be illustrated by, e.g., a capacitor model where the voltages are applied at the electrodes inside the model. These constraints are implemented, however, following the technique elaborated for the implementation of the real BCs [32].

Two main types of BCs are in the focus of the present work [32]:

Electric BCs ("flux walls", "current gate"). If this type of BCs is applied, the tangential component of the electric field strength vanishes on the boundary, i.e., $\vec{\mathrm{E}} \times \vec{\mathrm{a}}_\mathrm{n} = 0$ holds. This corresponds to the assumption that the electric conductivity is infinite at the boundary. For magnetic vector potential formulation used in this work, electric BCs are represented by Dirichlet BCs and correspond to the elimination of the normal component of $\vec{\mathrm{B}}$ field, i.e., $\vec{\mathrm{B}} \cdot \vec{\mathrm{a}}_\mathrm{n} = 0$.

Magnetic BCs ("flux gate", "current wall"). If this type of BCs is applied, the tangential component of the magnetic field strength vanishes on the boundary, i.e., $\vec{\mathrm{H}} \times \vec{\mathrm{a}}_{\mathrm{n}} = 0$ holds. This corresponds to the perfectly permeable material, i.e., $\mu \rightarrow \infty$. For magnetic vector potential formulation, magnetic BCs are represented by homogeneous Neumann BCs.

2.4 Electrical Circuit Simulations

A third corner stone of a field-circuit coupled formulation is the theory of the electrical circuits that is briefly discussed in the present section. In the first subsection, fundamental notions typical for electrical circuit theory are given and basic circuit elements are enumerated together with their corresponding properties. In the next subsection, we discuss the laws governing the behavior of the circuit elements and those of the electrical circuits. The third subsection is devoted to the description of the switching circuit elements and their main characteristics.

2.4.1 Definitions and Basic Network Elements

Electrical networks are energy or signal/information processors consisting of interconnections of simple circuit elements or devices. If a network contains at least one closed path, it is called a *circuit*. The processing of energy or information takes place through various time signals called *voltages* and *currents*. The circuit elements called *sources* generate a voltage or a current that in their turn represent some type of information. The interconnection of circuit elements produces from this input signal a new voltage or current response. It is important to differentiate between the physical device itself and its mathematical model used to analyze its behavior in a circuit. In this work, the expression "circuit element" is referred to the mathematical model.

One distinguishes between a *general circuit element* and a *simple circuit element*. The first one is composed of more than one simple circuit elements, but a simple circuit element cannot be further subdivided into other simple circuit elements. In the notation that follows the term "circuit element" always refers to a simple circuit element [33], [34].

A simple circuit element is a mathematical model of a two-terminal electrical device. It can be completely characterized by its voltage-current relations but cannot be subdivided into other two-terminal devices. For practical reasons, only interconnections of *lumped* circuit elements. i.e., circuits whose physical dimensions are far smaller than the wavelengths of the signals that excite them, are considered in the present treatise [34].

An *ideal voltage source* is characterized by a terminal voltage which is independent of the current flowing through it. The graphical representation of an ideal voltage source is given in Fig. 2.11a. An ideal voltage source which is characterized with a constant terminal voltage is often called an ideal d-c voltage source. This

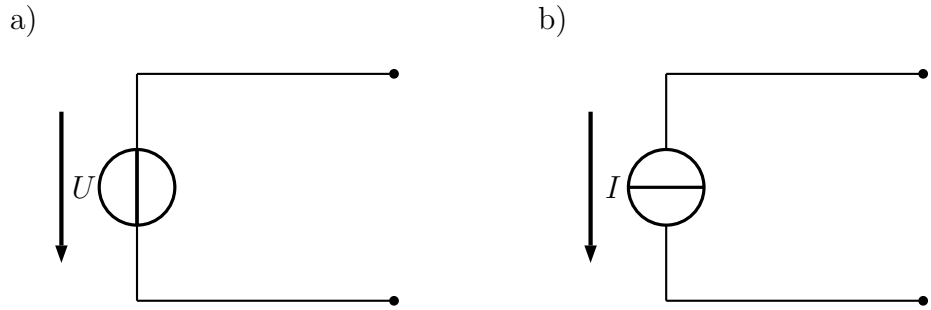

Figure 2.11: The graphical representation of (a) an ideal voltage source and (b) an ideal current source.

model source does not represent exactly any real physical device, since it could then theoretically deliver an infinite amount of energy from its terminal, which is impossible. However, an ideal voltage source gives a reasonable approximation to several practical voltage sources [34].

Another ideal source element is an *ideal current source*. Here the current through such an element is independent on the voltage across it. The graphical symbol used to represent an ideal current source in the electrical circuits is given in Fig. 2.11b. An ideal current source characterised with a constant value of the supplied current is called a d-c source. Analogously to the ideal voltage source, the ideal current source is a reasonable approximation for a real physical current source device.

Both of these sources are *active* elements, i.e., they are capable of delivering power to some external device. A network which contains at least one active element, such as a voltage or current source, is called an *active network*. *Passive* circuit elements are not capable of delivering energy. A network that does not contain any active sources is called a *passive network*.

In order to introduce the basic circuit elements, such important notions as electrical power and energy have to be determined. The *electrical power* is defined as a product of applied voltage u and resulting current i, i.e.,

$$p(t) = u(t)\, i(t). \tag{2.63}$$

When $p(t)$ has a negative value at some time instant t it means that at this time instant the source transfers energy to the circuit. Since the power p is defined as the time rate of energy transfer, i.e., $p = \frac{\partial w}{\partial t}$, then

$$W = \int_{t_1}^{t_2} p(t)\; dt \tag{2.64}$$

where W is the *energy* transferred during the time interval $[t_1, t_2]$.

When electrical energy is transferred to a circuit element, it reacts in one of the following three ways. If the energy is consumed, the circuit element is a pure *resistor*. If the energy is stored in a magnetic field, the circuit element is a pure *inductor*.

Finally, if the energy is stored in an electric field, the circuit element is a *capacitor*. Practical circuit devices exhibit naturally more than one of the above given behaviors and often all three at the same time, but one may be predominant. For instance, a coil may be designed to have a high inductance, but the wire with which it is wound has some resistance; hence the coil features both of the mentioned behaviors [35].

A resistor is a device that impedes the flow of current. Additionally, resistors are a good approximate model for a wide variety of technical devices, such as light bulbs and heating elements in ovens. For a linear resistor, the potential difference $u(t)$ across its terminals is directly proportional to the current $i(t)$ in it. The constant of proportionality R in Ohm is called the *resistance* of the resistor and it is a measure of the ability of the device to impede the current flow [33], [36]. Thus, one can write:

$$u(t) = R\, i(t) \tag{2.65a}$$

which has the equivalent formulation

$$i(t) = \frac{u(t)}{R}. \tag{2.65b}$$

In equation (2.65b), the proportionality constant is the reciprocal of R, i.e., $G = 1/R$, which is the *conductance* of the device. A device having a zero resistance, i.e., $R = 0$, is said to be a *short circuit*. Consequently, a short circuit has infinite conductance. Alternatively, a device or wire characterized with an infinite resistance (and hence having a zero conductance) is operated as an *open circuit*.

No restrictions are to be placed on the functions $u(t)$ and $i(t)$. They may be constant time functions, e.g., in case of d-c circuits, or they can exhibit sinusoidal behavior.

Equation (2.65a) has a fundamental meaning, since it represents a mathematical expression of Ohm's law for electrical networks that it is fulfilled under any circumstances. As an aid in writing the correct $u - i$ relationship for a resistor, Ohm's law is stated in words as follows:

For a resistor connected between terminals A and B, the voltage drop from A to B is equal to the resistance multiplied by the current flowing from A to B through the resistor.

Once the voltage and current associated with a resistor are known, the power absorbed by the resistor can be easily calculated [33]:

$$p(t) = u(t)\, i(t) = i^2(t)\, R = \frac{u^2(t)}{R} \tag{2.66}$$

which reduces to

$$P = UI = I^2 R = \frac{U^2}{R}$$

for the d-c case.

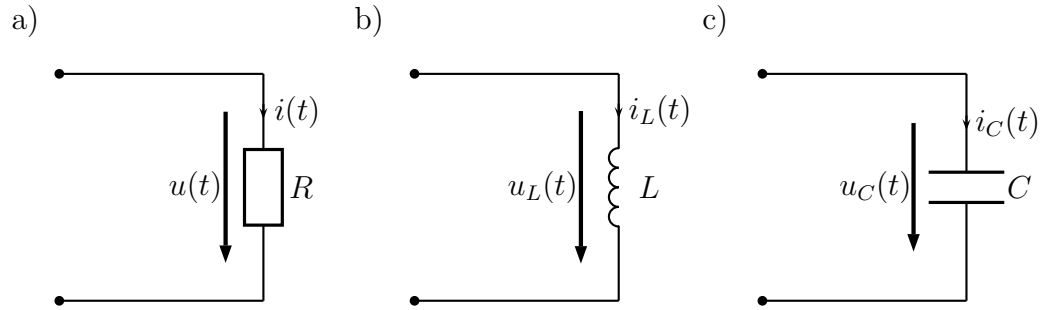

Figure 2.12: Basic network elements: (a) resistor, (b) inductor and (c) capacitor.

Equation (2.66) signifies a very important property of a resistor. Unlike other circuit elements which can store energy at one moment and return energy at another, a resistor always absorbs energy.

Fig. 2.12a shows the standard symbol for a resistor.

The linear inductor, symbolized by a coiled wire shown in Fig. 2.12b, is a two-terminal energy storage device whose voltage is proportional to the derivative of the current passing through it. The constant of proportionality, denoted by L, is called the *inductance* of the coil and is measured in Henry. The specific voltage-current relation of the linear inductor is given by

$$u_L(t) = L\,\frac{\mathrm{d}i_L(t)}{\mathrm{d}t}. \tag{2.67}$$

Physical configuration of an inductor influences the inductance value L. A segment of wire, e.g., has a rather negligible inductance. The inductance value increases significantly if the same wire is twisted in a coil. Because of this phenomenon, an inductor is often called a coil, which gave rise to the symbol specified in Fig. 2.12b [34].

Equation (2.67) contains an integral relationship:

$$i_L(t) = i_L(t_0) + \frac{1}{L}\int_{t_0}^{t} u_L(\tau)\mathrm{d}\tau. \tag{2.68}$$

The time t_0 can represent any time instant but is often used for characteristic values, e.g., when a switch is thrown or a source excitation is activated. The quantity $i_L(t_0)$ identifies the initial current thought the inductor at time instant t_0.

Equation (2.68) allows to derive the *continuity property of the inductor* [34]:

If the voltage $u_L(t)$ across an inductor is bounded over the time interval $t_1 \leq t \leq t_2$, then the current through the inductor is continuous for $t_1 < t < t_2$.

In particular, if $t_1 < t_0 < t_2$, then $i_L(t_0^-) = i_L(t_0^+)$, even when $u_L(t_0^-) \neq u_L(t_0^+)$. The notation $-$ and $+$ is used to designate the time instants directly before t_0 and directly after t_0, respectively, as shown schematically in Fig. 2.13 [34].

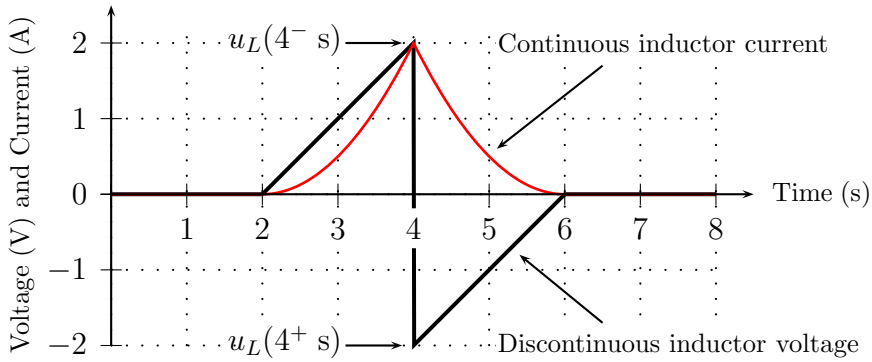

Figure 2.13: Continuity property of an inductor ($L = 1$ H): a possible discontinuous voltage $u_L(t)$ appearing across an inductor and the resulting continuous inductor current $i_L(t)$. Function $u_L(t)$ has a discontinuity point at $t_0 = 4$ s. The value $u_L(4^+\text{ s})$ is the limiting value of $u_L(t)$ when approaching t_0 from the right, whereas $u_L(4^-\text{ s})$ is a limiting value of $u_L(t)$ when approaching t_0 from the left [34].

The net energy $W_L(t_0, t_1)$ stored in the magnetic field surrounding the inductor within the time interval $[t_0, t_1]$ is

$$\begin{aligned} W_L(t_0, t_1) &= L \int_{t_0}^{t_1} \left(i_L(\tau) \frac{\mathrm{d}i_L(\tau)}{\mathrm{d}\tau} \right) \mathrm{d}\tau = L \int_{i_L(t_0)}^{i_L(t_1)} i_L \, \mathrm{d}i_L \\ &= \frac{1}{2} L \left(i_L^2(t_1) - i_L^2(t_0) \right). \end{aligned} \tag{2.69}$$

Equation (2.69) means that the energy stored in the inductor within the time interval $[t_0, t_1]$ depends only on the current flowing through the inductor at time instants t_0 and t_1, i.e., it is independent on the particular current waveform between t_0 and t_1. For the periodic waveform current, i.e., if $i_L(t) - i_L(t + T)$ for some $T > 0$ and all t, the value of the stored energy over any period T is obviously zero, since $i_L(t_0 + T) = i_L(t_1) = i_L(t_0)$. Further more, the energy stored by the inductor over the part of the cycle of positive power is delivered back to the circuit over the portion of the cycle when the power is negative. This property holds for any periodic signals over any period. Since no energy is dissipated, i.e., the energy is only stored and returned to the circuit, the inductor is said to be a *lossless* device [34].

The instantaneous energy stored in an inductor is

$$W_L(t) = \frac{1}{2} L \, i_L^2(t). \tag{2.70}$$

The capacitor, depicted in Fig. 2.12c, is also a two-terminal energy storing device characterized with the following voltage-current differential relation

$$i_C(t) = C \, \frac{\mathrm{d}u_c(t)}{\mathrm{d}t} \tag{2.71}$$

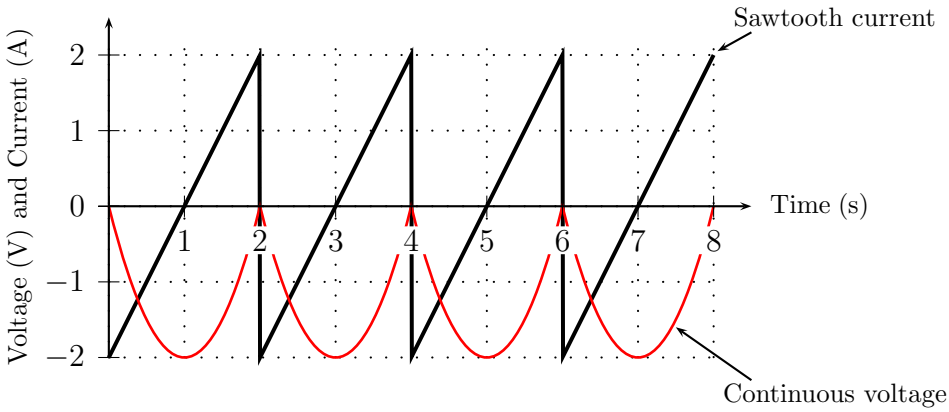

Figure 2.14: Continuity property of a capacitor ($C = 0.5$ F): Sawtooth driving current waveform and a continuous voltage response [34].

where C denotes *capacitance* measured in Farad. The capacitance quantifies the capacitor's ability to store energy in an electric field.

The integral form of (2.71) reads:

$$u_C(t) = u_C(t_0) + \frac{1}{C}\int_{t_0}^{t} i_C(\tau)\,\mathrm{d}\tau \tag{2.72}$$

where t_0 can represent any time instant but is often used for characteristic values, e.g., when a switch is thrown or a source excitation is activated. The quantity $u_C(t_0)$ represents the initial voltage across the capacitor at t_0.

Equation (2.72) allows to derive the *continuity property of the capacitor* [34]:

If the current $i_C(t)$ through a capacitor is bounded over the time interval $t_1 \leq t \leq t_2$, then the voltage across the capacitor is continuous for $t_1 < t < t_2$.

In particular, if $t_1 < t_0 < t_2$, then $u_C(t_0^-) = u_C(t_0^+)$, even when $i_C(t_0^-) \neq i_C(t_0^+)$ as shown in Fig. 2.14 [34].

A physical interpretation of equation (2.72) reveals another basic property of a capacitor. The positive and negative charges stored on the top and bottom capacitor plates separated by a dialectic insulating material produce a voltage drop $u_C(t)$ from the top plate to the bottom plate. For a linear capacitor, the value of the $u_C(t)$ is proportional to the charge $q(t)$ stored on its plates. The proportionality constant is the capacitance C, i.e.,

$$q(t) = C\,u_C(t). \tag{2.73}$$

Thus, equation (2.72) has the following physical interpretation: the first term $u_C(t_0)$ represents the capacitor voltage at t_0 and is therefore related to a given initial charge. The integral in the second term determines the additional charge transferred to the capacitor during the time interval (t_0, t). Dividing this by C gives the additional

voltage attained by the capacitor during (t_0, t). Therefore, the sum of these two terms is the voltage of the capacitor at time instant t [34].

As for all devices, the energy stored or utilized in a capacitor is defined by the integration of the power absorbed by the capacitor. The net energy entering the capacitor over the time interval $[t_0, t_1]$ is

$$\begin{aligned} W_C(t_0, t_1) &= \int_{t_0}^{t_1} u_C(\tau)\, i_C(\tau)\, \mathrm{d}\tau = C \int_{t_0}^{t_1} u_C(\tau)\, \frac{\mathrm{d}u_C(\tau)}{\mathrm{d}\tau}\, \mathrm{d}\tau \\ &= C \int_{u_C(t_0)}^{u_C(t_1)} u_C\, \mathrm{d}u_C = \frac{1}{2} C \left(u_C^2(t_1) - u_C^2(t_0) \right). \end{aligned} \tag{2.74}$$

The value of the energy is thus completely specified by the value of the capacitor voltage at times t_0 and t_1. This means that the change in the stored energy is independent on the particular waveform in time interval $[t_0, t_1]$. For the periodic voltage waveform, i.e., if $u_C(t) = u_C(t + T)$ for some $T > 0$ and all t, the change in the stored energy in the capacitor over any period of time T is zero, since $u_C(t_0{+}T) = u_C(t_1) = u_c(t_0)$ [34]. The instantaneous energy stored in a capacitor is

$$W_C(t) = \frac{1}{2} C u_C^2(t). \tag{2.75}$$

Finally, all linear circuit elements are introduced and a summary of the circuit response of single circuit elements is given in Tab. 2.3 below [35].

Element	**Voltage across element**	**Current in element**
Resistance R	$u(t) = R\, i(t)$	$i(t) = \frac{1}{R}\, u(t)$
Inductance L	$u(t) = L\, \frac{\mathrm{d}i(t)}{\mathrm{d}t}$	$i(t) = \frac{1}{L} \int u(t) \mathrm{d}t$
Capacitance C	$u(t) = \frac{1}{C} \int i(t) \mathrm{d}t$	$i(t) = C\, \frac{\mathrm{d}u(t)}{\mathrm{d}t}$

Table 2.3: Circuit response of single elements [35].

2.4.2 Kirchhoff's Current Law

Fig. 2.15a represents a *series circuit* consisting of a sequential connection of two-terminal circuit elements. An important property of a series connection is that all two-terminal elements carry the same current. Fig. 2.15b shows a *parallel circuit* in which the top terminals of each circuit element are wired together, as are the

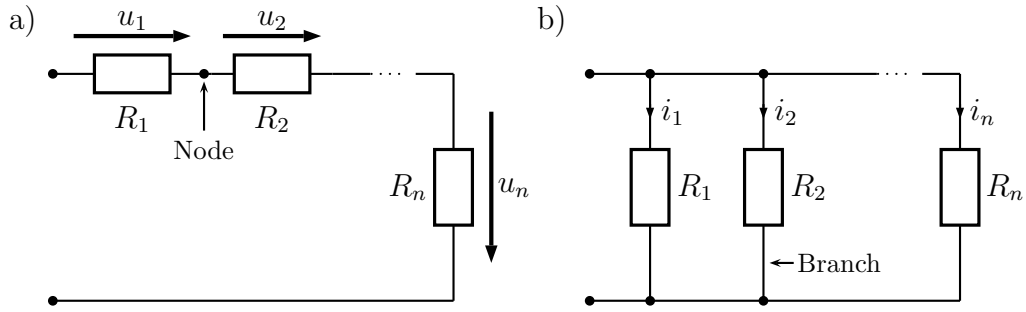

Figure 2.15: Interconnection of lumped circuit elements [34]: (a) a series circuit consisting of a sequential connection of two-terminal circuit elements and (b) a parallel circuit where the top terminals of each element are wired together, as are the bottom terminals. In each figure, a representative circuit branch and node is marked.

bottom terminals. An important property of parallel circuits is that each of the circuit elements has the same voltage across it [34].

According to Fig. 2.15, a *branch* of a circuit is simply a two-terminal circuit element whereas a *node* is a point of connection of two or more circuit elements (branches) [34]. These two notions are necessary to discuss in the present and subsequent sections of the treatise two fundamental laws of circuit theory, the *Kirchhoff's current law* (KCL) and the *Kirchhoff's voltage law* (KVL), which govern the distribution of current and voltages in a circuit.

Imagine a number of branches connected at a given node, as in node A of Fig. 2.16a. A reference direction of the current through each branch is indicated by an arrow. If the arrow points toward the node, the current is entering; if the arrow points away from the node, the current is leaving. If a current is referenced as leaving a node, then the negative of the current enters the node and conversely [34].

The KCL states that the sum of currents entering a node is equal to the sum of the currents leaving the node.

Since the charge is neither created nor destroyed, the charge transported into a node must equal the charge leaving the node because no charge can be accumulated there. Thus, the KCL expresses this conservation law in terms of branch currents [34].

Two corollaries of the KCL are of immediate interest. First, being a general rule, the KCL implies that current sources with different currents cannot be connected in series. A second consequence of the KCL is that a current source supplying zero current is equivalent to an open circuit. This means, that a current source has an *infinite internal resistance* [34]. The KCL holds regardless of the type of lumped two-terminal device represented by each branch of the circuit. This is true because the KCL determines how branch currents interact at nodes regardless of the type of lumped element connected to the node [34]. The graphical representation of the KCL is given in Fig. 2.16a.

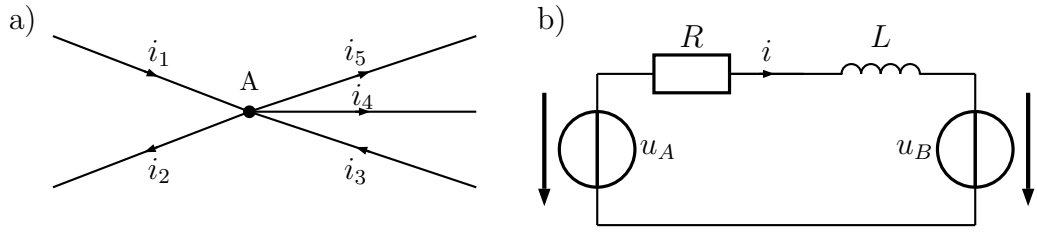

$$i_1 + i_3 = i_2 + i_4 + i_5$$
or
$$i_1 + i_3 - i_2 - i_4 - i_5 = 0$$

$$u_A - u_B = R\,i + L(\mathrm{d}i/\mathrm{d}t)$$
or
$$u_A - u_B - R\,i - L(\mathrm{d}i/\mathrm{d}t) = 0$$

Figure 2.16: Graphical representation of Kirchhoff's laws [35]: (a) KCL: the sum of the currents entering the node is equal to the sum of the currents leaving the node; (b) KVL: the sum of the potential rises in a loop is equal to the sum of the potential drops in it.

2.4.3 Kirchhoff's Voltage Law

The Kirchhoff's voltage law (KVL) determines how voltages distribute across the elements of a circuit. The notion of a *closed path* or a *loop* in a circuit is needed to formulate the KVL. With these terms one determines a connection of two-terminal elements that ends on the node where it began.

The KVL states that for lumped circuits, the algebraic sum of the voltage drops around any closed path or loop is zero at every time instant [34].

Two corollaries of the KVL are of immediate interest. First, being a general rule, the KVL implies that two voltage sources of different voltages, i.e., $u_1(t) \neq u_2(t)$, cannot be connected in parallel. Such a connection would violate the KVL, which requires that $u_1(t) = u_2(t)$ for a parallel connection. A second consequence of the KVL is that a voltage source supplying a zero voltage for all possible values of current through the source is equivalent to a short circuit. Thus, one can conclude that the *internal resistance* of a voltage source is zero [34]. Finally, we note that the KVL holds for all closed node sequences regardless of the lumped devices represented by each branch of the connected circuit. The graphical representation of the KVL is given in Fig. 2.16b.

2.4.4 Switching Circuit Elements

A lot of electrical phenomena can prohibit the proper work of the electrical circuits or even damage them. Reversing the polarity of the battery during its installation into a portable electronic equipment, high-voltage transients due to lightning or the effects of turning-on and turning-off of other electrical devices may enter the electrical circuits leading to an improper functioning or to a breakdown [34].

In this part of the work we discuss the devices that protect against both voltage reversal and over-voltage (electrical surges). These devices are called *diodes* [34]. In

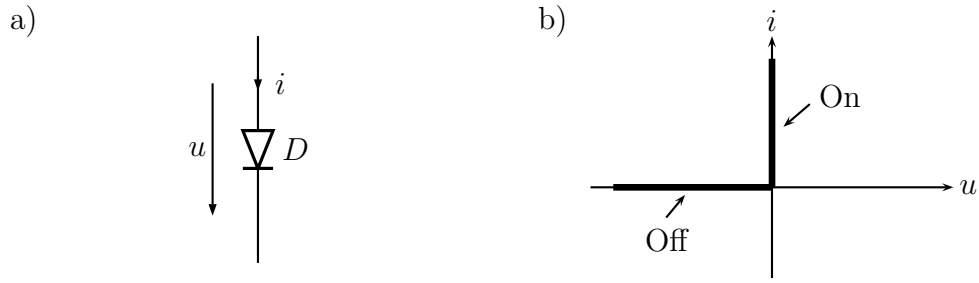

Figure 2.17: (a) Graphical symbol for an ideal diode; (b) voltage-current characteristic curve of an ideal diode [34].

this part of the work an *ideal diode* as a basic element of circuit analysis is introduced and its mathematical model is defined.

An ideal diode can be viewed as an electrically controlled *switch*. The essential property of a switch is as follows: when closed, an ideal switch behaves like a short circuit; when open, an ideal switch behaves like an open circuit. The presence of the switches does not alter the essential linear nature of the circuit [34].

A diode is a device similar to a switch and it is often in use in electronic circuits. A practical diode is a two-terminal element featuring a nonlinear characteristics and allowing current to pass much more easily in one direction than the other. Nowadays, diodes are mainly semiconductor devices produced of silicon or germanium [34].

A symbol for an ideal diode used in this work and its idealized $u-i$ curve are shown in Fig. 2.17. When the current i is positive, a diode is said to be *forward biased*. In this state, the diode behaves as a short circuit. A negative voltage presupposes a *reverse biased* state of a diode which corresponds to an open circuit since $i = 0$. Thus, an ideal diode has two main operation states, referred to by various equivalent nomenclatures:

1. forward biased, on, closed, or conducting
2. reverse biased, off, open, or nonconducting.

This terminology emphasizes an ideal diode's use as a switching element. There is a boundary state bordering the open and closed operating states of the diode called the *break point* [34].

It is convenient to characterize an ideal diode with the following set of equation:

$$i > 0,\ u = 0 \quad \text{(forward biased)} \tag{2.76a}$$

$$u < 0,\ i = 0 \quad \text{(reverse biased)} \tag{2.76b}$$

$$u = 0,\ i = 0 \quad \text{(break point).} \tag{2.76c}$$

A real diode may be approximately represented as an ideal diode in series with and/or in parallel with other circuit elements. Fig. 2.18 represents three increasingly

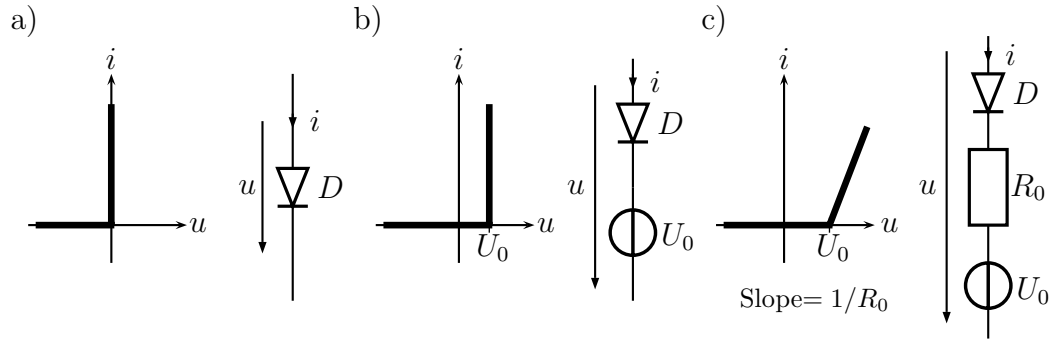

Figure 2.18: Three increasingly accurate models of a real diode [34].

more accurate models of a real diode. As one can conclude from the illustrations, the better approximation is achieved due to a more complicated circuit model [34].

The break point voltage U_0 appearing in the diode models of Fig. 2.18 is called the *cut-in voltage* or *threshold voltage*. This circuit parameter averages 0.6 V for silicon and 0.3 V for germanium diodes and also depends on the operating temperature of the diode. Starting at room temperature of 25°C, the value of U_0 increases by 2.3 mV for each 1°C decrease. When the effect of R_0 should be taken into account to obtain a good agreement between simulated and measured data, a model of Fig. 2.18c is used. The value of R_0 is typically less than 100 Ω [34].

When any of the diode models presented in Fig. 2.18 is used in praxis, the circuit to be considered is no longer a linear circuit. However, every diode at any time instant can be characterised by only one of the three possible states: on, off, or at the break point. Knowledge of these states then allows the replacement of each diode by a short circuit or an open circuit, respectively. The resulting circuit is thus linear and the governing laws discussed in the previous part can be applied. However, since the diode states are determined by inspection, it is necessary to have a checking algorithm able to verify that the assumed diode state is in fact correct. In the later parts of the treatise, such an algorithm is proposed for the numerical simulation of field-circuit coupled systems including switching elements.

Another switching circuit element is an electrical switch. A pair of contacts of the switch is closed if there is no space between them allowing the electrical current to flow from one side to the other. When the contacts are separated by a space, they are opened and no current can flow. The time periods of the open and closed phases of the switch functioning are defined a priory and no checking algorithm mentioned above is required.

Chapter 3

Coupled Field-Circuit Transient Formulation

3.1 Introduction

As the notion "field-circuit" presupposes, electromagnetic field theory and linear circuit analysis are essential. They were presented in the previous chapter of the treatise and are used in the present one to derive a field-circuit transient coupled formulation.

The derivation of a coupled formulation unfolds from a definition of the *topology* of the network and establishing its topological properties. The corresponding discussion is given in section 3.2. In section 3.3, several conductor models are considered. Finally, in section 3.4 a transient field-circuit coupled formulation is derived.

3.2 External Circuit Description

3.2.1 Network Topology

Any lumped network obeys three laws: the KCL, the KVL and the elements' law, i.e., branch voltage-current characteristics. The first two laws, KCL and KVL, introduced in the previous part of the work, are linear algebraic constraints on branch voltages and currents. They depend only on the interconnection of branches and are independent of the branch characteristics.

A large class of lumped networks, both linear and nonlinear, can be modeled as an interconnection of two-terminal elements with specified element characteristics [37]. A complete description of the network model must supply us with the following information:

1. How the branches are connected.
2. The reference directions for branch currents and voltages.

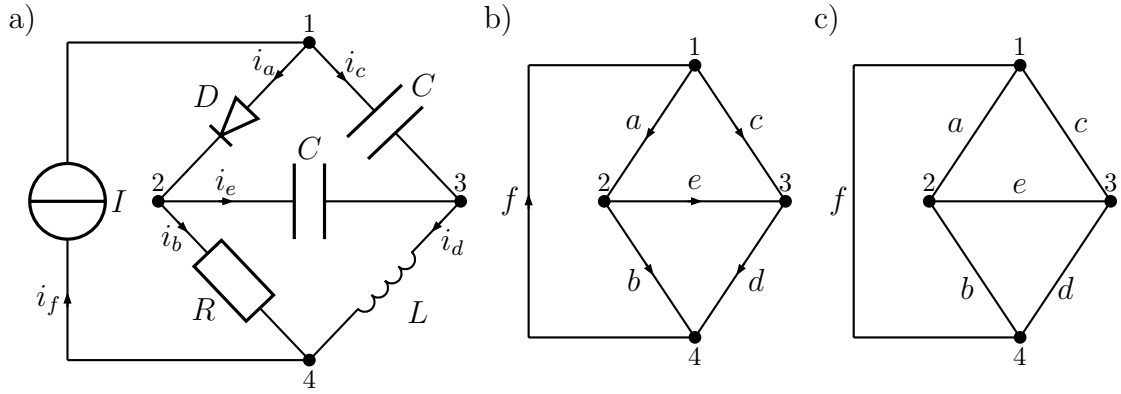

Figure 3.1: Network (a) and its associated directed (b) and undirected (c) graph.

3. The branch characteristics.

Naturally, to depict two items, say 1 and 2, one has to draw a *directed graph* G_d associated with the given network N according to the following rules: each two-terminal element of the network is replaced by a branch with an arrow showing in the same direction as the assumed positive current through that branch. The same arrows can be used for the branch voltage references, such that the positive voltage terminal is assumed to be at the tail of the arrow. Thus, the directed graph G_d provides us with the complete information for items 1 and 2. For instance, Fig. 3.1a,b depicts a network and its associated directed graph.

When the reference direction of the branch voltages and currents is not of interest, all the arrows in G_d may be removed. The resulting simplified graph G_n is called the *indirected* or the *nonoriented* graph (Fig. 3.1c).

Before we proceed further, some basic definitions of the network topology have to be introduced. A set of branches $b_1, b_2, \ldots, b_n$ in G_n is called a *path* between two nodes V_j and V_k if the branches can be labeled such that

1. Two consecutive branches b_i and b_{i+1} always have a common endpoint.
2. No node in G_n is the endpoint of more then two branches in the set.
3. V_j is the endpoint of exactly one branch in the set, and so is V_k.

An undirected graph G_n is said to be *connected* if there exists a path between any two nodes of the graph. A subgraph G_s of a graph G_n is a *loop* if

1. G_s is connected.
2. Every node of G_s has exactly two branches of G_s incident to this node.

A subgraph G_s of a connected graph G_n is called a *tree* if

1. G_s is connected.
2. G_s contains all nodes of G_n.

3. G_s has no loops.

The branches that belong to a tree T are called *tree branches* or *twigs*. Those branches that do no belong to a tree T are called *links* or *chords*. All the links of a given tree T form a *cotree* T_c with respect to the tree T.

If a connected graph G_n has n nodes, than any of its tree T has exactly $n-1$ branches.

A set of branches of a connected graph G_n forms a *cutset* in a graph if

1. The removal of the set of branches (but not their endpoints) results in a graph that is not connected.
2. After the removal of the set of branches, the restoration of any one branch from the set will result in a connected graph again.

The concepts of path, loop, cutset, tree and cotree are fundamental in the analysis of lumped networks. Loops are subgraphs to which we apply the KVL and the cutsets are subgraphs to which we apply the KCL.

The information contained in the directed graph G_d has to be stored in a form suitable for a subsequent usage on a digital computer. Such a storage scheme can be realized via a *node-branch incidence matrix*. For a directed graph G_d with n nodes and b branches, the incidence matrix is an $n \times b$ matrix $\mathbf{A} = [a_{ij}]$ whose entries are defined as follows:

$a_{ij} = 1$	if branch j is incident at node i, and the arrow is pointing away from node i,
$a_{ij} = -1$	if branch j is incident at node i, and the arrow is pointing toward node i,
$a_{ij} = 0$	if branch j is not incident at node i.

For example, for the directed graph given in Fig. 3.1b the incidence matrix A reads:

$$\mathbf{A} = \begin{array}{c} \\ \text{Node } 1 \\ 2 \\ 3 \\ 4 \end{array} \begin{array}{c} \begin{array}{cccccc} a & b & c & d & e & f \end{array} \\ \left[\begin{array}{cccccc} 1 & 0 & 1 & 0 & 0 & -1 \\ -1 & 1 & 0 & 0 & 1 & 0 \\ 0 & 0 & -1 & 1 & -1 & 0 \\ 0 & -1 & 0 & -1 & 0 & 1 \end{array}\right] \end{array} \begin{array}{c} \text{incident branches} \\ \text{(acf)} \\ \text{(abe)} \\ \text{(cde)} \\ \text{(bdf)} \end{array} \tag{3.1}$$

For directed graphs without self-loops,[1] every branch is connected to two distinct nodes. As a consequence, every column of the incidence matrix $\mathbf{A}$ has exactly two nonzero elements, namely -1 and 1, with the rest being zeroes. It follows that a single row of $\mathbf{A}$ matrix can be deleted without loosing information: it can always be restored by observing the rule that every column of an incident matrix adds up to zero. A matrix obtained from $\mathbf{A}$ by deleting any single row is called a *reduced incidence matrix*.

[1] A branch is called a *self-loop* if the two endpoints of the branch are the same.

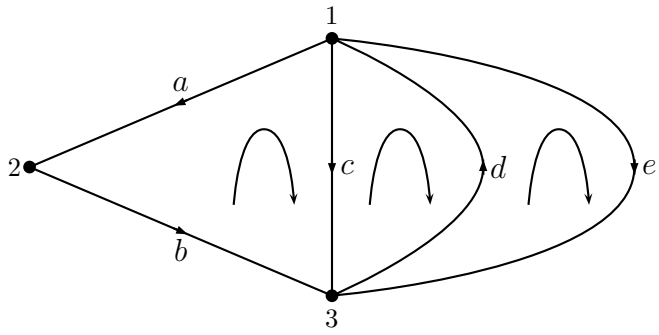

Figure 3.2: Construction of a loop matrix for a directed graph [37].

When the branch currents are collected together into a column vector $\mathbf{i}(t)$ having a dimension $b \times 1$, the KCL, applied to all nodes, is expressed compactly by the matrix equation:

$$\mathbf{A}\mathbf{i} = \mathbf{0}. \tag{3.2}$$

To be able to express the KVL in a compact form, another matrix - the *loop matrix* - is introduced. For a directed graph G_d with b branches and n_l oriented loops, the elements of this $n_l \times b$ matrix $\mathbf{B}_a = [b_{ij}]$ are defined as follows:

$b_{ij} = 1$	if branch j is in loop i, and their directions agree,
$b_{ij} = -1$	if branch j is in loop i, and their directions oppose,
$b_{ij} = 0$	if branch j is not in loop i.

For the directed graph given in Fig. 3.2 the loop matrix $\mathbf{B}_a$ reads:

$$\mathbf{B}_a = \begin{array}{c} \\ \text{Loop} \\ \\ \\ \\ \\ \\ \end{array} \begin{array}{c} \\ 1 \\ 2 \\ 3 \\ 4 \\ 5 \\ 6 \end{array} \begin{array}{c} \begin{array}{ccccc} a & b & c & d & e \end{array} \\ \left[\begin{array}{ccccc} -1 & -1 & 1 & 0 & 0 \\ 0 & 0 & -1 & -1 & 0 \\ 0 & 0 & 0 & 1 & 1 \\ -1 & -1 & 0 & -1 & 0 \\ -1 & -1 & 0 & 0 & 1 \\ 0 & 0 & -1 & 0 & 1 \end{array}\right] \end{array} \begin{array}{c} \text{branches in the loop} \\ \text{(abc)} \\ \text{(cd)} \\ \text{(de)} \\ \text{(abd)} \\ \text{(abe)} \\ \text{(ce)} \end{array} \tag{3.3}$$

If the branch voltages are collected into the $b \times 1$ column vector $\mathbf{u}(t)$ such that rows of $\mathbf{u}$ are in the same branch order as the columns of $\mathbf{B}_a$, then the KVL applied to all loops is expressed compactly by

$$\mathbf{B}_a\mathbf{u} = \mathbf{0}. \tag{3.4}$$

When written in a scalar form, system (3.4) leads to a system of n_l equations. However, in circuit analysis, we do not need all these n_l equations. Any maximum independent set of equations will suffice. Thus, a more useful submatrix of $\mathbf{B}_a$ can

be extracted. Actually, any submatrix of $\mathbf{B}_a$ that consists of the maximum number of linearly independent rows of $\mathbf{B}_a$ is called a *basic loop matrix* denoted as $\mathbf{B}_b$ [37].

A basic loop matrix can be constructed with the aid of a tree T. Each link of the cotree T_c together with a unique path through the tree makes a *fundamental loop* for that link. The orientation of the loop is that of the link. For a connected graph G_d with n nodes and b branches, there are $b-n+1$ links and, consequently, $b-n+1$ fundamental loops. A submatrix of $\mathbf{B}_a$ constructed from these $b-n+1$ fundamental loops is called a *fundamental loop matrix* and is denoted as $\mathbf{B}$ [37].

For the directed graph given in Fig. 3.2 if a tree T is constructed to consist of branches (a, d), the fundamental loop matrix $\mathbf{B}$ is

$$\mathbf{B} = \begin{array}{c} \begin{matrix} a & d & b & c & e \end{matrix} \\ \left[\begin{matrix} 1 & 1 & 1 & 0 & 0 \\ 0 & 1 & 0 & 1 & 0 \\ 0 & 1 & 0 & 0 & 1 \end{matrix}\right] \end{array} \tag{3.5}$$

From the way of construction, it is obvious that $\mathbf{B}$ can be partitioned as

$$\mathbf{B} = [\mathbf{B}_{\mathrm{ln,tw}} \mid \mathbf{I}] \tag{3.6}$$

consisting of the $\mathbf{B}_{\mathrm{ln,tw}}$ block and the identity matrix $\mathbf{I}$ of order $b - n + 1$. The subscripts "tw" and "ln" indicate twigs and links, respectively.

The maximum number of independent KVL equations for the fundamental loops is expressed in a compact form by

$$\mathbf{Bu} = \mathbf{0}. \tag{3.7}$$

The general form of the KCL states, that the algebraic sum of all currents through a cutset, from one part to the other, is zero at all times. To express the generalized KCL compactly, another matrix - the *cutset matrix* $\mathbf{D}_a$ - is introduced. A cutset with a prescribed orientation is called an *oriented cutset*.

For a directed graph G_d having b branches and n_c oriented cutsets, the entries of the $n_c \times b$ cutset matrix $\mathbf{D}_a = [d_{ij}]$ are defined as follows:

$d_{ij} = 1$ if branch j is in cutset i, and their directions agree,

$d_{ij} = -1$ if branch j is in cutset i, and their directions oppose,

$d_{ij} = 0$ if branch j is not in cutset i.

With the directed graph depicted in Fig. 3.3 one can associate six cutsets. The corresponding cutset matrix reads:

$$\mathbf{D}_a = \begin{array}{c} \\ \text{Cutset} \\ \\ \\ \\ \\ \\ \end{array} \begin{array}{c} \begin{matrix} a & b & c & d & e \end{matrix} \\ \left[\begin{matrix} 1 & 1 & 0 & 1 & 0 \\ 0 & 0 & -1 & 1 & 0 \\ 1 & 1 & 0 & 0 & 1 \\ 0 & 0 & 1 & 0 & -1 \\ 0 & 0 & 0 & 1 & -1 \\ -1 & -1 & -1 & 0 & 0 \end{matrix}\right] \end{array} \begin{array}{l} \text{branches in the cutset} \\ \text{(abd)} \\ \text{(cd)} \\ \text{(abe)} \\ \text{(ce)} \\ \text{(de)} \\ \text{(abc)} \end{array} \tag{3.8}$$

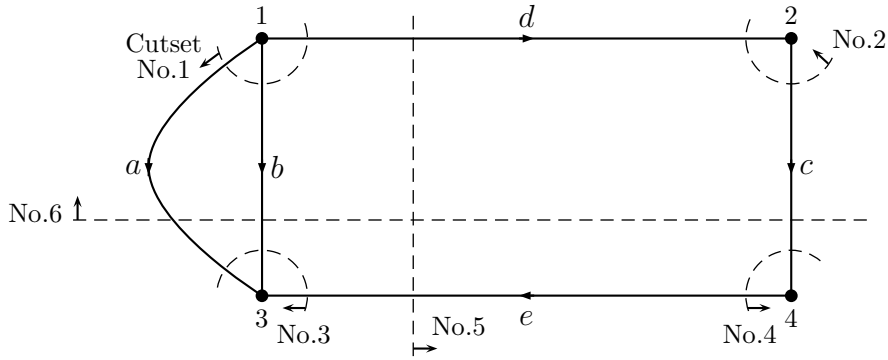

Figure 3.3: Construction of a cutset matrix for a directed graph.

If the rows of $\mathbf{i}$ and columns of $\mathbf{D}_a$ are arranged in the same branch order, the generalized KCL applied to all cutsets of G_d is expresses by

$$\mathbf{D}_a\mathbf{i} = \mathbf{0}. \tag{3.9}$$

When written in a scalar form, system (3.9) leads to a system of n_c equations. However, all what is needed in a circuit analysis, is the maximum number of independent equations from (3.9). Thus, a more useful submatrix of $\mathbf{D}_a$ can be extracted. Any submatrix that consists of the maximum number of linearly independent rows of $\mathbf{D}_a$ is called a *basic cutset matrix* and is denoted as $\mathbf{D}_b$ [37].

A systematic method of creating a basic cutset matrix is through the aid of a tree. Each tree branch of T together with some links from the corresponding cotree T_c forms a *fundamental cutset* for that tree branch, with respect to the chosen tree T. The reference arrow for the cutset is arbitrary chosen to agree with the reference arrow of the tree branch. For a connected graph having n nodes, there are $n-1$ tree branches and, consequently, $n-1$ fundamental cutsets for each chosen tree. A submatrix of $\mathbf{D}_a$ constructed with the $n-1$ fundamental cutsets is a called a *fundamental cutset matrix* and is denoted by $\mathbf{D}$.

For the directed graph presented in Fig. 3.3 if a tree T is constructed to consist of branches (a, c, e), the corresponding fundamental cutset matrix is

$$\mathbf{D} = \begin{array}{c} \begin{matrix} a & c & e & b & d \end{matrix} \\ \begin{bmatrix} 1 & 0 & 0 & 1 & 1 \\ 0 & 1 & 0 & 0 & -1 \\ 0 & 0 & 1 & 0 & -1 \end{bmatrix} \end{array} \tag{3.10}$$

Matrix $\mathbf{D}$ can be partitioned as

$$\mathbf{D} = [\mathbf{I} \mid \mathbf{D}_{\text{tw,ln}}] \tag{3.11}$$

consisting of the identity matrix $\mathbf{I}$ and the matrix $\mathbf{D}_{\text{tw,ln}}$. The linear independence of the rows of the fundamental cutset matrix $\mathbf{D}$ follows from the presence of the identity block $\mathbf{I}$. With the help of the fundamental cutset matrix $\mathbf{D}$ the generalized KCL is expressed compactly by

$$\mathbf{D}\mathbf{i} = \mathbf{0}. \tag{3.12}$$

Thus, all topological matrices are introduced.

3.2.2 Fundamental Relationship Among Branch Variables

Because of the constraints imposed by the KCL and the KVL on branch currents and voltages, respectively, only smaller sets of branch currents and voltages are independent, and the remaining branch variables may be expressed in terms of these [37].

For a connected network N with n nodes and b branches, the choice of a tree T leads to the following partitioned fundamental loop and fundamental cutset matrices:

$$\begin{aligned} \mathbf{B} &= [\mathbf{B}_{\mathrm{ln,tw}} \mid \mathbf{I}], \\ \mathbf{D} &= [\mathbf{I} \mid \mathbf{D}_{\mathrm{tw,ln}}]. \end{aligned} \tag{3.13}$$

The sizes of the identity blocks in the $\mathbf{B}$ and $\mathbf{D}$ matrices are equal to $b-n+1$ and $n-1$, respectively.

Let the branch variables be ordered in the following way:

$$\begin{aligned} \mathbf{u} &= [\mathbf{u}_{\mathrm{tw}} \mid \mathbf{u}_{\mathrm{ln}}]^T, \\ \mathbf{i} &= [\mathbf{i}_{\mathrm{tw}} \mid \mathbf{i}_{\mathrm{ln}}]^T. \end{aligned} \tag{3.14}$$

First we observe that with the usage of the generalized KVL (3.7) the link voltages are expressible as linear combination of tree branch voltages:

$$\mathbf{Bu} = \begin{bmatrix} \mathbf{B}_{\mathrm{ln,tw}} & \mathbf{I} \end{bmatrix} \begin{bmatrix} \mathbf{u}_{\mathrm{tw}} \\ \mathbf{u}_{\mathrm{ln}} \end{bmatrix} = \mathbf{B}_{\mathrm{ln,tw}}\mathbf{u}_{\mathrm{tw}} + \mathbf{u}_{\mathrm{ln}} = 0 \tag{3.15}$$

which reduces to

$$\mathbf{u}_{\mathrm{ln}} = -\mathbf{B}_{\mathrm{ln,tw}}\mathbf{u}_{\mathrm{tw}}. \tag{3.16}$$

Similarly, the twig currents are expressible as a linear combination of link currents using the generalized KCL (3.12):

$$\mathbf{Di} = \begin{bmatrix} \mathbf{I} & \mathbf{D}_{\mathrm{tw,ln}} \end{bmatrix} \begin{bmatrix} \mathbf{i}_{\mathrm{tw}} \\ \mathbf{i}_{\mathrm{ln}} \end{bmatrix} = \mathbf{i}_{\mathrm{tw}} + \mathbf{D}_{\mathrm{tw,ln}}\mathbf{i}_{\mathrm{ln}} = 0 \tag{3.17}$$

which leads to

$$\mathbf{i}_{\mathrm{tw}} = -\mathbf{D}_{\mathrm{tw,ln}}\mathbf{i}_{\mathrm{ln}}. \tag{3.18}$$

It is shown in [37] that the equality $\mathbf{DB}^T = 0$ holds. Using this, a relationship between two submatrices $\mathbf{B}_{\mathrm{ln,tw}}$ and $\mathbf{D}_{\mathrm{tw,ln}}$ can be established:

$$\mathbf{DB}^T = [\mathbf{I} \mid \mathbf{D}_{\mathrm{tw,ln}}][\mathbf{B}_{\mathrm{ln,tw}} \mid \mathbf{I}]^T = \mathbf{B}_{\mathrm{ln,tw}}^T + \mathbf{D}_{\mathrm{tw,ln}} = 0 \tag{3.19}$$

and thus

$$\mathbf{D}_{\mathrm{tw,ln}} = -\mathbf{B}^T_{\mathrm{ln,tw}} \quad \text{or} \quad \mathbf{B}_{\mathrm{ln,tw}} = -\mathbf{D}^T_{\mathrm{tw,ln}}. \tag{3.20}$$

Equalities (3.20) reflect the fundamental property of the circuit theory and lead to the idea of the *cutset/loop transformation* technique. Namely, all branch currents can be expressed in terms of link currents:

$$\begin{aligned} \mathbf{i} &= \begin{bmatrix} \mathbf{i}_{\mathrm{tw}} \\ \mathbf{i}_{\mathrm{ln}} \end{bmatrix} = \begin{bmatrix} -\mathbf{D}_{\mathrm{tw,ln}}\mathbf{i}_{\mathrm{ln}} \\ \mathbf{i}_{\mathrm{ln}} \end{bmatrix} = \begin{bmatrix} -\mathbf{D}_{\mathrm{tw,ln}} \\ \mathbf{I} \end{bmatrix} \mathbf{i}_{\mathrm{ln}} = \begin{bmatrix} \mathbf{B}^T_{\mathrm{ln,tw}} \\ \mathbf{I} \end{bmatrix} \mathbf{i}_{\mathrm{ln}} \\ &= \mathbf{B}^T \mathbf{i}_{\mathrm{ln}} \end{aligned} \tag{3.21}$$

and the branch voltages are expressed in terms of tree branch voltages as follows:

$$\begin{aligned} \mathbf{u} &= \begin{bmatrix} \mathbf{u}_{\mathrm{tw}} \\ \mathbf{u}_{\mathrm{ln}} \end{bmatrix} = \begin{bmatrix} \mathbf{u}_{\mathrm{tw}} \\ -\mathbf{B}_{\mathrm{ln,tw}}\mathbf{u}_{\mathrm{tw}} \end{bmatrix} = \begin{bmatrix} \mathbf{I} \\ -\mathbf{B}_{\mathrm{ln,tw}} \end{bmatrix} \mathbf{u}_{\mathrm{tw}} = \begin{bmatrix} \mathbf{I} \\ \mathbf{D}^T_{\mathrm{tw,ln}} \end{bmatrix} \mathbf{u}_{\mathrm{tw}} \\ &= \mathbf{D}^T \mathbf{u}_{\mathrm{tw}} \end{aligned} \tag{3.22}$$

The loop/cutset transformation technique can be presented by more general expressions involving basic loop/cutset matrices and written in terms of *loop currents* and *cutset voltages*. The corresponding expressions can be found in [37]. In the present work, we omit them since they are not well suited for the simulations on the digital computers. Instead, equations (3.21) and (3.22) are in use.

3.2.3 Tree-Cotree Partitioning

The tracing of a tree through a circuit is equal to selecting an orthogonal basis for the spaces formed by the loops and the cutsets in a circuit. A tree tracing process can be considered as a Gramm-Schmidt orthogonalization in the spaces formed by the loops and the cutsets [11].

The priority used for the decomposition in tree and cotree distinguishes between five categories of circuit branches depending on the form of the relation between the voltage drop and the current of the branch [38]:

1. For an *independent voltage source*, the voltage drop is known a priori.
2. A *voltage-driven branch* is a branch for which it is possible to express the voltage-current relation by

$$i_{\mathrm{br}} = Y_{\mathrm{br}} u_{\mathrm{br}} + f_{\mathrm{br,coup}} \tag{3.23}$$

   where Y_{br} is a branch admittance and $f_{\mathrm{br,coup}}$ is a coupling term.
3. A *voltage/current-driven branch* is a branch for which both relations (3.23) and (3.24) can be applied.

4. A *current-driven branch* is a branch for which it is possible to represent the voltage-current relation by

$$u_{\mathrm{br}} = Z_{\mathrm{br}} i_{\mathrm{br}} + f_{\mathrm{br,coup}} \tag{3.24}$$

   where Z_{br} is a branch impedance.

5. For a *independent current source*, the current is known a priori.

The list of branch types given above serves simultaneously as a priority list according to which the branches are selected to be the elements of a tree or a cotree, respectively. The priority of a twig is greater or equal to the priority of all links belonging to the associated fundamental cutset. In the same way, the priority of a link is less or equal to the priorities of the twigs of the corresponding fundamental loop. In a tree tracing process, the voltage-driven branches and the current-driven branches are selected to be twigs and links, respectively. Voltage/current-driven branches have a neutral nature as they can be described equivalently in terms of admittances or impedances and, consequently, take over the properties of voltage-driven branches or current-driven branches depending whether they are selected for the tree or the cotree, respectively. Thus, according to the voltage/current relations for the basic circuit elements, independent voltage sources, solid conductors and capacitors are selected as tree branches, while indictors, stranded conductors and independent current sources are cotree branches.[2]

Some exceptional cases when independent voltage and current sources appear in a cotree or a tree, respectively, deserve a special treatment. If an independent voltage source appears in the cotree, the corresponding fundamental loop consists of only independent voltage sources. If the KVL is satisfied for this loop, the voltage drop in the independent-voltage-source link can be expressed through the voltage drops in the other branches completing the loop. It means that this link should be eliminated from the consideration; otherwise, the circuit problem has no solution. Analogously, the independent-current-source twig in a corresponding fundamental cutset is eliminated from the consideration in order to satisfy the KCL [38].

After a priority list for the circuit branches has been established, they are indexed and sorted as follows: independent-voltage-source twigs ("twi"), unknown voltage-driven twigs ("twu"), eliminated current-driven twigs ("twe"), eliminated voltage-driven links ("lne"), unknown current-driven links ("lnu") and independent-current-source links ("lni"). The introduction of the indexing information for the circuit branches leads to the following partitioning in the fundamental matrices [38]:

$$\mathbf{D} = \begin{bmatrix} \mathbf{I} & \mathbf{0} & \mathbf{0} & \mathbf{D}_{\mathrm{twi,lne}} & \mathbf{D}_{\mathrm{twi,lnu}} & \mathbf{D}_{\mathrm{twi,lni}} \\ \mathbf{0} & \mathbf{I} & \mathbf{0} & \mathbf{D}_{\mathrm{twu,lne}} & \mathbf{D}_{\mathrm{twu,lnu}} & \mathbf{D}_{\mathrm{twu,lni}} \\ \mathbf{0} & \mathbf{0} & \mathbf{I} & \mathbf{0} & \mathbf{D}_{\mathrm{twe,lnu}} & \mathbf{D}_{\mathrm{twe,lni}} \end{bmatrix} \tag{3.25a}$$

[2] Basic types of conductors are discussed in the following section.

and

$$\mathbf{B} = \begin{bmatrix} \mathbf{B}_{\text{lne,twi}} & \mathbf{B}_{\text{lne,twu}} & \mathbf{0} & \mathbf{I} & \mathbf{0} & \mathbf{0} \\ \mathbf{B}_{\text{lnu,twi}} & \mathbf{B}_{\text{lnu,twu}} & \mathbf{B}_{\text{lnu,twe}} & \mathbf{0} & \mathbf{I} & \mathbf{0} \\ \mathbf{B}_{\text{lni,twi}} & \mathbf{B}_{\text{lni,twu}} & \mathbf{B}_{\text{lni,twe}} & \mathbf{0} & \mathbf{0} & \mathbf{I} \end{bmatrix}. \tag{3.25b}$$

The zero contributions at positions (3,4) in $\mathbf{D}$ and (1,3) in $\mathbf{B}$ matrices appear due to the application of the priority rules. A fundamental cutset associated with a current-driven twig cannot contain voltage-driven branches since these have a higher priority. The symmetry property of the fundamental cutset and loop matrices carries over to their subblocks: $\mathbf{B}_{a,b} = -\mathbf{D}_{b,a}^{T}$.

3.3 Basic Conductor Models

A *conductor model* is a model for a conductor or a set of conductors featuring a particular type of current distribution. The kind of current distribution in a conductor under application of a time-varying magnetic field is qualitatively described by the *skin depth*

$$\delta = \sqrt{\frac{1}{\pi f \mu \sigma}}. \tag{3.26}$$

The value of the skin depth depends on the conductivity σ and the permeability μ of the conductor material and on the frequency f of the time-varying magnetic field. The skin depth corresponds to the thickness of the layer of a conductive plane in which 63% of the current is concentrated. The skin depth also allows a qualitative classification of eddy current effects for conductors with an arbitrary geometry. *Massive bars* and *windings* are two main types of technical conductors that are typically in use for electrically coupled devices. The corresponding conductor models are *solid* and *stranded* conductors, respectively, illustrated in Fig. 3.4. In this figure, ℓ_{sol} and ℓ_{str} are the lengths of the solid and stranded conductors, respectively; I_{sol} and I_{str} are the total currents through the solid and stranded conductors; S_{sol} and S_{str} are the cross-sections of the solid and stranded conductors; U_{sol} and U_{str} are the voltage drops along the conductors, S_{w} is the cross-section of a single strand, and Ω_{FIT} is the FIT domain.

3.3.1 Solid Conductor Model

Solid conductors are voltage driven devices that exhibit significant skin effects and carry, consequently, non negligible eddy currents. For a solid conductor, the current density $\vec{\text{J}}_{\text{sol}}$ is related to the electric field strength by Ohm's law $\vec{\text{J}}_{\text{sol}} = \sigma\vec{\text{E}}$. By introducing the Faraday's law in integral form, the current density is expressed by:

$$\vec{\text{J}}_{\text{sol}} = -\sigma\frac{\partial\vec{\text{A}}}{\partial t} - \sigma\nabla V = \vec{\text{J}}_{\text{e}} + \vec{\text{J}}_{\text{s}} \tag{3.27}$$

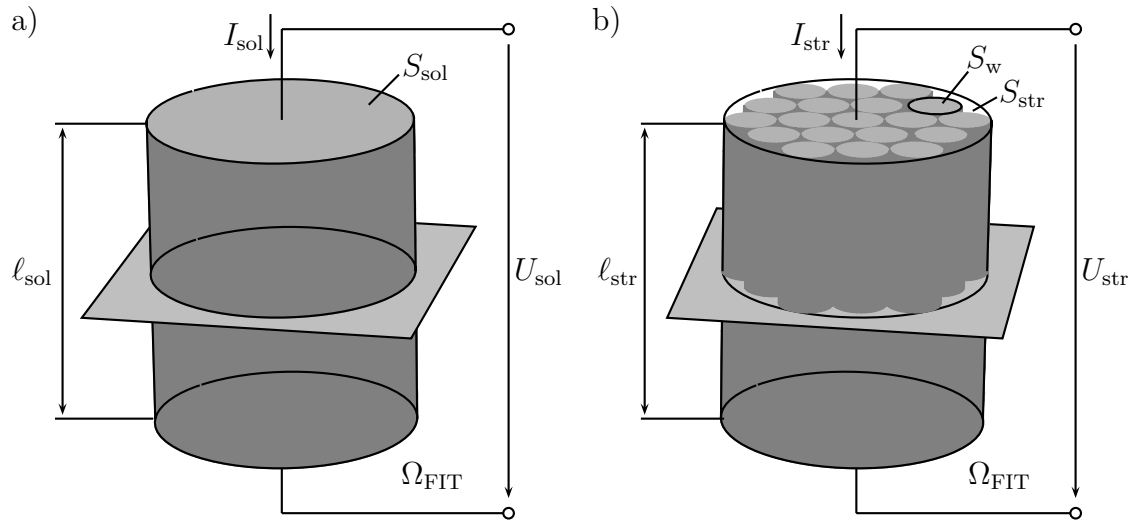

Figure 3.4: Basic conductor types: (a) solid conductor, (b) stranded conductor.

where $\vec{\mathrm{J}}_{\mathrm{e}}$ is the eddy current density and $\vec{\mathrm{J}}_{\mathrm{s}}$ is the source current density. Only the total current density $\vec{\mathrm{J}}_{\mathrm{sol}} = \vec{\mathrm{J}}_{\mathrm{e}} + \vec{\mathrm{J}}_{\mathrm{s}}$ is a physically measurable quantity. The separation of $\vec{\mathrm{J}}_{\mathrm{sol}}$ into two components is an effect flowing from the introduction of the potentials $\vec{\mathrm{A}}$ and V [10]. As becomes clear below, the division of $\vec{\mathrm{J}}_{\mathrm{sol}}$ into $\vec{\mathrm{J}}_{\mathrm{e}}$ and $\vec{\mathrm{J}}_{\mathrm{s}}$ is not unique which will lead to different coupling schemes.

In the FIT notation, expression (3.27) reads:

$$\widehat{\widehat{\mathbf{j}}}_{\mathrm{sol}} = \widehat{\widehat{\mathbf{j}}}_{\mathrm{e}} + \widehat{\widehat{\mathbf{j}}}_{\mathrm{s}} = \mathbf{M}_{\sigma}(-\frac{\mathrm{d}\widehat{\mathbf{a}}}{\mathrm{d}t} - \mathbf{G}\phi) \tag{3.28}$$

where $\mathbf{G}$ is the gradient operator defined on the primary grid and ϕ is a vector of nodal voltages. Since the discrete gradient operator $\mathbf{G}$ is related to the divergence operator $\widetilde{\mathbf{S}}$ of the dual grid by $\mathbf{G} = -\widetilde{\mathbf{S}}^T$, the following expression for the source current density $\widehat{\widehat{\mathbf{j}}}_{\mathrm{s}}$ holds:

$$\widehat{\widehat{\mathbf{j}}}_{\mathrm{s}} = -\mathbf{M}_{\sigma}\mathbf{G}\phi = \mathbf{M}_{\sigma}\widetilde{\mathbf{S}}^T\phi. \tag{3.29}$$

A first coupling scheme is organised at a *reference cross section* which is a cross section of the solid conductor composed of a set of dual facets (Fig. 3.5). The layer of primary cells of which the edges cross the reference cross section is the *reference layer* [39]. The voltage drop U_{sol} along the solid conductor is applied as a potential difference between the upper and the lower side of the reference layer. The electric-field distribution $\widehat{\mathbf{e}}_{\mathrm{app}}$, although a nonphysical quantity, can be then constructed by prescribing the value of the voltage drop U_{sol} to all primary edges crossing the reference cross section

$$\widehat{\mathbf{e}}_{\mathrm{app}} = \tilde{\mathbf{Q}}U_{\mathrm{sol}}. \tag{3.30}$$

The operator $\tilde{\mathbf{Q}}$ is a 2D incidence matrix containing the incidences 1, -1 and 0 between the primary edges at the reference cross section and the circuit [40]. With

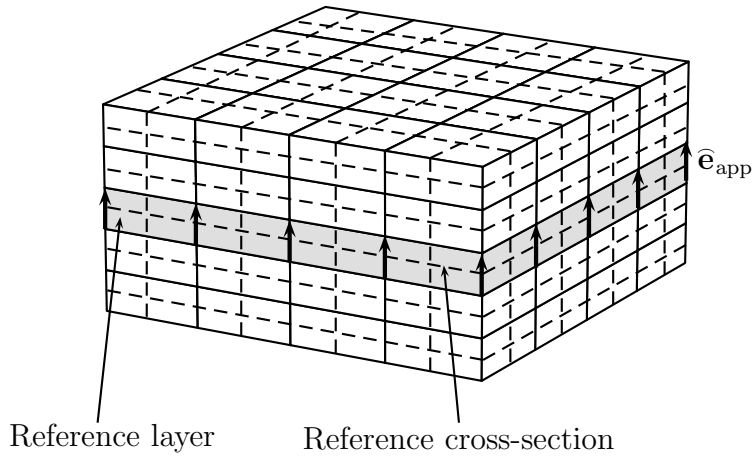

Figure 3.5: Reference cross section, reference layer and distribution of the applied electric field. The reference cross section coincides with the agglomeration of a number of dual facets whereas the reference layer corresponds to the extrusion of the reference cross section along the crossing primary edges.

this operator the *zero-dimensional* solid conductor voltage drop is coupled to the two-dimensional electric field components perpendicular to the reference cross section. Finally, the total current flowing through the solid conductor is calculated at the reference cross section summing up all the contributions of the dual facets associated with the primary edges:

$$\begin{aligned} I_{\mathrm{sol}} = \tilde{\mathbf{Q}}^T \widehat{\widehat{\mathbf{j}}}_{\mathrm{sol}} &= \tilde{\mathbf{Q}}^T \mathbf{M}_\sigma \widehat{\mathbf{e}}_{\mathrm{app}} - \tilde{\mathbf{Q}}^T \mathbf{M}_\sigma \frac{\mathrm{d}\widehat{\mathbf{a}}}{\mathrm{d}t} \\ &= \tilde{G}_{\mathrm{sol}} U_{\mathrm{sol}} - \tilde{\mathbf{Q}}^T \mathbf{M}_\sigma \frac{\mathrm{d}\widehat{\mathbf{a}}}{\mathrm{d}t} \end{aligned} \tag{3.31}$$

where $\tilde{G}_{\mathrm{sol}} = \tilde{\mathbf{Q}}^T \mathbf{M}_\sigma \tilde{\mathbf{Q}}$ can be interpreted as the dc conductance of the reference layer.

The *FIT solid conductor model* consists of magnetoquasistatic formulation (2.61) with the current density given by (3.28) which is coupled to the external electrical circuit via (3.31). The coupled system of equations for a model with a current-driven solid conductor reads:

$$\begin{bmatrix} \widetilde{\mathbf{C}}\mathbf{M}_{\mu^{-1}}\mathbf{C} & -\mathbf{M}_\sigma \tilde{\mathbf{Q}} \\ \mathbf{0} & \tilde{G}_{\mathrm{sol}} \end{bmatrix} \begin{bmatrix} \widehat{\mathbf{a}}_1 \\ U_{\mathrm{sol}} \end{bmatrix} + \begin{bmatrix} \mathbf{M}_\sigma & 0 \\ -\tilde{\mathbf{Q}}^T \mathbf{M}_\sigma & 0 \end{bmatrix} \frac{\mathrm{d}}{\mathrm{d}t} \begin{bmatrix} \widehat{\mathbf{a}}_1 \\ U_{\mathrm{sol}} \end{bmatrix} = \begin{bmatrix} \mathbf{0} \\ I_{\mathrm{sol}} \end{bmatrix}. \tag{3.32}$$

Formulation (3.32) corresponds to a particular choice of the electric potential, i.e., such that the support of the electric scalar potential equals the referencer layer.

The coupling at a reference cross section expressed by formulation (3.32) relies upon a source current field $\widehat{\widehat{\mathbf{j}}}_{\mathrm{s}} = \mathbf{M}_\sigma \tilde{\mathbf{Q}} U_{\mathrm{sol}} = \mathbf{M}_\sigma \widehat{\mathbf{e}}_{\mathrm{app}}$ which is not divergence-free.

A second field-circuit coupling scheme for a solid conductor is carried out based on a divergence-free source current field. The source current $\widehat{\widetilde{\mathbf{j}}}_{\mathrm{s}} = \mathbf{M}_\sigma \widehat{\mathbf{e}}$ based on the electric voltages $\widehat{\mathbf{e}} = \widehat{\mathbf{e}}_{\mathrm{app}} - \mathbf{G}\phi$ is derived from the solution of the stationary-current problem

$$\widetilde{\mathbf{S}}\mathbf{M}_\sigma \widetilde{\mathbf{S}}^T \phi_s = -\widetilde{\mathbf{S}}\mathbf{M}_\sigma \widehat{\mathbf{e}}_{\mathrm{app}}. \tag{3.33}$$

The solution for the stationary current $\widehat{\widetilde{\mathbf{j}}}_{\mathrm{s}} = \mathbf{M}_\sigma(\widehat{\mathbf{e}}_{\mathrm{app}} + \widetilde{\mathbf{S}}^T\phi_s)$ is divergence free and allows to define a coupling operator $\mathbf{Q}$ such that $\widehat{\widetilde{\mathbf{j}}}_{\mathrm{s}} = \mathbf{M}_\sigma \mathbf{Q} U_{\mathrm{sol}}$. Operator $\mathbf{Q}$ relates the voltages along the primary edges inside the solid conductor volume to the applied voltage drop U_{sol}. Both coupling operators are related by a projection, i.e., $\mathbf{Q} = \mathbf{N}_{\widehat{\mathbf{e}}}\tilde{\mathbf{Q}}$, where the projection operator

$$\mathbf{N}_{\widehat{\mathbf{e}}} = \mathbf{I} - \widetilde{\mathbf{S}}^T(\widetilde{\mathbf{S}}\mathbf{M}_\sigma\widetilde{\mathbf{S}}^T)^{-1}\widetilde{\mathbf{S}}\mathbf{M}_\sigma \tag{3.34}$$

maps an electric field $\widehat{\mathbf{e}}_{\mathrm{app}}$ onto an electric field $\mathbf{N}_{\widehat{\mathbf{e}}}\widehat{\mathbf{e}}_{\mathrm{app}}$ for which the source current is divergence free. The projector $\mathbf{N}_{\widehat{\mathbf{e}}}$ is orthogonal with respect to the matrix norm $(\widehat{\mathbf{e}}_1, \widehat{\mathbf{e}}_2)_{\mathbf{M}_\sigma} = \widehat{\mathbf{e}}_2^H \mathbf{M}_\sigma \widehat{\mathbf{e}}_1$.

The current through a solid conductor is then expressed as

$$I_{\mathrm{sol}} = G_{\mathrm{sol}} U_{\mathrm{sol}} - \mathbf{Q}^T \mathbf{M}_\sigma \frac{\mathrm{d}\widehat{\mathbf{a}}}{\mathrm{d}t}. \tag{3.35}$$

The second field-circuit coupled formulation for a solid conductor representing a coupling at the entire conductor domain is obtained when $\tilde{\mathbf{Q}}$ and $\tilde{G}_{\mathrm{sol}}$ are replaced by $\mathbf{Q}$ and $G_{\mathrm{sol}} = \mathbf{Q}^T\mathbf{M}_\sigma\mathbf{Q}$, respectively, and reads:

$$\begin{bmatrix} \widetilde{\mathbf{C}}\mathbf{M}_{\mu^{-1}}\mathbf{C} & -\mathbf{M}_\sigma\mathbf{Q} \\ \mathbf{0} & G_{\mathrm{sol}} \end{bmatrix} \begin{bmatrix} \widehat{\mathbf{a}}_2 \\ U_{\mathrm{sol}} \end{bmatrix} + \begin{bmatrix} \mathbf{M}_\sigma & 0 \\ -\mathbf{Q}^T\mathbf{M}_\sigma & 0 \end{bmatrix} \frac{\mathrm{d}}{\mathrm{d}t} \begin{bmatrix} \widehat{\mathbf{a}}_2 \\ U_{\mathrm{sol}} \end{bmatrix} = \begin{bmatrix} \mathbf{0} \\ I_{\mathrm{sol}} \end{bmatrix}. \tag{3.36}$$

The value G_{sol} is the dc conductance of the solid conductor. The coupling term $\mathbf{Q}$ couples the voltage drop along a solid conductor to a 3D field distribution prescribed for all primary edges inside the volume of the solid conductor. However, in contrast to $\tilde{\mathbf{Q}}$, $\mathbf{Q}$ is not an incidence matrix [39]. Notice that the solution for $\widehat{\mathbf{a}}$ in (3.36) will be different from the solution for $\widehat{\mathbf{a}}$ in (3.32). When $\widehat{\mathbf{a}}_1$ is a solution of (3.32), then $\widehat{\mathbf{a}}_2 = \mathbf{N}_{\widehat{\mathbf{e}}}\widehat{\mathbf{a}}_1$ solves (3.36).

In the following, the 3D solid conductor model described by system (3.36) is used.

3.3.2 Stranded Conductor Model

A stranded conductor represents a model for a current driven coil wound of many thin strands. The cross section of the individual strand of a stranded conductor is so small that for the expected frequencies no significant skin effect will occur and the eddy currents are negligible. In transient field-circuit coupled formulation, this fact is taken into account by introducing zeros at the corresponding positions of the

conductivity matrix $\mathbf{M}_\sigma$. Resolving the individual strands by the FIT grid is then not required.

As in the case of the solid conductor model, the coupling between a stranded conductor and an external circuit is carried out at all dual facets in the conductor volume or at the dual facets covering a reference cross section perpendicular to the strands. Assuming that each turn carries the current I_{str}, the average current density at the reference cross section for the second case is given by

$$\hat{\tilde{\mathbf{j}}}_{\mathrm{app}} = \underbrace{\frac{N_t}{S_{\mathrm{str}}}\tilde{\mathbf{D}}_A\tilde{\mathbf{Q}}}_{\tilde{\mathbf{P}}} I_{\mathrm{str}} \tag{3.37}$$

where $\tilde{\mathbf{D}}_A$ is the diagonal matrix of dual facet areas, N_t is the number of strands of the stranded conductor and S_{str} is the area of the reference cross section. The current distribution is forced to be homogeneous by defining an anisotropic conductivity aligned with the winding direction in the stranded conductor [41]. The voltage drop U_{str} along the winding is computed by averaging the voltage drops across cross section and summing them along the winding. This corresponds to

$$U_{\mathrm{str}} = \tilde{\mathbf{P}}^T\left(\mathbf{M}^{-1}_{\sigma,\mathrm{aniso}}\hat{\tilde{\mathbf{j}}}_{\mathrm{app}} + \frac{\mathrm{d}}{\mathrm{d}t}\hat{\mathbf{a}}\right) \tag{3.38}$$

where $\mathbf{M}^{-1}_{\sigma,\mathrm{aniso}}$ is obtained from the conductivity matrix $\mathbf{M}_{\sigma,\mathrm{aniso}}$ by inverting only the matrix blocks associated with the stranded conductor. The coupled system for a stranded conductor reads:

$$\begin{bmatrix} \widetilde{\mathbf{C}}\mathbf{M}_{\mu^{-1}}\mathbf{C} & -\tilde{\mathbf{P}} \\ \mathbf{0} & -\tilde{R}_{\mathrm{str}} \end{bmatrix}\begin{bmatrix} \hat{\mathbf{a}}_1 \\ I_{\mathrm{str}} \end{bmatrix} + \begin{bmatrix} \mathbf{M}_{\sigma,\mathrm{aniso}} & 0 \\ -\tilde{\mathbf{P}}^T & 0 \end{bmatrix}\frac{\mathrm{d}}{\mathrm{d}t}\begin{bmatrix} \hat{\mathbf{a}}_1 \\ I_{\mathrm{str}} \end{bmatrix} = \begin{bmatrix} \mathbf{0} \\ -U_{\mathrm{str}} \end{bmatrix}. \tag{3.39}$$

where $\tilde{R}_{\mathrm{str}} = \tilde{\mathbf{P}}^T\mathbf{M}_\sigma^{-1}\tilde{\mathbf{P}}$ is the dc resistance of the reference layer.

Since an anisotropic conductivity matrix $\mathbf{M}_{\sigma,\mathrm{aniso}}$ is not diagonal, the efficiency of the matrix-vector product in the FIT scheme decreases significantly. This is the reason why we turn to the less sparse coupling approach. Then, the anisotropic conductivity matrix has only to be applied in a pre-processing step where a divergence-free source current field is obtained from

$$\widetilde{\mathbf{S}}\mathbf{M}_{\sigma,\mathrm{aniso}}\widetilde{\mathbf{S}}^T\phi_s = -\widetilde{\mathbf{S}}\hat{\tilde{\mathbf{j}}}_{\mathrm{app}} \tag{3.40}$$

yielding the relation $\hat{\tilde{\mathbf{j}}}_{\mathrm{s}} = \hat{\tilde{\mathbf{j}}}_{\mathrm{app}} + \mathbf{M}_{\sigma,\mathrm{aniso}}\widetilde{\mathbf{S}}^T\phi_s = \mathbf{P}I_{\mathrm{str}}$ between the applied current and the source current field. The coupling operator $\mathbf{P}$ between the applied winding current and the source current field reads $\mathbf{P} = \mathbf{N}_{\hat{\tilde{\mathbf{j}}}}\tilde{\mathbf{P}}$ where the projector

$$\mathbf{N}_{\hat{\tilde{\mathbf{j}}}} = \mathbf{I} - \mathbf{M}_\sigma\widetilde{\mathbf{S}}^T(\mathbf{S}\mathbf{M}_{\sigma,\mathrm{aniso}}\widetilde{\mathbf{S}}^T)^{-1}\widetilde{\mathbf{S}} \tag{3.41}$$

maps a current field $\hat{\tilde{\mathbf{j}}}$ onto a divergence-free current field $\mathbf{N}_{\hat{\tilde{\mathbf{j}}}}\hat{\tilde{\mathbf{j}}}$. The projector $\mathbf{N}_{\hat{\tilde{\mathbf{j}}}}$ is orthogonal with respect to the inner product $(\hat{\tilde{\mathbf{j}}}_1, \hat{\tilde{\mathbf{j}}}_2)_{\mathbf{M}_\sigma^{-1}} = \hat{\tilde{\mathbf{j}}}_2^H\mathbf{M}_\sigma^{-1}\hat{\tilde{\mathbf{j}}}_1$ defined

for all current fields inside the stranded conductor. The projector $\mathbf{N}_{\widehat{\mathbf{j}}}$ is the dual counterpart of $\mathbf{N}_{\widehat{\mathbf{e}}}$, i.e., $\mathbf{N}_{\widehat{\mathbf{j}}} = \mathbf{N}_{\widehat{\mathbf{e}}}^T$. Moreover, both projectors commute with respect to $\mathbf{M}_\sigma$, i.e., $\mathbf{N}_{\widehat{\mathbf{j}}}\mathbf{M}_\sigma = \mathbf{M}_\sigma\mathbf{N}_{\widehat{\mathbf{e}}}$ [39].

Because this second coupling scheme explicitly forces the current distribution to be homogeneous in the whole stranded conductor volume, the application of the anisotropic conductivity matrix $\mathbf{M}_{\sigma,\text{aniso}}$ is equivalent to the application of isotropic conductivity matrix $\mathbf{M}_\sigma$.

The voltage drop U_{str} along the winding at primary edges is computed by averaging the voltage drops across cross sections and summing them along the whole winding, i.e.,

$$U_{\text{str}} = R_{\text{str}} I_{\text{str}} + \mathbf{P}^T \frac{\mathrm{d}\widehat{\mathbf{a}}}{\mathrm{d}t} \tag{3.42}$$

where $R_{\text{str}} = \mathbf{P}^T \mathbf{M}_\sigma^{-1} \mathbf{P}$ is a dc resistance of the winding.

The *FIT stranded conductor model* consists of magnetoquasistatic formulation (2.61) with a source current density $\widehat{\widehat{\mathbf{j}}}_{\text{s}} = \mathbf{P} I_{\text{str}}$ which is coupled to the external electrical circuit via (3.42) and reads:

$$\begin{bmatrix} \widetilde{\mathbf{C}}\mathbf{M}_{\mu^{-1}}\mathbf{C} & -\mathbf{P} \\ \mathbf{0} & -R_{\text{str}} \end{bmatrix} \begin{bmatrix} \widehat{\mathbf{a}}_2 \\ I_{\text{str}} \end{bmatrix} + \begin{bmatrix} \mathbf{0} & 0 \\ -\mathbf{P}^T & 0 \end{bmatrix} \frac{\mathrm{d}}{\mathrm{d}t} \begin{bmatrix} \widehat{\mathbf{a}}_2 \\ I_{\text{str}} \end{bmatrix} = \begin{bmatrix} \mathbf{0} \\ -U_{\text{str}} \end{bmatrix}. \tag{3.43}$$

Note that conductivity matrix $\mathbf{M}_\sigma$ is not needed in the first equation.

Since a coupling term $\mathbf{P}$ does not depend on time, the following auxiliary quantity $\psi = \mathbf{P}^T \widehat{\mathbf{a}}$ can be introduced. It represents a magnetic flux linked to the winding. When only linear materials are present, we obtain from the first part of system (3.43)

$$\psi = \mathbf{P}^T (\widetilde{\mathbf{C}}\mathbf{M}_{\mu^{-1}}\mathbf{C})^{-1} \mathbf{P} I_{\text{str}}. \tag{3.44}$$

The inductance of the winding is $L_{\text{str}} = \mathbf{P}^T (\widetilde{\mathbf{C}}\mathbf{M}_{\mu^{-1}}\mathbf{C})^{-1}\mathbf{P}$. Hence, we can rewrite system (3.43) in terms of magnetic flux ψ and a current I_{str}:

$$\begin{bmatrix} 1/L_{\text{str}} & -1 \\ 0 & -R_{\text{str}} \end{bmatrix} \begin{bmatrix} \psi \\ I_{\text{str}} \end{bmatrix} + \begin{bmatrix} 0 & 0 \\ -1 & 0 \end{bmatrix} \frac{\mathrm{d}}{\mathrm{d}t} \begin{bmatrix} \psi \\ I_{\text{str}} \end{bmatrix} = \begin{bmatrix} 0 \\ -U_{\text{str}} \end{bmatrix}. \tag{3.45}$$

This system is equivalent to the ordinary differential equation

$$L_{\text{str}} \frac{\mathrm{d}}{\mathrm{d}t} I_{\text{str}} + R_{\text{str}} I_{\text{str}} = U_{\text{str}}. \tag{3.46}$$

The solution of equation (3.46) can be easily found analytically and used as a reference solution for the formulation (3.43).

In the following, the 3D stranded conductor model described by system (3.43) is used.

3.4 Transient Field-Circuit Coupled Formulation

In practical applications, magnetic branches are coupled to an electrical circuit containing voltage and current sources, resistors, inductors, capacitors, diodes and other power electronic components. In the present part of the treatise, a coupled transient formulations for the circuits without switching elements is derived.

3.4.1 Coupling Requirements

Both the FIT and the circuit models have their own typical properties reflected by the corresponding system matrices. The FIT matrix is large and sparse. In the absence of motion, it is also symmetric. If we consider a static or a transient formulation, it is also semi-positive definite. The circuit system matrix is usually small and rather dense, symmetric and indefinite.

The coupling mechanism should be organised in such a way, that the corresponding coupled system matrix preserves as much as possible the properties of the FIT matrix [11].

The sparsity of the FIT system part can be preserved if for each solid conductor and for each stranded conductor a voltage drop and a current, respectively, are added as unknowns in the coupled formulation. To conform to this requirements, a circuit model is developed combining both types of unknowns without loosing the symmetry of the system [42]. In the absence of the motional effects and controlled sources, the coupled system of equations is symmetric [11].

3.4.2 Basic Ideas

The source current $\hat{\hat{\mathbf{j}}}_\mathrm{s}$ is a combination of the currents of the coils and the source currents of the massive conductors present in the field model:

$$\hat{\hat{\mathbf{j}}}_\mathrm{s} = \sum_q \mathbf{M}_\sigma \mathbf{Q}_{\mathrm{sol},q} \mathbf{u}_{\mathrm{sol},q} + \sum_p \mathbf{P}_{\mathrm{str},p} \mathbf{i}_{\mathrm{str},p}. \tag{3.47}$$

where $\mathbf{u}_{\mathrm{sol},q}$ is the voltage drop along the solid conductor q and $\mathbf{i}_{\mathrm{str},p}$ is a current flowing through the stranded conductor p. The coupling matrices $\mathbf{Q}$ and $\mathbf{P}$ are determined in the previous section.

Relations (3.35) and (3.42) are entered as generalized current-voltage relations in the circuit description. To determine a set of state variables for the circuit, a partitioning in a tree and a cotree is implemented according to the procedure described in Section 3.2.3. Following a priority rule, independent voltage sources, solid conductors and capacitors are selected as tree branches (twigs), whereas inductors, coils and independent current sources are determined to become cotree branches (links). Resistors may appear in the tree as well as in cotree. The circuit state variables are then the voltage drops $\mathbf{u}_\mathrm{twu}$ and the currents $\mathbf{i}_\mathrm{lnu}$ of the twigs and links, respectively.

The excitations due to voltage and current sources are collected in vectors $\mathbf{u}_{\text{twi}}$ and $\mathbf{i}_{\text{lni}}$, respectively.

The KCL formulated for all fundamental cutsets in the absence of the eliminated links reads:

$$\mathbf{i}_{\text{twu}} + \mathbf{D}_{\text{twu,lnu}}\mathbf{i}_{\text{lnu}} = -\mathbf{D}_{\text{twu,lni}}\mathbf{i}_{\text{lni}} \tag{3.48a}$$

where $\mathbf{D}_{\text{twu,lnu}}$ and $\mathbf{D}_{\text{twu,lni}}$ are parts of the fundamental cutset matrix $\mathbf{D}$ given by (3.25a) which is constructed during the tree tracing process.

The KVL formulated for all fundamental loops in the absence of the eliminated twigs reads:

$$\mathbf{B}_{\text{lnu,twu}}\mathbf{u}_{\text{twu}} + \mathbf{u}_{\text{lnu}} = -\mathbf{B}_{\text{lnu,twi}}\mathbf{u}_{\text{twi}} \tag{3.48b}$$

where $\mathbf{B}_{\text{twu,lnu}}$ and $\mathbf{B}_{\text{lnu,twi}}$ are parts of the fundamental loop matrix $\mathbf{B}$ given by (3.25b) which is constructed during the tree tracing process.

3.4.3 Partial Cutset/Loop Transformation Technique

At the next stage of the coupling process, the partial cutset/loop transformation technique described in Section 3.2.2 has to be applied to eliminate the current-driven twigs (index "twe") and the voltage-driven links (index "lne") from the consideration.

Suppose that $\mathbf{C}_{\text{twu}}$ is the capacitance matrix for the capacitive elements in the tree and $\mathbf{C}_{\text{lne}}$ is the capacitance matrix for the capacitive elements in the cotree. Let $\mathbf{G}_{\text{twu}}$ represent the conductance matrix for the conductive elements in the tree and $\mathbf{G}_{\text{lne}}$ is the conductance matrix for the conductive elements in the cotree. The matrix $\mathbf{L}_{\text{lnu}}$ contains the inductances of the inductive elements in the cotree and the matrix $\mathbf{L}_{\text{twe}}$ contains the inductances of the inductive elements in the tree. Finally, the matrix $\mathbf{R}_{\text{lnu}}$ collects the resistances of the resistors in the cotree and matrix $\mathbf{R}_{\text{twe}}$ collects the resistances of the resistors in the tree.

Eliminated Links. For voltage-driven links, the corresponding branch current-voltage relations read:

$$\mathbf{i}_{\text{lne}} = \mathbf{G}_{\text{lne}}\mathbf{u}_{\text{lne}} + \mathbf{C}_{\text{lne}}\frac{\mathrm{d}\mathbf{u}_{\text{lne}}}{\mathrm{d}t} \tag{3.49}$$

where $\mathbf{i}_{\text{lne}}$ and $\mathbf{u}_{\text{lne}}$ are the currents and the voltage drops, respectively, for the considered eliminated links.

Each of the eliminated link belongs to a fundamental loop. The KVL applied to all fundamental loops containing the eliminated links gives:

$$\mathbf{u}_{\text{lne}} = -\mathbf{B}_{\text{lne,twu}}\mathbf{u}_{\text{twu}} - \mathbf{B}_{\text{lne,twi}}\mathbf{u}_{\text{twi}}. \tag{3.50}$$

Substitution of (3.50) into (3.49) leads to:

$$\begin{aligned}\mathbf{i}_{\mathrm{lne}} &= -\mathbf{G}_{\mathrm{lne}}\mathbf{B}_{\mathrm{lne,twu}}\mathbf{u}_{\mathrm{twu}} - \mathbf{C}_{\mathrm{lne}}\mathbf{B}_{\mathrm{lne,twu}}\frac{\mathrm{d}\mathbf{u}_{\mathrm{twu}}}{\mathrm{d}t} \\ &- \mathbf{G}_{\mathrm{lne}}\mathbf{B}_{\mathrm{lne,twi}}\mathbf{u}_{\mathrm{twi}} - \mathbf{C}_{\mathrm{lne}}\mathbf{B}_{\mathrm{lne,twi}}\frac{\mathrm{d}\mathbf{u}_{\mathrm{twi}}}{\mathrm{d}t}.\end{aligned} \tag{3.51}$$

Now, we apply the KCL to all the fundamental cutsets containing the eliminated links:

$$\mathbf{i}_{\mathrm{twu}} + \mathbf{D}_{\mathrm{twu,lnu}}\mathbf{i}_{\mathrm{lnu}} + \mathbf{D}_{\mathrm{twu,lne}}\mathbf{i}_{\mathrm{lne}} + \mathbf{D}_{\mathrm{twu,lni}}\mathbf{i}_{\mathrm{lni}} = \mathbf{0}. \tag{3.52}$$

The currents in the voltage-driven twigs are expressed by

$$\mathbf{i}_{\mathrm{twu}} = \mathbf{G}_{\mathrm{twu}}\mathbf{u}_{\mathrm{twu}} + \mathbf{C}_{\mathrm{twu}}\frac{\mathrm{d}\mathbf{u}_{\mathrm{twu}}}{\mathrm{d}t}. \tag{3.53}$$

Finally, expressions (3.51) and (3.53) are substituted into (3.52) leading to the transformed fundamental cutset equations:

$$\begin{aligned}\mathbf{N}_{\mathrm{G}}\mathbf{u}_{\mathrm{twu}} &+ \mathbf{N}_{\mathrm{C}}\frac{\mathrm{d}\mathbf{u}_{\mathrm{twu}}}{\mathrm{d}t} + \mathbf{D}_{\mathrm{twu,lnu}}\mathbf{i}_{\mathrm{lnu}} = -\mathbf{D}_{\mathrm{twu,lni}}\mathbf{i}_{\mathrm{lni}} \\ &+ \mathbf{D}_{\mathrm{twu,lne}}\mathbf{G}_{\mathrm{lne}}\mathbf{B}_{\mathrm{lne,twi}}\mathbf{u}_{\mathrm{twi}} + \mathbf{D}_{\mathrm{twu,lne}}\mathbf{C}_{\mathrm{lne}}\mathbf{B}_{\mathrm{lne,twi}}\frac{\mathrm{d}\mathbf{u}_{\mathrm{twi}}}{\mathrm{d}t}\end{aligned} \tag{3.54}$$

where the matrices $\mathbf{N}_{\mathrm{G}}$ and $\mathbf{N}_{\mathrm{C}}$ are defined by:

$$\begin{aligned}\mathbf{N}_{\mathrm{G}} &= \mathbf{G}_{\mathrm{twu}} - \mathbf{D}_{\mathrm{twu,lne}}\mathbf{G}_{\mathrm{lne}}\mathbf{B}_{\mathrm{lne,twu}}, \\ \mathbf{N}_{\mathrm{C}} &= \mathbf{C}_{\mathrm{twu}} - \mathbf{D}_{\mathrm{twu,lne}}\mathbf{C}_{\mathrm{lne}}\mathbf{B}_{\mathrm{lne,twu}}.\end{aligned} \tag{3.55}$$

Eliminated Twigs. For current-driven twigs, the corresponding branch current-voltage relations read:

$$\mathbf{u}_{\mathrm{twe}} = \mathbf{R}_{\mathrm{twe}}\mathbf{i}_{\mathrm{twe}} + \mathbf{L}_{\mathrm{twe}}\frac{\mathrm{d}\mathbf{i}_{\mathrm{twe}}}{\mathrm{d}t} \tag{3.56}$$

where $\mathbf{u}_{\mathrm{twe}}$ and $\mathbf{i}_{\mathrm{twe}}$ are the voltage drops and the currents, respectively, for the considered eliminated twigs.

Each of the eliminated twig belongs to a fundamental cutset. The KCL applied to all fundamental cutsets containing the eliminated twigs gives:

$$\mathbf{i}_{\mathrm{twe}} = -\mathbf{D}_{\mathrm{twe,lnu}}\mathbf{i}_{\mathrm{lnu}} - \mathbf{D}_{\mathrm{twe,lni}}\mathbf{i}_{\mathrm{lni}}. \tag{3.57}$$

Substitution of (3.57) into (3.56) leads to:

$$\begin{aligned}\mathbf{u}_{\mathrm{twe}} &= -\mathbf{R}_{\mathrm{twe}}\mathbf{D}_{\mathrm{twe,lnu}}\mathbf{i}_{\mathrm{lnu}} - \mathbf{L}_{\mathrm{twe}}\mathbf{D}_{\mathrm{twe,lnu}}\frac{\mathrm{d}\mathbf{i}_{\mathrm{lnu}}}{\mathrm{d}t} \\ &- \mathbf{R}_{\mathrm{twe}}\mathbf{D}_{\mathrm{twe,lni}}\mathbf{i}_{\mathrm{lni}} - \mathbf{L}_{\mathrm{twe}}\mathbf{D}_{\mathrm{twe,lni}}\frac{\mathrm{d}\mathbf{i}_{\mathrm{lni}}}{\mathrm{d}t}.\end{aligned} \tag{3.58}$$

Now, we apply the KVL to all the fundamental loops containing the eliminated twigs:

$$\mathbf{u}_{\mathrm{lnu}} + \mathbf{B}_{\mathrm{lnu,twu}}\mathbf{u}_{\mathrm{twu}} + \mathbf{B}_{\mathrm{lnu,twe}}\mathbf{u}_{\mathrm{twe}} + \mathbf{B}_{\mathrm{lnu,twi}}\mathbf{u}_{\mathrm{twi}} = \mathbf{0}. \tag{3.59}$$

The voltage drops in the current-driven links are expressed by

$$\mathbf{u}_{\mathrm{lnu}} = \mathbf{R}_{\mathrm{lnu}}\mathbf{i}_{\mathrm{lnu}} + \mathbf{L}_{\mathrm{lnu}}\frac{\mathrm{d}\mathbf{i}_{\mathrm{lnu}}}{\mathrm{d}t}. \tag{3.60}$$

Finally, expressions (3.58) and (3.60) are substituted into (3.59) leading to the transformed fundamental loop equations:

$$\begin{aligned} -\mathbf{N}_{\mathrm{R}}\mathbf{i}_{\mathrm{lnu}} \;-\; & \mathbf{N}_{\mathrm{L}}\frac{\mathrm{d}\mathbf{i}_{\mathrm{lnu}}}{\mathrm{d}t} + \mathbf{D}^{T}_{\mathrm{twu,lnu}}\mathbf{u}_{\mathrm{twu}} = \mathbf{B}_{\mathrm{lnu,twi}}\mathbf{u}_{\mathrm{twi}} \\ -\; & \mathbf{B}_{\mathrm{lnu,twe}}\mathbf{R}_{\mathrm{twe}}\mathbf{D}_{\mathrm{twe,lni}}\mathbf{i}_{\mathrm{lni}} - \mathbf{B}_{\mathrm{lnu,twe}}\mathbf{L}_{\mathrm{twe}}\mathbf{D}_{\mathrm{twe,lni}}\frac{\mathrm{d}\mathbf{i}_{\mathrm{lni}}}{\mathrm{d}t} \end{aligned} \tag{3.61}$$

where the equality $\mathbf{B}_{\mathrm{lnu,twu}} = -\mathbf{D}^{T}_{\mathrm{twu,lnu}}$ is taken into account. The matrices $\mathbf{N}_{\mathrm{R}}$ and $\mathbf{N}_{\mathrm{L}}$ are defined by:

$$\begin{aligned} \mathbf{N}_{\mathrm{R}} &= \mathbf{R}_{\mathrm{lnu}} - \mathbf{B}_{\mathrm{lnu,twe}}\mathbf{R}_{\mathrm{twe}}\mathbf{D}_{\mathrm{twe,lnu}}, \\ \mathbf{N}_{\mathrm{L}} &= \mathbf{L}_{\mathrm{lnu}} - \mathbf{B}_{\mathrm{lnu,twe}}\mathbf{L}_{\mathrm{twe}}\mathbf{D}_{\mathrm{twe,lnu}}. \end{aligned} \tag{3.62}$$

3.4.4 Derivation of the Coupled Formulation

A first transient coupled formulation is derived on the assumption that no eliminated twigs and links occur. In this case, equations (2.61), (3.48a) and (3.48b) are combined and the relations (3.35), (3.42) and the branch current-voltage relations for the capacitors, resistor and inductors are substituted. Finally, known voltage drops and currents supplied by the independent sources are transferred to the right-hand side of the system leading to the following transient field-circuit coupled formulation:

$$\begin{bmatrix} \mathbf{M}_{\sigma} & \mathbf{0} & \mathbf{0} \\ -\mathbf{Q}^{T}\mathbf{M}_{\sigma} & \mathbf{N}_{C} & \mathbf{0} \\ -\mathbf{P}^{T} & \mathbf{0} & -\mathbf{N}_{L} \end{bmatrix} \frac{\mathrm{d}}{\mathrm{d}t} \begin{bmatrix} \widehat{\mathbf{a}} \\ \mathbf{u}_{\mathrm{twu}} \\ \mathbf{i}_{\mathrm{lnu}} \end{bmatrix} + \begin{bmatrix} \widetilde{\mathbf{C}}\mathbf{M}_{\mu^{-1}}\mathbf{C} & -\mathbf{M}_{\sigma}\mathbf{Q} & -\mathbf{P} \\ \mathbf{0} & \mathbf{N}_{G} & \mathbf{D}_{\mathrm{twu,lnu}} \\ \mathbf{0} & \mathbf{D}^{T}_{\mathrm{twu,lnu}} & -\mathbf{N}_{R} \end{bmatrix} \begin{bmatrix} \widehat{\mathbf{a}} \\ \mathbf{u}_{\mathrm{twu}} \\ \mathbf{i}_{\mathrm{lnu}} \end{bmatrix} = \\ = \begin{bmatrix} \mathbf{0} \\ -\mathbf{D}_{\mathrm{twu,lni}}\mathbf{i}_{\mathrm{lni}} \\ \mathbf{B}_{\mathrm{lnu,twi}}\mathbf{u}_{\mathrm{twi}} \end{bmatrix} \tag{3.63}$$

where the capacitance matrix $\mathbf{N}_{\mathrm{C}} = \mathbf{C}_{\mathrm{twu}}$, the conductance matrix $\mathbf{N}_{\mathrm{G}} = \mathbf{G}_{\mathrm{twu}}$, the inductance matrix $\mathbf{N}_{\mathrm{L}} = \mathbf{L}_{\mathrm{lnu}}$ and the resistance matrix $\mathbf{N}_{\mathrm{R}} = \mathbf{R}_{\mathrm{lnu}}$ represent the circuit elements.

In the general situation, when the tree/cotree partitioning procedure leads to the occurrence of the current-driven twigs or/and voltage-driven links, partial cutset/loop transformations are performed. For the eliminated branches, the transformed fundamental cutset and loop equations (3.54) and (3.61) are used instead of equations (3.48a) and (3.48b), respectively. A second transient field-circuit coupled formulation reads:

$$\begin{bmatrix} \mathbf{M}_\sigma & \mathbf{0} & \mathbf{0} \\ -\mathbf{Q}^T\mathbf{M}_\sigma & \mathbf{N}_C & \mathbf{0} \\ -\mathbf{P}^T & \mathbf{0} & -\mathbf{N}_L \end{bmatrix} \frac{\mathrm{d}}{\mathrm{d}t} \begin{bmatrix} \widehat{\mathbf{a}} \\ \mathbf{u}_{\mathrm{twu}} \\ \mathbf{i}_{\mathrm{lnu}} \end{bmatrix} + \begin{bmatrix} \widetilde{\mathbf{C}}\mathbf{M}_{\mu^{-1}}\mathbf{C} & -\mathbf{M}_\sigma\mathbf{Q} & -\mathbf{P} \\ \mathbf{0} & \mathbf{N}_G & \mathbf{D}_{\mathrm{twu,lnu}} \\ \mathbf{0} & \mathbf{D}^T_{\mathrm{twu,lnu}} & -\mathbf{N}_R \end{bmatrix} \begin{bmatrix} \widehat{\mathbf{a}} \\ \mathbf{u}_{\mathrm{twu}} \\ \mathbf{i}_{\mathrm{lnu}} \end{bmatrix} =$$

$$= \begin{bmatrix} \mathbf{0} \\ -\mathbf{D}_{\mathrm{twu,lni}}\mathbf{i}_{\mathrm{lni}} + \mathbf{D}_{\mathrm{twu,lne}}\mathbf{G}_{\mathrm{lne}}\mathbf{B}_{\mathrm{lne,twi}}\mathbf{u}_{\mathrm{twi}} + \mathbf{D}_{\mathrm{twu,lne}}\mathbf{C}_{\mathrm{lne}}\mathbf{B}_{\mathrm{lne,twi}}\frac{\mathrm{d}\mathbf{u}_{\mathrm{twi}}}{\mathrm{d}t} \\ \mathbf{B}_{\mathrm{lnu,twi}}\mathbf{u}_{\mathrm{twi}} - \mathbf{B}_{\mathrm{lnu,twe}}\mathbf{R}_{\mathrm{twe}}\mathbf{D}_{\mathrm{twe,lni}}\mathbf{i}_{\mathrm{lni}} - \mathbf{B}_{\mathrm{lnu,twe}}\mathbf{L}_{\mathrm{twe}}\mathbf{D}_{\mathrm{twe,lni}}\frac{\mathrm{d}\mathbf{i}_{\mathrm{lni}}}{\mathrm{d}t} \end{bmatrix} \quad (3.64)$$

where the circuit elements are represented by the matrices $\mathbf{N}_{\mathrm{C}}$, $\mathbf{N}_{\mathrm{G}}$ and $\mathbf{N}_{\mathrm{L}}$, $\mathbf{N}_{\mathrm{R}}$ specified by (3.55) and (3.62), respectively.

The differential-algebraic system (3.64) represents a general transient field-circuit coupled formulation. The special simplified case described by formulation (3.63) can be easily derived from (3.64).

In the following part of the work, the main properties of system (3.64) are discussed and the application of different classes of time integration schemes is investigated.

Chapter 4

Numerical Integration of Field-Circuit Coupled Problems

4.1 Introduction

This chapter deals with the methods for numerical integration applicable to the transient field-circuit coupled formulation derived in the previous chapter. In Section 4.2, main properties of quasistatic and field-circuit coupled systems are analysed. One-step time integration methods and their characteristics are presented in Section 4.3. In Section 4.4, we discuss the standard classical time integration schemes and apply them for the numerical integration of the coupled field-circuit formulation with linear circuit elements. Section 4.5 introduces Runge-Kutta time integration methods and a technique allowing an adaptive control of the time steps in the process of numerical integration.

4.2 Characteristics of the Transient Quasistatic and Field-Circuit Coupled Systems

There are several important characteristics that are used to describe the properties of the differential equations. The first one is called *stiffness* of a differential equation. For stiff differential equations, explicit integration methods do not work efficiently [43]. Secondly, one differentiates between ordinary differential equations (ODEs) and differential-algebraic equations (DAEs). The DAE system incorporates two type of equations - differential and algebraic equations. The concept of *differential index* is of the great importance in the numerical treatment of the DAEs. According to the definitions given in [44] and [45], the differential index along a solution is the minimum number of differentiations of the DAE system which would be required to transform the algebraic part of the DAE system into an ODE form. The notion of the differential index is introduced to characterize the structure of the algebraic part of the DAE and to choose an appropriate method for numerical integration.

The electro- and magnetoquasistatic formulations (2.59) and (2.61) as well as a field-circuit transient formulation (3.64) can be written in the following form:

$$\mathbf{M}\frac{\mathrm{d}}{\mathrm{d}t}\mathbf{x}(t) + \mathbf{K}\mathbf{x}(t) = \mathbf{r}(t) \tag{4.1}$$

where the corresponding system unknowns are composed into a vector $\mathbf{x}$. The matrices $\mathbf{M}$ and $\mathbf{K}$ are square matrices of real-valued numbers and t is a real-valued variable denoting the time. System (4.1) represents a system of equations with linear coefficients.

For a nonsingular system matrix $\mathbf{M}$, system (4.1) can be written in the explicit form

$$\frac{\mathrm{d}}{\mathrm{d}t}\mathbf{x}(t) = \mathbf{M}^{-1}(\mathbf{r}(t) - \mathbf{K}\mathbf{x}(t)) \tag{4.2}$$

which represents a system of ODEs.

In the presence of a singular matrix $\mathbf{M}$, the conversion of (4.1) into (4.2) is not possible and one speaks about a system of DAEs. A DAE written in the form (4.1) represents a particular case of the general *fully implicit* linear[1] time varying DAE given by

$$\mathbf{M}(t)\frac{\mathrm{d}}{\mathrm{d}t}\mathbf{x}(t) + \mathbf{K}(t)\mathbf{x}(t) = \mathbf{r}(t). \tag{4.3}$$

The separation of the algebraic and differential constituents in (4.3) leads to the DAE in the semi-explicit form:

$$\begin{aligned} \frac{\mathrm{d}}{\mathrm{d}t}\mathbf{x}_1(t) \quad + \quad & \mathbf{A}_{11}(t)\mathbf{x}_1(t) + \mathbf{A}_{12}(t)\mathbf{x}_2(t) = \mathbf{r}_1(t) \\ & \mathbf{A}_{21}(t)\mathbf{x}_1(t) + \mathbf{A}_{22}(t)\mathbf{x}_2(t) = \mathbf{r}_2(t). \end{aligned}$$

For the linear constant coefficient DAE system (4.1), the matrix $\lambda\mathbf{M} + \mathbf{K}$ where λ is a complex parameter, is called the *matrix pencil*. If the determinant of $\lambda\mathbf{M} + \mathbf{K}$, denoted as $det(\lambda\mathbf{M} + \mathbf{K})$, is not identically zero for at least one value of λ, then the pencil is said to be *regular*. It is rather difficult to elaborate a solvability criterium for DAEs in the general form, but for (4.1) there is a convenient characterization. It states that the linear constant coefficient DAE (4.1) is solvable if and only if its matrix pencil $\lambda\mathbf{M} + \mathbf{K}$ is a regular matrix [44]. Consequently, if consistent initial conditions are specified, system (4.1) has a unique solution only in the case of nonsingular matrix pencil.

Since in electroquasistatic formulations the permittivity ε never equals zero, the matrix $\mathbf{M} = \widetilde{\mathbf{S}}\mathbf{M}_\varepsilon\mathbf{G}$ in (2.59) is a regular matrix. As a consequence, the electroquasistatic formulation (2.59) represents a linear constant coefficient ODE system.

In magnetoquasistatic formulations, the conductivity σ equals zero for the parts of the model filled with non-conductive materials. In this case, the diagonal matrix $\mathbf{M} = \mathbf{M}_\sigma$ contains zero entries and is therefore singular. Then, system (2.61) represents a linear constant coefficient index 1 DAE system.

[1]The general fully-implicit nonlinear DAE, which is, however, not discussed here, reads: $\mathbf{F}(t,\mathbf{x},\mathbf{x}')=\mathbf{0}$.

Since transient field-circuit coupled formulation (3.64) incorporates the magneto-quasistatic equation (2.61), it also constitutes a linear constant coefficient index 1 DAE system.

4.3 General Properties of One-Step Time Integration Methods

In the context of this work, the numerical integration of transient formulations described by system (4.1) is implemented with one-step time integration methods. In the present chapter, a brief review of the main characteristics and properties of such methods is given.

Consider the numerical solution of the initial value problem for an ODE given in the explicit form:

$$\frac{\mathrm{d}}{\mathrm{d}t}x(t) = f(t, x),\ x(t_0) = x_0 \tag{4.4}$$

in the time interval $\Omega_t = [t_0, t_N] \subset R$. We denote by $t_0 < t_1 < \ldots < t_N$ gridpoints in the interval Ω_t and by x_{n+1} approximations to the solution $x(t_{n+1})$. For the sake of simplicity, only equidistant time grids are considered, i.e., $t_n = t_0 + nh,\ n = 0, \ldots, N$ and $t_N - t_0 = Nh$, but the theory also remains valid for non-equidistant time grids. Two *evolution operators* are applied: a continuous operator Φ of an equation (4.4) defined as $x(t) = \Phi^{t,t_0}x(t_0)$ and a corresponding discrete evolution operator Ψ defined as $x_{n+1} = \Psi^{t_{n+1},t_n}x_n$ [46].

The integration of equation (4.4) leads to the following integral equation:

$$x_{n+1} = x_n + \int_{t_n}^{t_{n+1}} f(\tau, x(\tau))\mathrm{d}\tau. \tag{4.5}$$

Numerical integration is the approximate computation of the integral in (4.5) using numerical techniques. Time integration methods fall into two categories: those which use only *one* starting value at each integration step are called *one-step* methods and those which are based on *several* values of the solution calculated at the previous time instants are called *multistep* methods [47].[2]

Numerical time integration methods are further subdivided into *explicit* and *implicit* ones. For the explicit time integration methods, the discrete evolution operator Ψ can be written in the form

$$\Psi = x_n + h\psi(t_n, x_n, h) \tag{4.6a}$$

where the *increment function* ψ is calculated using the already available value of x_n. It means that the numerical approximation x_{n+1} to the solution $x(t_{n+1})$ can

[2]The multistep time integration methods are not considered in this work.

be calculated explicitly using (4.6a). For an implicit time integration method, the discrete evolution operator Ψ has the form

$$\Psi = x_n + h\psi(t_n, x_n, t_{n+1}, x_{n+1}, h) \tag{4.6b}$$

which means that the approximation x_{n+1} can only be obtained by solving the system of equations described by (4.6b).

There are two types of *errors* associated with any method for numerical integration:

1. The *local (or consistency) discretization error* is the error accumulated after one integration step:

$$\epsilon_l(t, x, h) = \Phi^{t+h,t}x - \Psi^{t+h,t}x. \tag{4.7}$$

2. The *global discretization error* is the error of the computed solution after several integration steps due to the accumulated local errors:

$$\epsilon_g(t_n) = \Phi^{t_n,t_0} - x_n. \tag{4.8}$$

Consistency. A one-step time integration method is called *consistent* if, under assumption that $x_n = x(t_n)$, the local discretization error satisfies:

$$\epsilon_l(t, x, h) = \mathcal{o}(h) \quad \text{for} \quad h \to 0$$

where $\mathcal{o}$ is the Landau symbol.[3] The comparison of the Taylor expansions of $\Phi^{t+h,t}x$ and $\Psi^{t+h,t}x$ at $h = 0$ leads to an alternative definition of consistency: the discrete evolution Ψ is consistent if it has the form

$$\Psi^{t+h,t}x = x + h\psi(t, x, h), \quad \text{where} \quad \psi(t, x, 0) = f(t, x), \tag{4.9}$$

involving some continuous increment function ψ of h. Thus, statement (4.9) represents a useful criterium allowing to determine whether an integration method is consistent or not.

A discrete evolution operator Ψ has *consistency order* p if the local error satisfies:

$$\epsilon_l(t, x, h) = \mathcal{O}(h^{p+1}), \tag{4.10}$$

i.e., if the Taylor series for the exact solution and the Taylor series for the approximated one coincide up to (and including) the term h^p. The Landau symbol $\mathcal{O}$ is used to describe the asymptotic behavior of functions.[4]

Stability. A one-step time integration method is said to be *stable* if for two arbitrary solutions x and $\tilde{x}$, there exists a Lipschitz constant L such that

$$|\Psi^{t_{n+1},t_n}x - \Psi^{t_{n+1},t_n}\tilde{x}| \leq L|x - \tilde{x}| \tag{4.11}$$

[3] For two functions $f(x)$ and $g(x)$ defined on some subset of the real numbers, we write $f(x) = \mathcal{o}(g(x))$ if and only if for every $C > 0$ there exists a real number N such that for all $x > N$ we have $|f(x)| < C|g(x)|$; if $g(x) \neq 0$ this is equivalent to $\lim_{x\to\infty} \frac{f(x)}{g(x)} = 0$.

[4] We write $f(x) = \mathcal{O}(g(x))$ for $x \to \infty$ if and only if there exist constants N and C such that $|f(x)| \leq C|g(x)|$ for all $x > N$.

Convergence. A one-step time integration method *converges* to the exact solution if for sufficiently small timesteps the global error satisfies:

$$\max_{t\in[t_0,T]} \epsilon_g(t) = o(h). \tag{4.12}$$

The *convergence is of order p* if

$$\max_{t\in[t_0,T]} \epsilon_g(t) = \mathcal{O}(h^p). \tag{4.13}$$

For one-step time integration methods, a consistency of order p implies the convergence of the method of order p [46].

Stability Characteristics. In this part of the work, we address the question when and for which step sizes h the stability of a continuous problem is inherited by the chosen method of numerical integration.

Consider a test linear initial value problem

$$\frac{\mathrm{d}}{\mathrm{d}t}\mathbf{x}(t) = \mathbf{A}\mathbf{x}(t) \tag{4.14}$$

having a solution $\mathbf{x}(t) = e^{\mathbf{A}t}$. The test equation (4.14) has a stable solution if the maximum real parts of the eigenvalues of $\mathbf{A}$ satisfy the condition $max_\lambda \Re\{\lambda\} \leq 0$ and the eigenvalues with $\Re\{\lambda\} = 0$ are simple ones.[5]

A one-step method for numerical integration, $\mathbf{x}_{n+1} = \Psi^h \mathbf{x}_n$, inherits the stability of the solution of the test problem (4.14) when the spectral radius ρ of the increment operator Ψ^h satisfies the condition $\rho(\Psi^h) \leq 1$ and its eigenvalues μ of modulus $|\mu| = 1$ satisfy certain additional conditions [46]. A matrix exponential function is approximated using a rational function $R(h\mathbf{A})$, which specifies the spectral radius $\rho(\Psi^h)$ using the eigenvalues of matrix $\mathbf{A}$ in the following way:

$$\rho(\Psi^h) = \max_{\lambda\in\sigma(A)} |R(h\lambda)|. \tag{4.15}$$

The rational function $R(h\lambda)$ is called the *stability function* of the integration method. For stability inheritance, only time steps h are applicable for which $|R(h\lambda)| \leq 1$ for all eigenvalues $\lambda \in \sigma(\mathbf{A})$. Thus, the set

$$S = \{z \in \mathbb{C} : |R(z)| \leq 1\} \tag{4.16}$$

with $z = h\lambda$ represents the *region of absolute stability* of the time integration method.

A method whose stability domain satisfies

$$S \supset \mathbb{C}^- = \{z \in \mathbb{C} : \Re(z) \leq 0\} \tag{4.17}$$

[5] Test equation (4.14) has been introduced by Dahlquist. In spite of its simplicity, equation (4.14) was readily acknowledged of being of major importance for the stability analysis of numerical time integration methods for ODE.

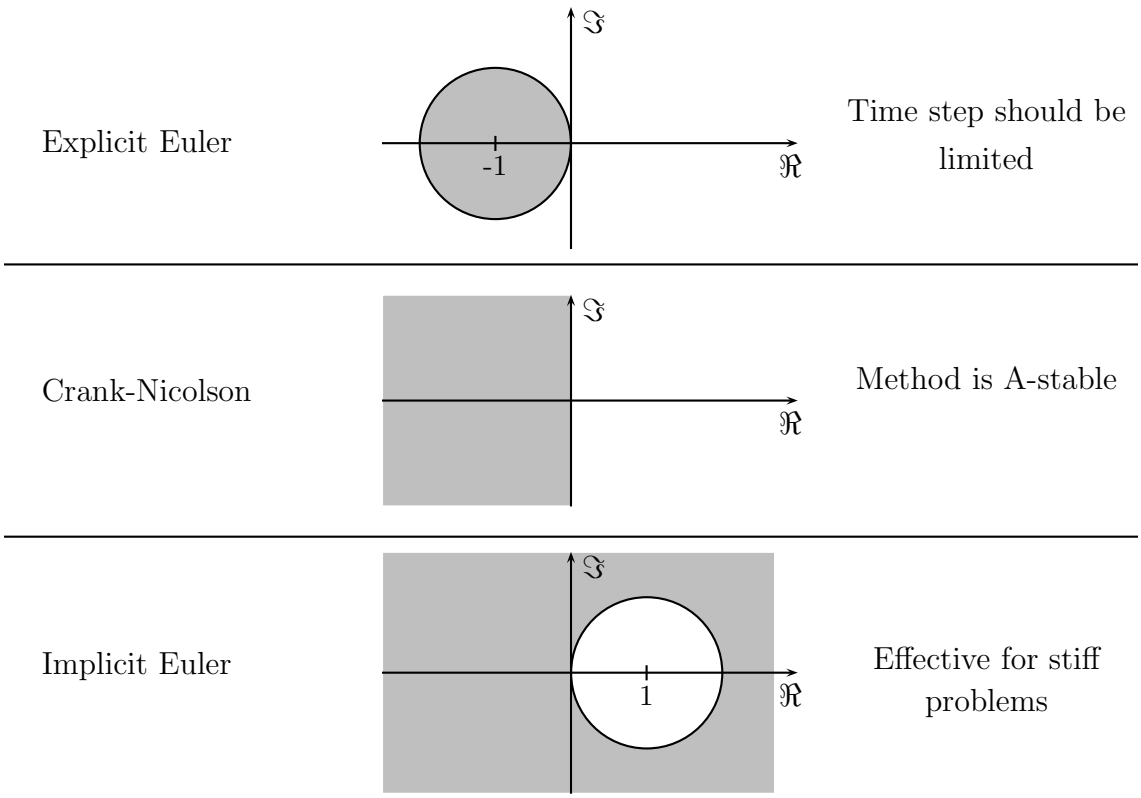

Figure 4.1: The regions of the absolute stability (gray areas) for some one-step time integration methods.

is called *A-stable*. If the region of absolute stability S represents a sector having an angle α located entirely in the negative complex half-plane, the corresponding integration method is called $A(\alpha)$-stable. A-stability is an important property for stiff problems.[6] The regions of absolute stability for some one-step time integration methods are illustrated in Fig. 4.1. Explicit one-step time integration methods always have bounded regions of absolute stability, while implicit methods are often A-stable.

Concept of Stiffness. Estimation (4.13) shows how the global discretization error improves when a sufficiently small step size is further decreased. However, it does not allow to conclude how small the step size has to be to guarantee a reasonable accuracy. The reason for this is the fact that the estimation (4.13) contains an unknown constant. It is evident, that if for some problem the best possible constant in the estimate (4.13) is too large, then the convergence result loses its value, since it is not possible in practice to work with arbitrarily small time steps.

The answer to the question "How large the constant in the estimation (4.13) can become?" leads to the concept of the *stiffness* of a differential equation. There are initial value problems for which explicit one-step integration methods require extremely small time steps and, as a consequence, a lot of computational effort making the integration process highly ineffective. Such problems are called *stiff*

[6]The concept of A-stability is introduced by Dahlquist in 1963.

in the literature. Whenever a nonstiff integration method encounters stiffness, the product of the step size with the dominant eigenvalue of matrix **A** lies near the border of the stability domain [43]. For stiff problems, the eigenvalues of the matrix **A** differ significantly in magnitude. Since DAE systems possess zero eigenvalues, they also belong to the class of stiff problems. For A-stable methods, the stepsize is never restricted by stability, regardless of the stiffness. The problems for which one-step explicit time integration methods work rather effective in practice, are called *nonstiff*. Thus, according to [46], not the problem class leads to a choice of methods, but the class of methods classifies the problems under stiff and nonstiff ones.

There are time integration methods with a rational stability function $R(z)$, for which A-stability is not as desirable as it seems to be, because for z being real and very negative, $|R(z)|$ is less than 1 but very close to 1. As a consequence, the stiff components are damped out very slowly. However, in some situations it may be desirable to damp the very stiff components of the numerical solution. This motivates the following definition: a method is said to be *L-stable* if it is A-stable and if in addition

$$\lim_{z\to\infty} R(z) = 0. \tag{4.18}$$

This property is sometimes called *stiff A-stability* or *strong A-stability*.

It is worth noting the stability hierarchy:

$$\boxed{\textit{L-stability} \longrightarrow \textit{A-stability} \longrightarrow \textit{A}(\alpha)\textit{-stability}}$$

Several one-step integration methods suffer from a severe order reduction when they are applied for the numerical integration of stiff problems and DAEs. The order reduction does, however, not occur for so-called *stiffly accurate methods*. Therefore these methods are particularly suited for solving index 1 DAEs and stiff initial value problems. Most of the Runge-Kutta methods[7] for stiff problems are stiffly accurate [48], [49].

4.4 Classical Time Integration Schemes

In the present section we consider the application of classical one-step time integration schemes of θ-type to the coupled field-circuit transient formulation derived in the previous chapter. In Subsection 4.4.1, a general formulation of θ-type time integration methods is given. In Subsection 4.4.2, a derived transient field-circuit coupled formulation (3.64) is discretized with a θ-type time integration scheme. Subsection 4.4.3 introduces numerical examples illustrating the application of θ-type time integration methods for the numerical integration of equations arising from the combined simulation of electromagnetic fields and electrical circuits.

[7] Runge-Kutta time integration methods are discussed in the following sections.

4.4.1 θ-Type Time Integration Schemes

Consider the following time integration method applied to the differential equation (4.4):

$$x_{n+1} = x_n + (1-\theta)hf(t_n, x_n) + \theta h f(t_{n+1}, x_{n+1}) \tag{4.19}$$

with parameter $\theta \in [0,1]$. For any $\theta > 0$ this method is implicit since the new approximation is given by an implicit algebraic relation. This method is known under the name of θ-method. If we take $\theta = 0$, (4.19) represents the *explicit Euler* method or the *forward Euler* method. Among the infinite set of choices, $\theta = 1/2$, $\theta = 2/3$ and $\theta = 1$ are often used. The method with $\theta = 1/2$ is called the *trapezoidal rule* or the *Crank-Nicolson method*, on the analogy of the quadrature trapezoidal rule for integrals. The method with $\theta = 2/3$ is called the Galerkin method and $\theta = 1$ gives the *implicit Euler* or the *backward Euler* method.

Stability of the θ-Method. For the test problem (4.14), the application of the θ-method gives an approximation [50]:

$$\mathbf{x}_{n+1} = R(h\mathbf{A})\mathbf{x}_n, \quad \text{with} \quad R(z) = \frac{1+(1-\theta)z}{1-\theta z}. \tag{4.20}$$

Using a maximum modulus theorem[8] it can be shown that the θ-methods are A-stable for $\theta \geq 1/2$. The value of $\theta = 1$ gives the only L-stable method in the family of the time integration schemes of θ-type. The stability regions for $\theta = 0, 1/2, 1$ are plotted in Fig. 4.1.

4.4.2 Field-Circuit Coupled Formulation Discretized with a θ-Scheme

A time discretization for the linear coefficient system (4.1) implemented with a θ-method reads:

$$\frac{1}{h}\mathbf{M}(\mathbf{x}_{n+1} - x_n) + \mathbf{K}(\theta\mathbf{x}_{n+1} + (1-\theta)\mathbf{x}_n) = \theta\mathbf{r}(t_{n+1}) + (1-\theta)\mathbf{r}(t_n) \tag{4.21}$$

where h is the time step. For system (4.1) involving a singular matrix $\mathbf{M}$, system (4.1) is formally multiplied with $\mathbf{M}^{-1}$. Then the θ-type discretization scheme is applied and the resulting formula is finally multiplied with $\mathbf{M}$.

The components in the formula (4.21) are rearranged leading to the following linear system of equations:

$$\left(\frac{\mathbf{M}}{h} + \theta\mathbf{K}\right)\mathbf{x}_{n+1} = \left(\frac{\mathbf{M}}{h} - (1-\theta)\mathbf{K}\right)\mathbf{x}_n + \theta\mathbf{r}_{n+1} + (1-\theta)\mathbf{r}(t_n). \tag{4.22}$$

[8] Let φ be a non-constant complex function which is analytic on a set $D \subset \mathbb{C}$ and continuous on its closure. The maximum modulus theorem states, that the maximum of $|\varphi(z)|$ on D is assumed on the boundary of D and not in the interior. In particular, if φ is a rational function without poles in $\mathbb{C}^-$ then $\max_{z\in\mathbb{C}^-} |\varphi(z)| = \max_{y\in\mathbb{R}^-} |\varphi(iy)|$ [50].

Thus, the update of the solution in the next time instant is realized through the solution of the linear system (4.22).

The matrix $\mathbf{M}/h + \theta\mathbf{K}$ is involved in the solution of system (4.22). One obvious condition is that it must be invertible, i.e., nonsingular. As we have mentioned in Section 4.2, the study of DAE systems of form (4.1) involves the matrix pencil $\lambda\mathbf{M} + \mathbf{K}$ of matrices $\mathbf{M}$ and $\mathbf{K}$ where λ is an arbitrary parameter. If the matrix pencil is not a regular matrix, it is impossible to find a step length h and a value of θ so that $\mathbf{M}/h + \theta\mathbf{K}$ is not singular [51]. For a regular matrix pencil $\lambda\mathbf{M} + \mathbf{K}$, matrices $\mathbf{A}_1$ and $\mathbf{A}_2$ can be found such that:

$$\begin{aligned} \mathbf{M}^* &= \mathbf{A}_1\mathbf{M}\mathbf{A}_2 = diag(\mathbf{I}, \mathbf{J}) \\ \mathbf{K}^* &= \mathbf{A}_1\mathbf{K}\mathbf{A}_2 = diag(\mathbf{W}, \mathbf{I}) \end{aligned} \tag{4.23}$$

where "diag" denotes a square matrix constructed from the argument square matrices placed on its diagonal, $\mathbf{I}$ is a unit matrix of the suitable dimension, $\mathbf{W}$ is a regular square matrix, and $\mathbf{J}$ is a nilpotent Jordan block matrix with blocks of the form [51]:

$$\begin{bmatrix} 0 & 0 & \dots & 0 \\ 1 & 0 & \dots & 0 \\ \vdots & \vdots & \ddots & \vdots \\ 0 & 0 & 1 & 0 \end{bmatrix}. \tag{4.24}$$

The size of the largest of these block is the *nilpotency* of the system.[9] Introducing the notation $\mathbf{x}^* = \mathbf{A}_2^{-1}\mathbf{x}$ and $\mathbf{r}^* = \mathbf{A}_1\mathbf{r}$, we can rewrite system (4.1) in the *Kronecker normal form* [51]:

$$\begin{aligned} \dot{\mathbf{x}}_1 + \mathbf{W}\mathbf{x}_1 &= \mathbf{r}_1 \\ \mathbf{J}\dot{\mathbf{x}}_2 + \mathbf{x}_2 &= \mathbf{r}_2 \end{aligned} \tag{4.25}$$

where $\mathbf{x}^* = [\mathbf{x}_1, \mathbf{x}_2]^T$ and $\mathbf{r}^* = [\mathbf{r}_1, \mathbf{r}_2]^T$. The numerical behaviour of a DAE system depends on the nilpotency. If the nilpotency is greater than one, the system is rather difficult to solve. For systems having a nilpotency of one, i.e., when $\mathbf{J}$ is identically equal to zero, the system is easy to solve and classical integration methods for ODEs can be used [51].

In the case of the magnetodynamic and field-circuit coupled systems, two kinds of equations must be considered. The first kind are the equations corresponding to the conducting region. Such equations do not influence the nilpotency of the system, since they give nonzero entries on the diagonal of matrix $\mathbf{M}$. The second kind are equations corresponding to the nonconducting regions. These equations

[9] Alternatively, the nilpotency of a matrix $\mathbf{J}$ is defined as a largest integer m so that $J^m = 0$ but $J^{m-1} \neq 0$.

do not have any differential term, they are purely algebraic and their contributions to the matrix $\mathbf{M}$ are zero lines. Obviously, they lead to a system of nilpotency 1. Therefore, classical methods described with the scheme (4.22) may be used. However, if the explicit Euler method is applied, the singular matrix $\mathbf{M}/h$ becomes the system matrix and the solution is impossible. Generally, purely explicit methods are not applicable to solve (4.1) since they involve singular matrices and implicit time integrators should be used [51].

The application of (4.22) to the general field circuit-coupled formulation (3.64) gives the following update scheme:

$$\begin{bmatrix} \frac{1}{\theta h^2}\mathbf{M}_\sigma + \frac{1}{h}\widetilde{\mathbf{C}}\mathbf{M}_{\mu^{-1}}\mathbf{C} & -\frac{1}{h}\mathbf{M}_\sigma\mathbf{Q} & -\frac{1}{h}\mathbf{P} \\ -\frac{1}{h}\mathbf{Q}^T\mathbf{M}_\sigma & \frac{1}{h}\mathbf{N}_C + \theta\mathbf{N}_G & \theta\mathbf{D}_{\text{twu,lnu}} \\ -\frac{1}{h}\mathbf{P}^T & \theta\mathbf{D}^T_{\text{twu,lnu}} & -\frac{1}{h}\mathbf{N}_L - \theta\mathbf{N}_R \end{bmatrix} \begin{bmatrix} \widehat{\mathbf{a}} \\ \mathbf{u}_{\text{twu}} \\ \mathbf{i}_{\text{lnu}} \end{bmatrix}_{n+1}$$

$$= \begin{bmatrix} \frac{1}{\theta h^2}\mathbf{M}_\sigma + \frac{\theta-1}{\theta h}\widetilde{\mathbf{C}}\mathbf{M}_{\mu^{-1}}\mathbf{C} & -\frac{\theta-1}{\theta h}\mathbf{M}_\sigma\mathbf{Q} & -\frac{\theta-1}{\theta h}\mathbf{P} \\ -\frac{1}{h}\mathbf{Q}^T\mathbf{M}_\sigma & \frac{1}{h}\mathbf{N}_C + (\theta-1)\mathbf{N}_G & (\theta-1)\mathbf{D}_{\text{twu,lnu}} \\ -\frac{1}{h}\mathbf{P}^T & (\theta-1)\mathbf{D}^T_{\text{twu,lnu}} & -\frac{1}{h}\mathbf{N}_L - (\theta-1)\mathbf{N}_R \end{bmatrix} \begin{bmatrix} \widehat{\mathbf{a}} \\ \mathbf{u}_{\text{twu}} \\ \mathbf{i}_{\text{lnu}} \end{bmatrix}_n + \begin{bmatrix} \mathbf{0} \\ \theta\mathbf{r}_1(t_{n+1}) \\ \theta\mathbf{r}_2(t_{n+1}) \end{bmatrix} + \begin{bmatrix} \mathbf{0} \\ (1-\theta)\mathbf{r}_1(t_n) \\ (1-\theta)\mathbf{r}_2(t_n) \end{bmatrix} \quad (4.26)$$

where the right hand side functions $\mathbf{r}_1(t)$ and $\mathbf{r}_2(t)$ are defined as

$$\mathbf{r}_1(t) = -\mathbf{D}_{\text{twu,lni}}\mathbf{i}_{\text{lni}}(t) + \mathbf{D}_{\text{twu,lne}}\mathbf{G}_{\text{lne}}\mathbf{B}_{\text{lne,twi}}\mathbf{u}_{\text{twi}}(t) + \mathbf{D}_{\text{twu,lne}}\mathbf{C}_{\text{lne}}\mathbf{B}_{\text{lne,twi}}\frac{\mathrm{d}\mathbf{u}_{\text{twi}}(t)}{\mathrm{d}t}$$

$$\mathbf{r}_2(t) = \mathbf{B}_{\text{lnu,twi}}\mathbf{u}_{\text{twi}}(t) - \mathbf{B}_{\text{lnu,twe}}\mathbf{R}_{\text{twe}}\mathbf{D}_{\text{twe,lni}}\mathbf{i}_{\text{lni}}(t) - \mathbf{B}_{\text{lnu,twe}}\mathbf{L}_{\text{twe}}\mathbf{D}_{\text{twe,lni}}\frac{\mathrm{d}\mathbf{i}_{\text{lni}}(t)}{\mathrm{d}t}.$$

In formulation (4.26), the symmetry of the matrix pencil $[\frac{\mathbf{M}}{h} + \theta\mathbf{K}]$ is restored by multiplying the field equation block by the scalar factor $1/(\theta h)$.

4.4.3 Numerical Examples

In this part of the work, θ-type integration methods are applied for the numerical treatment of solid and stranded conductor models represented by the formulations (3.36) and (3.43), respectively. A test model consists of a conductive ring (Fig. 4.2a) which is either treated as a current-driven solid conductor (Fig. 4.2b) or a voltage-driven stranded conductor (Fig. 4.2c). The excitations of the independent sources are $I_{\text{sol}}(t) = I_{\max}\sin(\omega t)$ and $U_{\text{str}}(t) = U_{\max}\cos(\omega t)$.

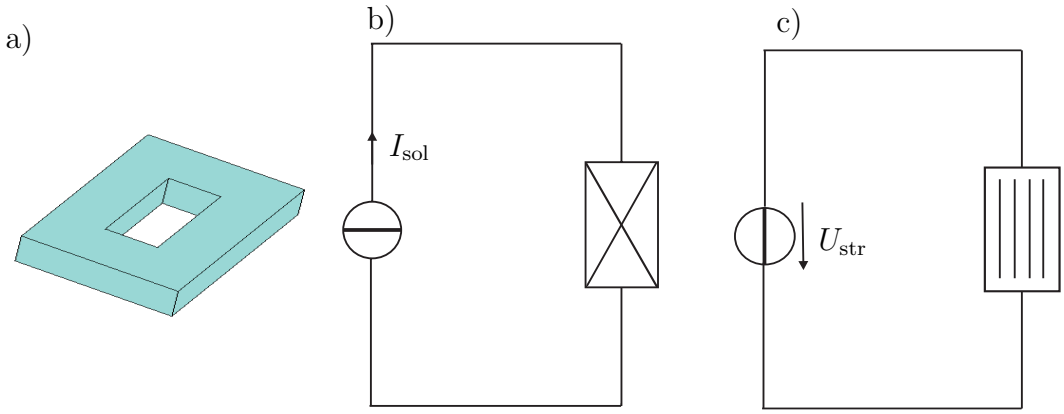

Figure 4.2: (a) Conductive ring; electrical circuit models with (b) solid conductor and (c) stranded conductor.

Due to the mixed nature of the circuit formulation, the application of the θ-method leads to an indefinite system of equations. Therefore, for reasons of numerical stability, the transient formulation is turned into its positive semi-definite equivalent obtained by eliminating the circuit equations (in a Schur complement). The θ-method (for the values of $\theta = 1, 2/3, 1/2$) is then performed only for the magnetic vector potential unknowns $\widehat{\mathbf{a}}$ followed by the update of the circuit degrees of freedom with the corresponding Schur complement. The simulated currents and voltage drops are shown in Fig. 4.3-4.5.

For coupled formulation (3.43), system (3.45) can be used as an auxiliary one to obtain an analytical solution. Hence, the estimation of the absolute error can be performed during the computation.

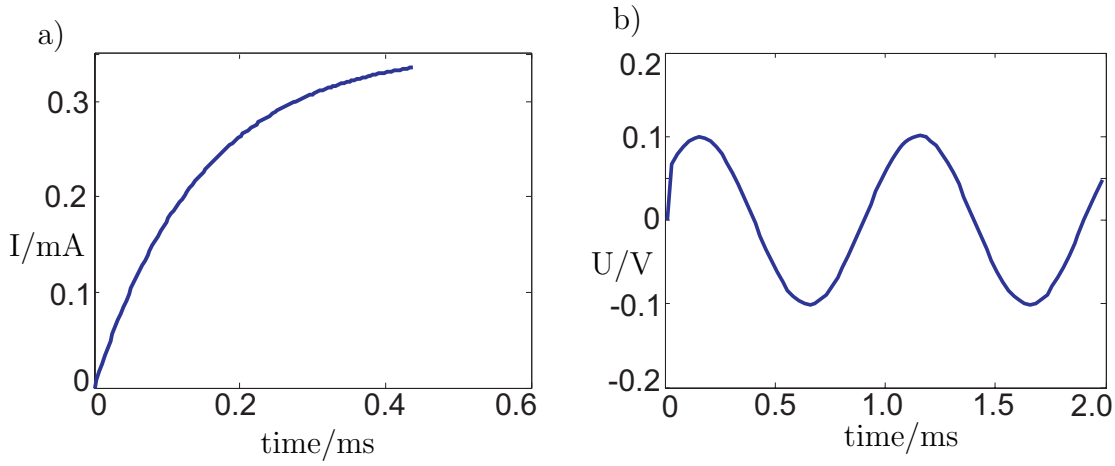

Figure 4.3: Implicit Euler method: (a) calculated current for the stranded conductor and (b) calculated voltage for the solid conductor.

For formulation (3.36) describing the solid conductor, an analytical solution can not be derived. However, a special approach to check the obtained solution can

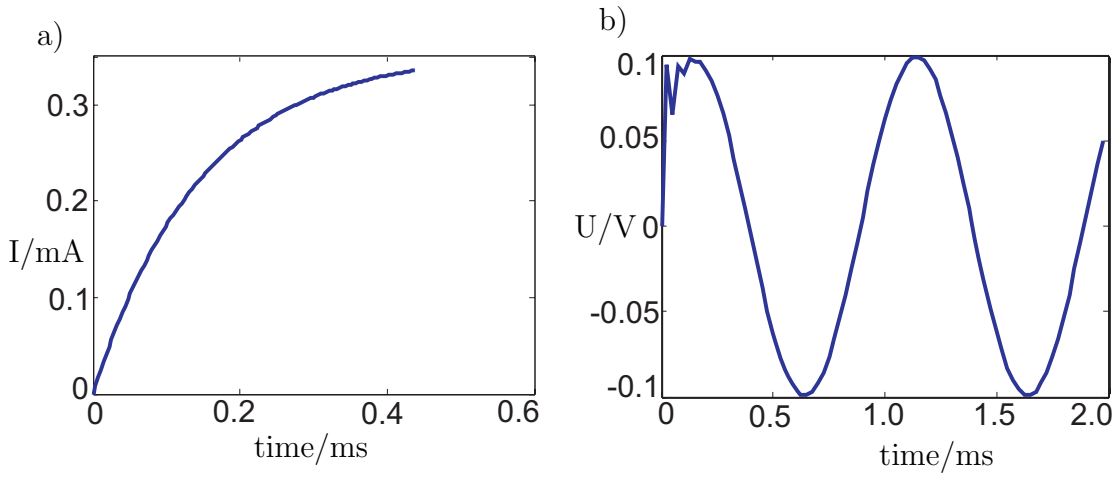

Figure 4.4: Galerkin method: (a) calculated current for the stranded conductor and (b) calculated voltage for the solid conductor.

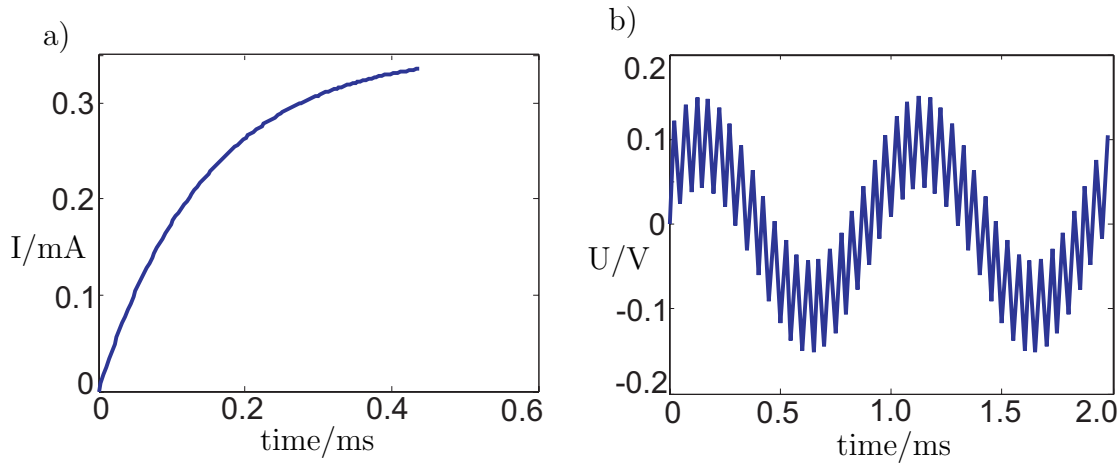

Figure 4.5: Crank-Nicolson method: (a) calculated current for the stranded conductor and (b) calculated voltage for the solid conductor.

be proposed where a frequency-domain equivalent of the treated transient formulation (3.36) is used. Afterwards, the voltage-current relation is derived from this frequency-domain formulation. This relation can be treated as a phasor equivalent of Ohm's law for some electrical circuit the admittance of which serves as the constant of proportionality between the phasor quantities of the applied current excitation and the obtained voltage response. This proportionality constant accounts for the circuit containing a conductor and a capacitor connected in parallel. Therefore, according to electrical circuit theory, a situation when the applied current leads the response voltage should be observed. The reference values for the phasor angle and the amplitude of the response can be calculated and then compared with the ones obtained by numerical integration. Hence, in this case the time-integrated simulation results can only be compared to analytical data starting from that time instant when the transient phenomenon has vanished.

From the simulation results presented in Fig. 4.3-4.5, it is observed that only the implicit Euler method and the Galerkin method are suitable time integration methods for field-circuit coupled problems. The Crank-Nicolson method shows high oscillations in the solution and is found to be unreliable for these type of simulations [13].

4.5 Runge-Kutta Time Integration Methods

The test examples of the previous section demonstrate that the classical θ-type methods can suffer from the stability problems when they are applied for the numerical integration of field-circuit coupled formulations. The point here is that the FIT discretization of the magnetodynamic part of the model and its following coupling with external circuits leads to large differential-algebraic systems of equations that cannot be treated numerically like regular ordinary differential equations [51]. Since they are index 1 problems, they should be treated by implicit time integration schemes, e.g., by *implicit Runge-Kutta-type* methods. Their realization also makes it possible to implement adaptive time-stepping within the integration process which effectively reduces the CPU time.

4.5.1 General Properties and Terminology

Consider first an integral equation obtained from the first order ordinary differential equations $\dot{x}(t) = f(t, x)$

$$x_{n+1} = x_n + \int_{t_n}^{t_{n+1}} f(\tau, x(\tau))d\tau. \tag{4.27}$$

The idea of a Runge-Kutta method is to approximate function $f(\tau, x(\tau))$ with an interpolation polynomial function of degree s having the nodes $c_i \in [0, 1], i = 1, \ldots, s$. If a *weight vector* $b_i, i = 1, \ldots, s$ is applied in a way that

$$\int_{t_n}^{t_{n+1}} f(\tau, x(\tau))d\tau \approx h \sum_{i=1}^{s} b_i f(t_n + c_i h, x(t_n + c_i h)) \tag{4.28}$$

then we obtain classical integration schemes as described in the previous subsection. In Runge-Kutta methods, however, auxiliary intermediate values have to be computed to approximate the values of $f(t_n + c_i h, x(t_n + c_i h))$. They are computed recursively and serve to obtain a sufficiently high accuracy of the current approximation x_{n+1}. To deduce the formula for these intermediate approximations, we consider the following integral equation

$$f(t_n + c_i h, x(t_n + c_i h)) = f\left(t_n + c_i h, x_n + \int_{t_n}^{t_n + c_i h} f(\tau, x(\tau))dt\right) \tag{4.29}$$

and approximate the integral appearing in this formula with a quadrature formula built using the same nodes c_i but with new weight coefficients a_{ij}:

$$\int_{t_n}^{t_n+c_ih} f(\tau, x(\tau))dt \approx h\sum_{j=1}^{s} a_{ij} f(t_n + c_ih, x(t_n + c_ih)).$$

The values $X'_{n,i} := f(t_n + c_ih, x(t_n + c_ih))$ and $X_{n,i} = x_n + h\sum_{j=1}^{s} a_{ij}X'_{n,j}$ are called *stage derivatives* and *stage values*, respectively, and serve as the approximations to the derivative and to the solution of the differential equation at the time instants $t_n + c_ih$.

For every integration time step in the Runge-Kutta method, the solutions of s (non)linear equations should be computed delivering either the stage values $X_{n,i}$

$$X_{n,i} = x_n + h\sum_{j=1}^{s} a_{ij} f(t_n + c_jh, X_{n,j}), \quad i = 1, \ldots, s \tag{4.30}$$

or the stage derivatives $X'_{n,i}$

$$X'_{n,i} = f(t_n + c_jh, x_n + h\sum_{j=1}^{s} a_{ij}X'_{n,j}), \quad i = 1, \ldots, s. \tag{4.31}$$

The update of the solution is then implemented as

$$x_{n+1} = x_n + h\sum_{i=1}^{s} b_i f(t_n + c_jh, X_{n,i}) = x_n + h\sum_{i=1}^{s} b_iX'_{n,i}. \tag{4.32}$$

The coefficients of the Runge-Kutta method are usually collected in a so-called Butcher table:

$$\begin{array}{c|cccc} c_1 & a_{11} & a_{12} & \ldots & a_{1s} \\ c_2 & a_{21} & a_{22} & \ldots & a_{2s} \\ \vdots & \vdots & \vdots & \ddots & \vdots \\ c_s & a_{s1} & a_{s2} & \ldots & a_{ss} \\ \hline & b_1 & b_2 & \ldots & b_s \\ \hline & \hat{b}_1 & \hat{b}_2 & \ldots & \hat{b}_s \end{array} . \tag{4.33}$$

In this table, the components of vector $\mathbf{c}$ are called the *abscissae*. Vector $\mathbf{b}$ represents a weight vector and $\mathbf{A}$ is a matrix specifying the method. The introduction of the second weight vector is necessary to construct an embedded Runge-Kutta method.[10]

[10]Embedded Runge-Kutta methods are discussed below in the section.

The Runge-Kutta methods may be sorted according to the structure of $\mathbf{A} = [a_{ij}]$ matrix in the Butcher table (4.33). The classical explicit methods are the methods for which $a_{ij} = 0$ for $j \geq i$, i.e., matrix $\mathbf{A}$ is a lower triangular matrix with vanishing coefficients on the main diagonal. If this condition is not satisfied (i.e., if $a_{ij} \neq 0$ for $j \geq i$), the methods are called *implicit Runge-Kutta* methods [51]. For this type of methods, each time step incorporates the solution of a (non)linear system of dimension s.[11]

There are special classes of implicit Runge-Kutta methods called *diagonally implicit* and *singly diagonally implicit* Runge-Kutta (SDIRK) methods. The first class is characterized by the condition $a_{ij} = 0$ for $j > i$. These methods were developed to make it possible for each stage to successively solve the s equations delivering the stage values or the stage derivatives. If all diagonal coefficients have the same value, the method is a singly diagonally implicit Runge-Kutta method. The main advantage of methods of this type is that the system matrix should not be changed within one integration time step which allows to reduce the computational time considerably.

The functionality of an implicit Runge-Kutta methods depends directly on the following properties:

1. The stability function of an implicit Runge-Kutta method is given by:

$$R(z) = 1 + z\mathbf{b}^T(\mathbf{I} - z\mathbf{A})^{-1}\mathbf{e}_s \tag{4.34}$$

   where $\mathbf{e}_s = (1, \ldots, 1)^T$.

2. Implicit Runge-Kutta methods that satisfy the conditions

$$a_{sj} = b_j, j = 1, \ldots, s, \tag{4.35}$$

   i.e., the weight vector b is equal to the last row of matrix $\mathbf{A}$, are stiffly accurate time integration methods [48].

3. Stiffly accurate implicit Runge-Kutta methods are L-stable [43].

4. For an s-stage implicit Runge-Kutta method the maximum attainable convergence order is $p \leq 2s$. The maximum attainable convergence order for an SDIRK method is $p = s + 1$.

4.5.2 SDIRK Method for a Field-Circuit Coupled Formulation

From the large variety of the today available implicit Runge-Kutta methods, we choose for our research the class of SDIRK methods. There are the following decisive reasons stipulating this decision:

[11] For the system containing n differential equations, a system of the dimension ns should be solved.

1. SDIRK methods belong to the group of implicit time integration methods and one can consequently expect their adequate and proper functionality for index 1 DAE systems.
2. One should not introduce any changes in the system matrix within one integration step; this allows to reduce the CPU time.
3. Like all Runge-Kutta-type methods, these methods allow the implementation of *adaptive time-step selection* which is discussed in the following subsection.
4. Runge-Kutta methods can be equipped with a *dense output* algorithm allowing to approximate the solution at intermediate time instants.

An SDIRK method can be formulated in terms of either the vector of stage values $\mathbf{X}_{n,i}$ or the vector of stage derivatives $\mathbf{X}'_{n,i}$. The formulation with the stage derivatives is preferred since it allows a simple introduction of the boundary conditions into a system and simplifies the numerical integration for systems where the coefficient matrix $\mathbf{K}$ is not just a constant coefficient matrix, but may depend on the solution vector $\mathbf{x}$. Nonlinear field-circuit coupled formulations are, however, not the subject of the present research but they can obviously be considered as a possible extension and/or continuation of the work.

For a differential-algebraic nonlinear system

$$\mathbf{M}\dot{\mathbf{x}} + \mathbf{K}(\mathbf{x})\mathbf{x} = \mathbf{r}(t)$$

the first step in the implementation of an SDIRK method consists of the determination of the stage value $\mathbf{X}_{n,i}$ from the following (non)linear system

$$\left(\frac{\mathbf{M}}{ha_{ii}} + \mathbf{K}(\mathbf{X}_{n,i})\right)\mathbf{X}_{n,i} = \frac{\mathbf{M}}{ha_{ii}}\left(\mathbf{x}_n + \sum_{j=1}^{i-1} a_{ij}\mathbf{X}'_{n,i}\right) + \mathbf{r}(t_n + c_i h) \tag{4.36a}$$

where $i = 1, \ldots, s$. After that, the corresponding stage derivative $\mathbf{X}'_{n,i}$ is calculated from the expression

$$\mathbf{X}'_{n,i} = \frac{1/h\,(\mathbf{X}_{n,i} - \mathbf{x}_n) - \sum_{j=1}^{i-1} a_{ij}\mathbf{X}'_{n,j}}{a_{ii}}. \tag{4.36b}$$

During the computation process, all stage derivatives are saved. Finally, the update of the solution at the time point t_{n+1} is carried out:

$$\mathbf{x}_{n+1} = \mathbf{x}_n + h\sum_{i=1}^{s} b_i\mathbf{X}'_{n,i}. \tag{4.36c}$$

There is an important peculiarity of some SDIRK methods that should be mentioned: if there is an abscissa $c_s = 1$, i.e., when the last stage solution is calculated exactly at a new time point,[12] then the obtained stage derivative $\mathbf{X}'_{n,s}$ serves simultaneously as an approximation for $\dot{\mathbf{x}}_{n+1}$.

[12]For the stiffly accurate methods it means that the last stage solution coincides with a solution at the new time point.

4.5.3 Adaptive Time-Stepping Technique

As we have already mentioned, one of the reasons for choosing implicit Runge-Kutta methods is the possibility to implement an adaptive time stepping procedure, i.e., to construct a *problem-adapted* time grid. In the construction of time grids, the following aspects have to be taken into account:

1. The accuracy of the obtained approximation $\mathbf{x}_{n+1}$.
2. The number of grid points.
3. The cost of generating the approximation.

In the approximation theory, only items 1 and 2 are of the particular interest and one searches for *optimal* grids that minimize the number of nodes with given accuracy. The user of the simulation software is, however, interested in items 1 and 3 and expects *minimal* effort in generating an approximation with a prescribed accuracy [46].

There are two major factors affecting the choice of the step size: accuracy and stability. Popular numerical schemes produce results in qualitative agreement with the solution of the problem only when the step sizes are sufficiently small. For stiff problems, the stability requirement is much more restrictive than the accuracy requirement and, consequently, only implicit methods can be used. It is much more expensive to evaluate an implicit formula when solving a stiff problem, but the strong stability properties of implicit formulas are much better than that of explicit formulas.

A general-purpose code that adapts the step size to the solution behavior requires a user-defined tolerance ϵ_{tol}. At each time step, the code selects a step size so that some measure of time integration error is smaller than ϵ_{tol}. In order to solve the problem efficiently, the code tries to select a step size that is about as big as possible. The *work/precision efficiency* of a time-stepping scheme depends on the discretization as well as on problem properties and size. The nature of time-stepping is local: given the state $\mathbf{x}(t)$, the time integration method is a procedure for computing an approximation to $\mathbf{x}(t+h)$ which is a time step h ahead. The size of h is used to trade accuracy for efficiency and vice versa and is therefore the principal means of controlling the error and making the computational procedure adaptive. It is a well established practice to *control the local error*. This is an approach which is not expensive and far simpler than controlling the global error. With the help of differential inequalities, one can show that if the local error per unit time of integration is kept below ϵ_{tol}, then the global error at time t is bounded. Thus a local error control indirectly affects the global error.

Embedded implicit Runge-Kutta methods offer an effective way of estimating the local error. Such integration schemes deliver for each time step a solution $\mathbf{x}^{(p)}$ of a given order p obtained with a weight vector $\mathbf{b}$ and an embedded solution $\mathbf{x}^{(\hat{p})}$ of a lower order $\hat{p}$ obtained with a weight vector $\hat{\mathbf{b}}$ (see Butcher table (4.33)). The main and the embedded methods share the same coefficient matrix $\mathbf{A}$, and, as a consequence, use the same stage values/stage derivatives to compute the approximation

to the solution. Thus, the computation of the second, embedded solution, does not require significant additional computational efforts.

The first step in the adaptive time stepping procedure is the construction of the error vector

$$\mathbf{y} = \mathbf{x}^{(p)} - \mathbf{x}^{(\hat{p})} \tag{4.37}$$

which represents the difference between the higher and the lower order solutions. Since we are restricted to control only the local error, we need to find some computable estimation for it, because the value of the local error itself cannot be computed in a general case. Such an estimation is given by a value $\hat{\epsilon}_n$ defined as

$$\hat{\epsilon}_n = \|\mathbf{y}\|_{\text{err}} := \|\mathbf{x}^{(p)} - \mathbf{x}^{(\hat{p})}\| \tag{4.38}$$

and is used further as an estimate for the local integration error ϵ_l [46].

It is advisable that the main and the embedded methods both possess the property of L-stability, otherwise the stiff error components are damped out very slowly and are, therefore, substantially overestimated. In practice, some codes improve such inadequate error estimates by premultiplying the estimate by a "filter" matrix which damps or removes the large, stiff error components. Although this approach may improve the computational performance, it has been criticized due to its arbitrariness and due to the lack of a sound theoretical background [52].

The following step in the adaptive time stepping procedure is to find a suitable norm for the error vector $\mathbf{y}$, i.e., to determine the value of $\|\mathbf{y}\|_{\text{err}}$. In the literature, one can find a lot of different norms allowing to estimate the error vector. We list some of them:

1. a norm suggested in [53] reads:

$$\|\mathbf{y}\|_{\text{err}} = \sqrt{\frac{\|\mathbf{y}\|_2^2}{\|\mathbf{x}^{(p)}\|_2^2 + \epsilon^{(p)}}} \tag{4.39}$$

   where $\epsilon^{(p)}$ is an absolute error tolerance value. The parameter $\epsilon^{(p)}$ is chosen as a proper fraction $\nu \in [10^{-3}, 10^{-2}]$ of the maximum norm of the values that were calculated so far during the time marching process

$$\epsilon^{(p)} := \nu \max_{t \in [t_0, t_i]} \{\|\mathbf{x}(t)\|_2^2\}. \tag{4.40}$$

2. another norm is given in [54]:

$$\|\mathbf{y}\|_{\text{err}} = \sqrt{\sum_{i=1}^{N} \left(\frac{y_i}{|x_i^{(p)}| + \epsilon_{x,i}^{(p)}} \right)^2} \tag{4.41}$$

   where $\epsilon_{x,i}^{(p)}$ is an absolute error tolerance for the component $x_i^{(p)}$ [54] and N is the dimension of the solution vector. System (4.1) describes a field-circuit

coupled formulation incorporating variables having different physical nature which have, consequently, different units. Therefore, it makes sense to choose different absolute tolerances for each solution component:

$$\epsilon_{x,i}^{(p)} := \nu \max_{t\in[t_0,t_i]} \{|x_i^{(p)}(t)|\} \tag{4.42}$$

where $\nu \in [10^{-2}, 10^{-1}]$. The introduction of absolute tolerances takes the history of the integration process into account. This leads to a more effective realization of the adaptive time stepping scheme.

3. in [47] the following norm is proposed:

$$\|\mathbf{y}\|_{\text{err}} = \sqrt{\frac{1}{N}\sum_{i=1}^{N}\left(\frac{y_i}{a_{\text{tol,i}} + \max(|x_{n,i}^{(p)}|, |x_i^{(p)}|)r_{\text{tol,i}}}\right)^2} \tag{4.43}$$

where $a_{\text{tol,i}}$ and $r_{\text{tol,i}}$ are the tolerances prescribed by the user (relative errors are considered for $a_{\text{tol,i}} = 0$, absolute errors for $r_{\text{tol,i}} = 0$). In formula (4.43), $x_{n,i}^{(p)}$ is a value of the ith component of the solution obtained at the previous time instant.

4. maximum norms are also in use [85]:

$$\|\mathbf{y}\|_{\text{err}} = \max_i \frac{|y_i|}{||x_i^{(p)}| + \epsilon_{x,i}^{(p)}|}. \tag{4.44}$$

The adaptive time stepping scheme comprises criteria allowing to decide whether the last calculated integration step has to be repeated with a smaller time step or a new simulation step can be performed. According to the standard rule aiming at keeping the error estimate $\|\mathbf{y}\|_{\text{err}}$ close to the user-specified tolerance ϵ_{tol}, the solution is rejected if $\|\mathbf{y}\|_{\text{err}} > \mu\,\epsilon_{\text{tol}}$ holds true and a new attempt is made with a smaller step size; otherwise the time step is accepted. In this scheme, μ is an accelerating factor usually taken as 1.2 [54].

Finally, the length of a next time step is calculated using a formula

$$\Delta t_{n+1} = \rho\left(\frac{\epsilon_{\text{tol}}}{\|\mathbf{y}\|_{\text{err}}}\right)^{1/(\hat{p}+1)} \Delta t_n \tag{4.45}$$

where ρ denotes a safety factor that is usually set to 0.9 [55].

4.5.4 Dense Output

The Runge-Kutta methods described in the previous sections estimate the states and return the approximation to the solution at times $t_i, i = 1, 2, \ldots, n$. The stepsize $h_i = t_i - t_{i-1}$ has not to be constant, since an adaptive time stepping algorithm can be built into the integration process. However, one often needs to estimate the

solution at some time t^* where $t_n < t^* < t_{n+1}$. The problem of obtaining such estimates is the *interpolation* or *dense output* problem. Consider an off-grid time instant defined as $t^* = t_n + \sigma h, 0 \leq \sigma \leq 1$. The interpolator or *continuous extension* is constructed using the stage derivatives computed in updating the state from t_n to t_{n+1}. Such an interpolator has the form:

$$\mathbf{x}_{n+1}(\sigma) = \mathbf{x}(t_n + \sigma h) = \mathbf{x}_n + \sigma h \sum_{i=1}^{s} \bar{b}_i(\sigma) \mathbf{X}'_{n,i} \tag{4.46}$$

where $\bar{b}_i$ are typically polynomials in σ.

Usually, there are two main reasons for interpolating:

1. To obtain an approximation to the solution at the off-grid time points.
2. For predicating time instants when discontinuities occur.

Extrapolators are mainly used for producing starting values for an iterative solution of nonlinear equations in the next time step. Assume that the nonlinear equations in question must be solved for the stage variables $\mathbf{X}_{n,i}, i = 1, \ldots, s$. Let $\mathbf{X}^0_{n,i}$ be the starting value for $\mathbf{X}_{n,i}$ produced by an extrapolator. According to the way how the values of $\mathbf{X}^0_{n,i}$ are produced, two types of extrapolators are considered:

1. Continuous extension extrapolators.
2. Stage value extrapolators.

The extrapolators of the first type use (4.46). Suppose that a step from $(t_n, \mathbf{x}_n)$ to $(t_n + h_n, \mathbf{x}_{n+1})$ is taken and the next proposed step has the length h_{n+1}. The estimate for the solution at the time instant $t_n + h_n + c_i h_{n+1}$ can be directly obtained from (4.46) by putting $\sigma = 1 + \omega c_i$ where $\omega = h_{n+1}/h_n$. This estimate in some sense approximates $\mathbf{X}_{n+1,i}$ and hence can be used as $\mathbf{X}^0_{n+1,i}$.

The extrapolators of the second type directly estimate $\mathbf{X}_{n,i}$ without estimating the solution at the stage abscissa i, i.e., at $t_n + h_n + c_i h_{n+1}$. Let $\mathbf{X}_{n,1}, \mathbf{X}_{n,2}, \ldots, \mathbf{x}_{n,s}$ be the stage values computed during the solution update from $(t_n, \mathbf{x}_n)$ to $(t + h_n, \mathbf{x}_{n+1})$. A stage value extrapolator producing $\mathbf{X}^0_{n+1,i}$ for the starting at $(t_n + h_n, \mathbf{x}_{n+1})$ has the form [56]:

$$\mathbf{X}^0_{n+1,i} = \beta^{ex}_{i0} \mathbf{x}_n + \sum_{j=1}^{s} \beta^{ex}_{ij} \mathbf{X}_{n,i}. \tag{4.47}$$

The extrapolator parameters β^{ex}_{ij} are chosen to satisfy certain order conditions.

There are also so called *augmented stage value extrapolators*, where the stages of the previous and current steps are used to approximate the future stage values [56].

In the frame of the present work, only interpolator techniques are used: the dense output formula (4.46) is employed in Chapter 6 to predict the time instants where

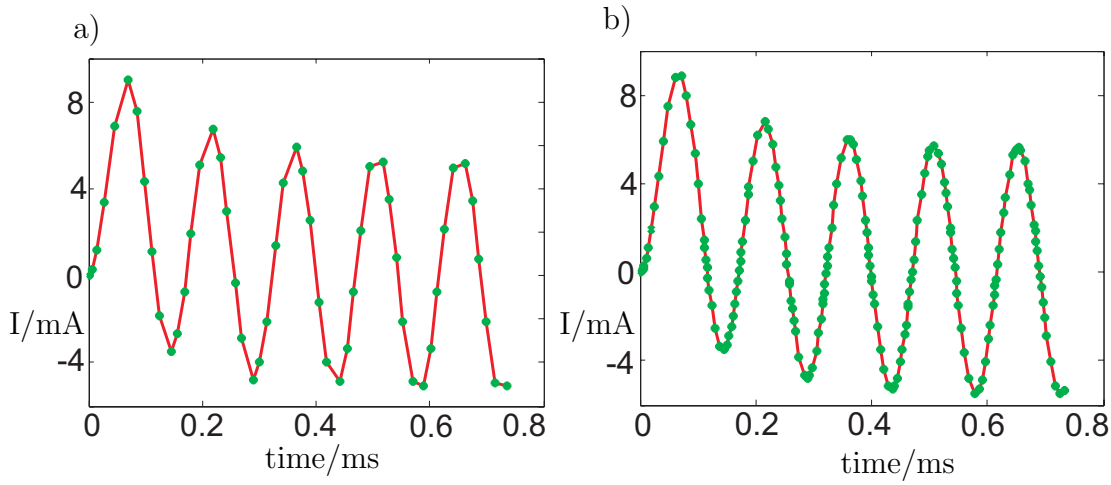

Figure 4.6: Stranded conductor: higher order currents calculated using : (a) norm (4.39) and (b) norm (4.41) .

the switching circuit elements change their state. For the numerical examples presented below, an embedded SDIRK method delivering a main solution of order three and the embedded solution of order two (i.e., SDIRK 3(2) method) is chosen for time discretization. Its Butcher table is given in [56] (second pair of the coefficients, page 51). Both methods are L-stable. The corresponding coefficients of the continuous extension polynomials can be found in [56] on page 59. For convenience, the coefficients of the method itself and its continuous extension formula are given in Appendix A.

4.5.5 Numerical Example

The last subsection of this chapter is devoted to the comparison of the different norms applied to estimate an error vector within the adaptive time stepping procedure. As a test model, consider again an electrical network with a conductive ring (Fig. 4.2a) treated as a stranded conductor excited by the voltage source of the form $U(t) = U_{\max} \sin(\omega t)$ (Fig. 4.2c). The corresponding numerical model of this network is described by system (3.43).

The numerical integration of system (3.43) is carried out by SDIRK 3(2) method (see Appendix A). Fig. 4.6 shows the behavior of the higher order solutions for the current for one and the same values of ϵ_{tol} and ν, namely $\epsilon_{\text{tol}} = 10^{-2}$ and $\nu = 10^{-2}$, but with different norms applied to the error vector. Fig. 4.6a illustrates the solution obtained using error norm (4.39) whereas Fig. 4.6b presents the solution obtained using error norm (4.41). From the presented results one can conclude that the choice of the norm for the error vector significantly influences the adaptive time integration process. The results of Fig. 4.6a demonstrate that the adaptive time stepping procedure does not reflect the sinusoidal dynamics of the current curve exactly. Error norm (4.41) (see Fig. 4.6b) allows to obtain satisfactory results, however, the behavior of the time stepping process is not adequate: namely, at the

regions, where obviously the step size should be significantly reduced, it is increased. Where one would expect an increase of the step size, it appeared to be reduced. In the next chapter a special technique is proposed allowing an adequate adaptive integration of the electromagnetic problems with sinusoidal dynamics.

Tab. 4.1 contains the overall monitored data on the influence of the chosen error norms ((4.39) and (4.41)) and the absolute tolerances on the number of accepted and rejected time-steps and the observed maximum relative error.

Norm \ ϵ_{tol}		10^{-1}		10^{-2}		10^{-3}	
		steps	error	steps	error	steps	error
(4.39)	ν=10^{-2}	21/11	6.8e-2	50/24	3.8e-2	95/48	1.6e-2
	ν=10^{-3}	22/16	6.2e-2	55/30	1.76e-2	104/57	1.3e-1
(4.41)	ν=10^{-1}	76/42	7.6e-2	177/99	2.9e-3	369/217	3.8e-4
	ν=10^{-2}	92/63	1.7e-2	177/106	1.3e-2	355/164	6.8e-3

Table 4.1: Influence of the chosen error norm and the absolute tolerance on the number of accepted/rejected time-steps and on the observed maximum relative error.

The results summarized in Tab. 4.1 demonstrate a strong dependence of the number of accepted/rejected step on the chosen error vector norm. The usage of the norm (4.41) increases the number of the time steps (both accepted and rejected) significantly. However, the changes in the parameter ν within one chosen norm does not make a decisive influence on the number of time steps. Naturally, the decrease of the user-specified tolerance ϵ_{tol} leads to the significant increase of the total number of time steps.

Chapter 5

Efficiency Improvements in Adaptive Numerical Techniques

In this chapter we discuss some numerical techniques that can be used to improve the efficiency of the classical adaptive time integration procedure described previously in the work. In Section 5.1, a non-standard approach for the numerical adaptive integration of the electromagnetic systems with sinusoidal dynamics is proposed. Section 5.2 covers the aspects of the so-called *envelope* integration of the electromagnetic formulations.

5.1 Adaptive Time Stepping for Systems with Sinusoidal Dynamics

The adaptive numerical integration schemes described in the previous chapter allow to reduce the computational time considerably guaranteeing at the same time the achievement of a user-prescribed tolerance for the local error. For one particular selected time step, Runge-Kutta adaptive integration methods deliver two approximations to the solution with different order of approximation. The difference between both approximations is used to estimate the local error [47].

For some types of problems, the implementation of the adaptive schemes commonly proposed in the literature delivers rather surprising results: namely, at time spans, where obviously the step size should be significantly reduced, it is increased. When one would expect an increase of the step size, it appeared to be reduced.

As a test example, consider a model of a plate capacitor, one plate of which is supplied with the voltage excitation $U_1(t) = U_0 \sin(2\pi f t)$ whereas the other plate is grounded (Fig. 5.1). A suitable mathematical model for this example is electroquasistatic formulation (2.35a) given in terms of the electric scalar potential φ, the conductivity σ and the permittivity ε. The spatial discretization can be carried out by means of the FIT [82] leading to the discrete electroquasistatic formulation (2.59).

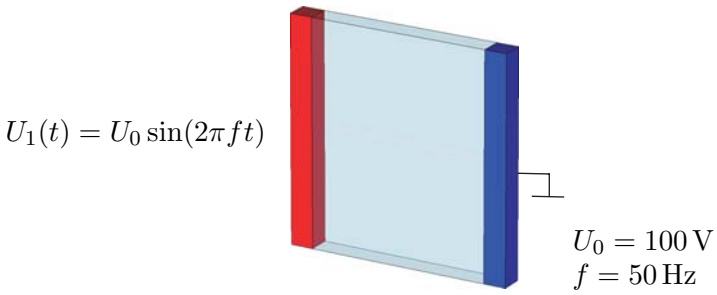

Figure 5.1: Electroquasistatic model: plate capacitor.

Formulation (2.59) is integrated with the SDIRK3(2) method (see Appendix A). The solution for one degree of freedom as well as the corresponding dynamics of the step size selection are illustrated in Fig. 5.2. At time moments $t = \frac{1}{4}T + nT$, $T = \frac{1}{f}$, $n \in \mathbb{N}$, the excitation signal reaches a maximum value and exhibits a rather fast change. Though, the time step prediction increases the time step length.

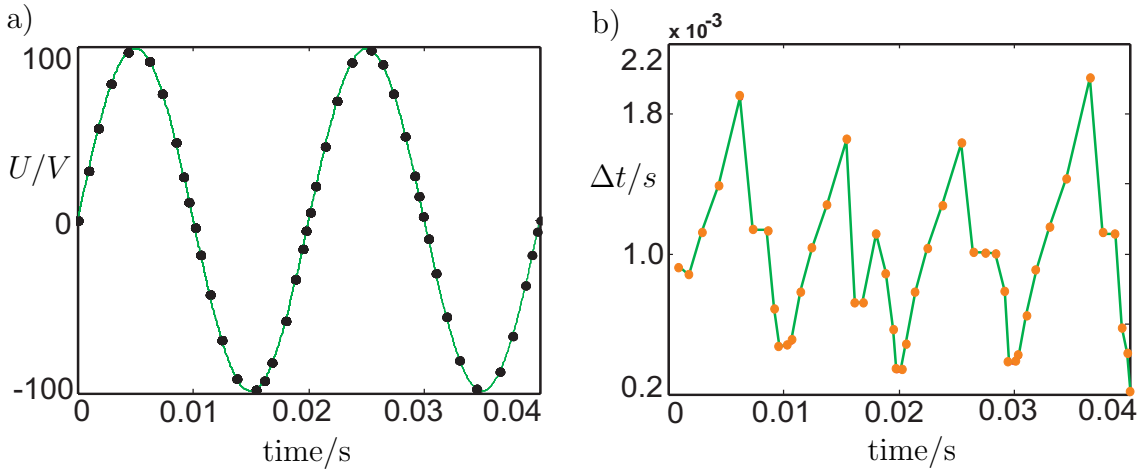

Figure 5.2: Simulation results for SDIRK 3(2): (a) voltage distribution for one of the degrees of freedom; (b) selected time step lengths.

The results of a detailed study show that the described phenomena always take place when sinusoidal and/or cosinusoidal functions are subjected to numerical time integration. The only finding in the literature that concerns this phenomenon is given in [53]: "However, in the case of sine and cosine drives... the fixed-time approach will be more efficient... ".

Sinusoidal excitations are of primordial importance for transient simulations of electromagnetic devices. The highlighted problem is, however, not only specific for purely sinusoidal functions. Obviously, the described phenomenon also occurs for excitation functions that are approximately sinusoidal.

This section is dedicated to the analysis of the unexpected behavior of the adaptive time stepping procedure described above and to the development of the time integration scheme combined with a reliable time step prediction approach able to tackle this class of problems.

5.1.1 Reason for the Unexpected Behavior

To the author's knowledge, all adaptive Runge-Kutta methods developed and implemented up to the present have in common that the difference between the order of the main solution and the order of the embedded solution is equal to one, e.g., SDIRK 3(2) method [56], Merson 5(4), Zonneveld 4(3) [47]. All of them are reported to perform in an effective and reliable way without any exceptions. For problems with sinusoidal dynamics this is, however, not the case as explained below.

The Taylor expansion of a sinusoidal function indicates the reason for the unexpected behavior mentioned above:

$$\begin{aligned}\sin(\omega t) &= \sin(\omega t_0) + \omega\cos(\omega t_0)\,[\omega(t-t_0)] \\ &- \omega^2\frac{\sin(\omega t_0)}{2}\,[\omega(t-t_0)]^2 - \omega^3\frac{\cos(\omega t_0)}{6}\,[\omega(t-t_0)]^3 \\ &+ \cdots + \frac{\sin^{(n)}(\omega t_0)}{n!}\,[\omega(t-t_0)]^n + R_{n+1}(\omega t) \qquad (5.1)\end{aligned}$$

where $R_{n+1}(\omega t)$ is the reminder. From (5.1) it follows that e.g. at the point $\omega t_0 = \pi/2$ the terms including $\cos(\omega t_0)$ vanish and, hence, the expansion of the function of third order coincides with the expansion of second order. For common adaptive time integrators implemented e.g., with SDIRK 3(2), this means that at this very point or in its vicinity no or a negligible difference between the lower and the higher order solutions is detected. As a consequence, the integration process will proceed with an enormously large time step which, however, does not correspond to the dynamics of the solution.

This problem can be successfully overcome by constructing Runge-Kutta methods where the difference between the orders of the solutions is more than one.

5.1.2 Construction of a Dedicated Runge-Kutta Method

Here we discuss how the proposed technique can be implemented for the SDIRK 3(2) method (see Appendix A). Instead of having a weight vector delivering an embedded solution of order two, we construct a modified weight vector allowing to obtain an embedded solution of order one, i.e., SDIRK3(1).

For a Runge-Kutta method to be of one particular order, its coefficients have to satisfy so-called order conditions. The number of the order conditions to be put on the coefficients of the Butcher table to obtain a Runge-Kutta integration scheme of one particular order increases significantly with the required order (see Tab. 5.1) [47]. As one can conclude from Tab. 5.1, a construction of a Runge-Kutta method of higher order is not a trivial task.

To obtain a weight vector delivering a first order embedded solution, only one order condition is applied on the coefficients of the weight vector $\hat{\mathbf{b}} = [b_j], j = 1,\ldots,4$ (see Tab. 5.1) [47]:

$$\sum_{j=1}^{s}\hat{b}_j = 1\,. \qquad (5.2)$$

Table 5.1: Number of order conditions for Runge-Kutta methods

order p	1	2	3	4	5	6	7	8	9	10
order conditions	1	2	4	8	17	37	85	200	486	1205

From Tab. 5.1 one can observe that two order conditions should be applied to obtain a second order Runge-Kutta method. The first one is condition (5.2) guaranteeing a first order Runge-Kutta method. The other order condition is

$$\sum_{j=1}^{s} \hat{b}_j c_j = 1/2\,. \tag{5.3}$$

Conditions (5.2) and (5.3) together allow to describe all the variety of possible Runge-Kutta methods of order two.

Now, we turn back again to the proposed technique. Condition (5.2) allows us to obtain Runge-Kutta method of first order. However, to be sure that a second order accurate solution will not be obtained by accident, the following inequality has to hold as well [47]:

$$\sum_{j=1}^{s} \hat{b}_j c_j \neq 1/2\,. \tag{5.4}$$

Solving simultaneously an algebraic system consisting of the equation (5.2) and inequality (5.4), a family of the weight vectors delivering a first order solution is obtained.

For the SDIRK method from Appendex A this family of methods is given by:

$$\begin{cases} \hat{b}_1 = \alpha \\ \hat{b}_3 = \beta \neq \frac{\sqrt{2}-1}{2-\sqrt{2}}\alpha \\ \hat{b}_4 = \gamma \\ \hat{b}_2 = 1-\alpha-\beta-\gamma \neq 1-\alpha-\frac{\sqrt{2}-1}{2-\sqrt{2}}\alpha-\gamma \end{cases}$$

where α, β, γ are parameters. For example, one possible embedded method of order one is given by $\hat{\mathbf{b}} = \left[\frac{1}{2}\ \frac{1}{8}\ \frac{1}{4}\ \frac{1}{8}\right]^T$. Thus, the Butcher table in Appendix A can be augmented with this additional weight vector.

5.1.3 Numerical Examples

The already introduced test example given in Fig. 5.1 is simulated again with the SDIRK method using an embedded solution of order one instead of order two, i.e., SDIRK 3(1) (Appendix A). The simulation results are presented in Fig. 5.3.

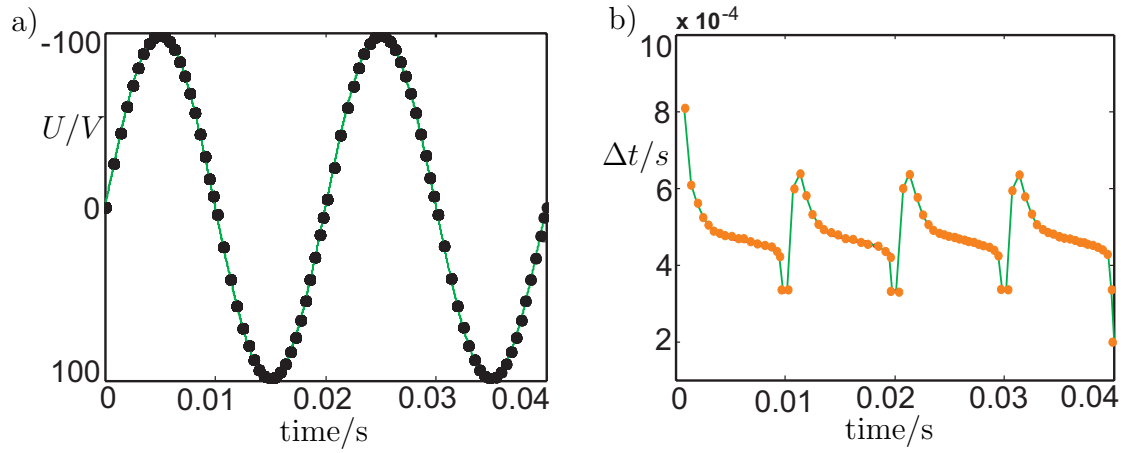

Figure 5.3: Simulation results for SDIRK 3(1): (a) voltage distribution for one of the degrees of freedom; (b) selected time steps.

From the results one can conclude that the time marching process is now adequate: at the time instants $\omega t = \frac{\pi}{2} + \pi n, n \in \mathbb{N}$ and in their vicinity very small time steps are performed. The asymmetry of the time step selection dynamics (Fig. 5.3b) is explained by the fact that the adaptive time stepping scheme needs a certain time to recognize the behavior of the transient process and also due to the limits put on the length of the time step.

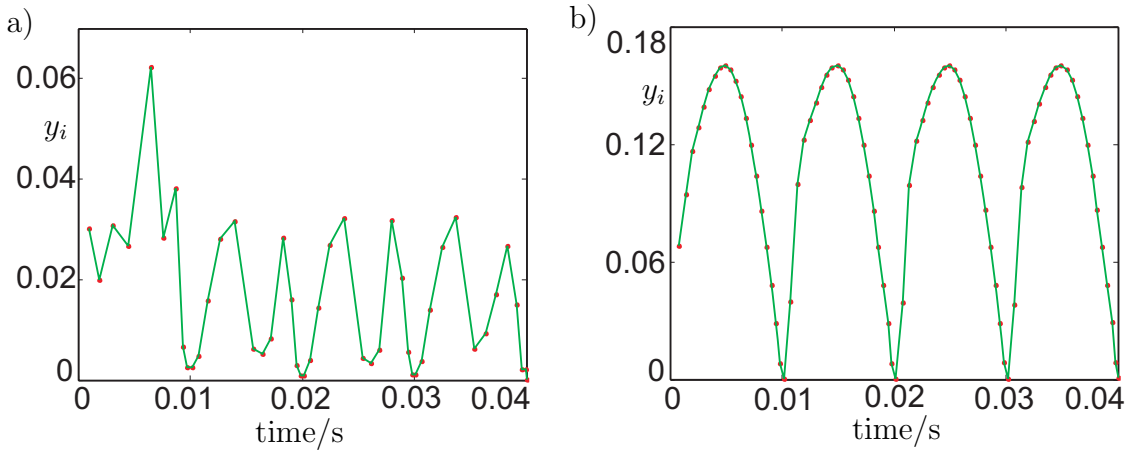

Figure 5.4: Magnitude of the error for one selected degree of freedom : (a) simulation with the SDIRK 3(2) method; (b) simulation with the SDIRK 3(1) method. In both simulations, the same set of tolerances and step-size limits is used.

Fig. 5.4 shows the magnitude of the error, i.e., the difference between the higher and lower order solutions for one selected degree of freedom in case when the simulation is carried out with the SDIRK 3(2) method (Fig. 5.4a) and with the SDIRK 3(1) method (Fig. 5.4b). As one can conclude from the results, the SDIRK 3(1) method detects the highest value for the error at the time points $\omega t = \frac{\pi}{2} + \pi n, n \in \mathbb{N}$ and in their vicinity. The SDIRK 3(2) method, however, does not demonstrate a reliable behavior for this case.

Error norm (4.44) is used for the simulation. With the user prescribed tolerance

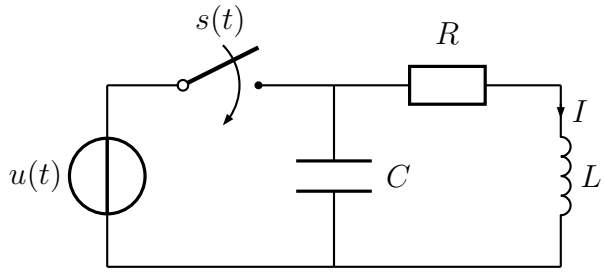

Figure 5.5: Test problem: electrical network.

ϵ_{tol} put to 10^{-3}, the total number of time steps for the SDIRK 3(2) method is 64, of which 17 steps are rejected. For the SDIRK 3(1), 91 steps are computed, but only 6 are rejected in case when ϵ_{tol} is equal to 10^{-2}. This allows to conclude, that despite of the increase in the total number of time steps, SDIRK 3(1) method is more suitable for the simulations of the models with sinusoidal excitation because the number of rejected steps reduces significantly. The usage of the bigger tolerance $\epsilon_{\text{tol}} = 10^{-2}$ in the simulation with SDIRK 3(1) method is due to the fact that the magnitude of the error (see Fig. 5.4), and since the value of $\|\mathbf{y}\|_{\text{err}}$, increase.

As a second test example, consider the electrical circuit depicted in Fig. 5.5 where the resonance frequency is determined by the system itself and not by the excitation. The following parameters are used in the simulation: $u(t) = U(1 - e^{-t/\tau})$, where $U = 1$ V and $\tau = 0.1$ ms. The switch is initially closed and is opened at $t_{\text{switch}} = 5$ s. The parameters of the circuit elements are as follows: $L = 1$ mH, $C = 10$ μF and $R = 1$ mΩ.

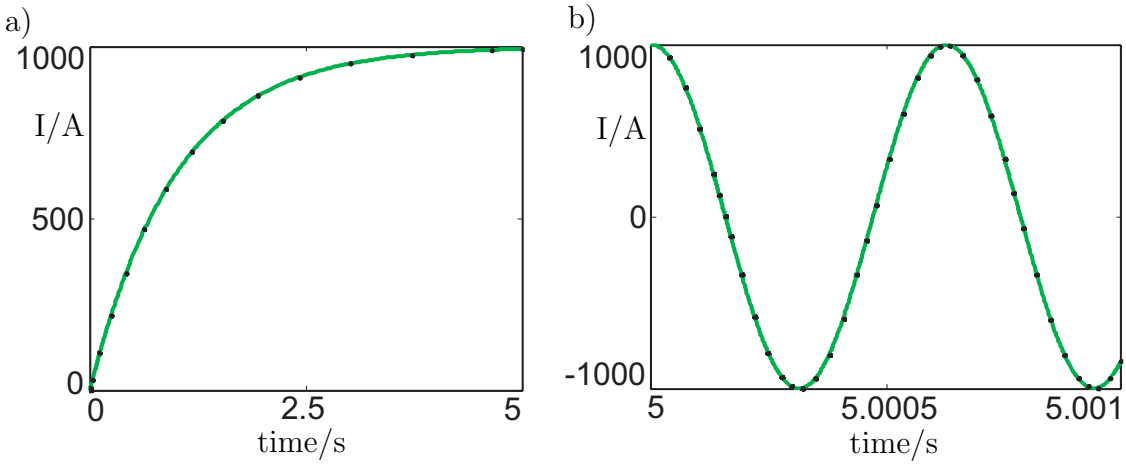

Figure 5.6: Simulated current through the inductor: (a) the time integration is started with SDIRK 3(2); (b) the time integration is continued with SDIRK 3(1).

The time span corresponding to the configuration with the closed switch is simulated with the SDIRK 3(2) method. With the user specified tolerance ϵ_{tol} put to 10^{-3}, the number of the accepted and rejected steps is 30 and 2, respectively. The simulation results are presented in Fig. 5.6a. After 5 s, the switch is opened, and the simulation is continued with the SDIRK 3(1) method. The simulated current through the

inductor is presented in Fig. 5.6b. For this part of the simulation, ϵ_{tol} is equal to 10^{-2} and the number of the accepted/rejected steps is 40 and 8, respectively. Error norm estimate (4.44) is used for the simulation.

5.2 Adaptive Envelope Integration of Electromagnetic Problems

Traditionally, electromagnetic devices operating on a definite fundamental frequency are simulated by either a transient approach or using a frequency domain method. The choice between the simulation regimes is made according to the fact whether a non-repetitive phenomena or a steady-state condition are to be studied. The transient time step size is related to the time constant of the phenomenon dynamics. Problems arise when differential equations exhibiting fast and slow dynamics have to be numerically integrated. A typical example is a coupled thermal-magnetic problem, where the time constant associated with the period of the fundamental electrical supply is in the range of $\tau_{\text{el}} = 1$ s and the thermal time constant is about $\tau_{\text{therm}} = 1$ h [57]. Mathematically, such problems are stiff differential or differential-algebraic systems of equations and, accordingly, robust integration techniques able to effectively resolve very diverse time constants should be applied. Pure transient analysis is inefficient when it is necessary to resolve low frequencies in the presence of a high frequency component because the high-frequency dynamics forces a small time step while the low-frequency dynamics forces a long simulation time interval. In this section, a transient time-harmonic approach [57] is proposed able to tackle problems including fast and slow dynamics. This approach can be considered as a bridge between a purely transient method and a time-harmonic method. The transient complex systems arising from this approach are integrated with implicit Runge-Kutta methods.

5.2.1 Derivation of Method

A solution to index 1 DAE system (4.1) involving a sinusoidal function of a single known angular frequency can be expressed using the phasor notation as

$$\mathbf{x}(t) = \Re\{\underline{\mathbf{X}}(t)e^{j\omega t}\} \tag{5.5}$$

with the time dependent complex phasor solution $\underline{\mathbf{X}}(t)$ describing the slow dynamic phenomenon and the factor $e^{j\omega t}$ in terms of the angular frequency ω describing the fast varying dynamics of the problem. The absolute value of the phasor $\underline{\mathbf{X}}(t)$ can be interpreted as an "envelope" around the fast oscillating solution. For the excitation function $\mathbf{r}(t)$ having a favorable spectrum. i.e., when a clear distinction between the low frequency components and the single frequency component stipulated by the angular frequency ω can be made in the spectrum, we have:

$$\mathbf{r}(t) = \Re\{\underline{\mathbf{R}}(t)e^{j\omega t}\} \tag{5.6}$$

where the complex-valued vector $\underline{\mathbf{R}}(t)$ contains the low frequency excitation components.

The time derivative of (5.5) reads:

$$\begin{aligned}\frac{\mathrm{d}}{\mathrm{d}t}\mathbf{x}(t) &= \frac{\mathrm{d}}{\mathrm{d}t}\left(\Re\{\underline{\mathbf{X}}(t)e^{j\omega t}\}\right)\\ &= \Re\left[\frac{\mathrm{d}}{\mathrm{d}t}\left(\underline{\mathbf{X}}(t)e^{j\omega t}\right)\right]\\ &= \Re\{\frac{\mathrm{d}}{\mathrm{d}t}\underline{\mathbf{X}}(t)e^{j\omega t}+\underline{\mathbf{X}}(t)j\omega e^{j\omega t}\}. \end{aligned} \tag{5.7}$$

Now, we substitute expressions (5.5), (5.6) and (5.7) into system (4.1) composed of the $\mathbf{K}$ and $\mathbf{M}$ matrices which are constant in time and linear:

$$\mathbf{M}\Re\{\frac{\mathrm{d}\underline{\mathbf{X}}(t)}{\mathrm{d}t}e^{j\omega t}+\underline{\mathbf{X}}(t)j\omega e^{j\omega t}\}+\mathbf{K}\Re\{\underline{\mathbf{X}}(t)e^{j\omega t}\}=\Re\{\underline{\mathbf{R}}(t)e^{j\omega t}\}$$

which gives:

$$\Re\{\mathbf{M}\frac{\mathrm{d}\underline{\mathbf{X}}(t)}{\mathrm{d}t}e^{j\omega t}+\mathbf{M}\underline{\mathbf{X}}(t)j\omega e^{j\omega t}\}+\Re\{\mathbf{K}\underline{\mathbf{X}}(t)e^{j\omega t}\}=\Re\{\underline{\mathbf{R}}(t)e^{j\omega t}\}$$

and finally obtain:

$$\Re\{\mathbf{M}\frac{\mathrm{d}\underline{\mathbf{X}}(t)}{\mathrm{d}t}e^{j\omega t}+\mathbf{M}\underline{\mathbf{X}}(t)j\omega e^{j\omega t}+\mathbf{K}\underline{\mathbf{X}}(t)e^{j\omega t}\}=\Re\{\underline{\mathbf{R}}(t)e^{j\omega t}\}. \tag{5.8}$$

Equation $\Re\{\underline{a}(t)e^{j\omega t}\}=\Re\{\underline{b}(t)e^{j\omega t}\}$ holds for every t if and only if $\underline{a}(t)e^{j\omega t}=\underline{b}(t)e^{j\omega t}$. Consequently, from equation (5.8) one can derive:

$$\mathbf{M}\frac{\mathrm{d}\underline{\mathbf{X}}(t)}{\mathrm{d}t}e^{j\omega t}+\mathbf{M}\underline{\mathbf{X}}(t)j\omega e^{j\omega t}+\mathbf{K}\underline{\mathbf{X}}(t)e^{j\omega t}=\underline{\mathbf{R}}(t)e^{j\omega t}$$

Now, the fast dynamics described with the multiplier $e^{j\omega t}$ can be cancelled leading to the following homogeneous phasor DAE:

$$\mathbf{M}\frac{\mathrm{d}}{\mathrm{d}t}\underline{\mathbf{X}}(t)+(\mathbf{K}+j\omega\mathbf{M})\underline{\mathbf{X}}(t)=\underline{\mathbf{R}}(t) \tag{5.9}$$

which includes only the time derivative with respect to slow varying dynamics of the problem whereas the fast-varying components corresponding to the angular frequency ω are incorporated in the phasor formulation. Thus, instead of solving problem (4.1) containing both slow and fast dynamics, one only has to resolve the slow varying transient phenomena described by system (5.9) and deduce the overall time dependence of the solution using formula (5.5).

This methodology is used for a long time in circuit analysis to study electronic circuits with modulated signals [58], but it has been only recently applied in combination with the electromagnetic field analysis [57], [59].

In many systems such as e.g., electrical energy distribution applications, the frequency ω is known and constant. However, for e.g., free oscillating systems it may

be unknown and should be determined separately. Here, it is assumed that ω is known.

The numerical time integration of problem (5.9) is carried out with the SDIRK 3(2) method which is to the author's knowledge the first experience in applying Runge-Kutta-type time integrators to the phasor systems.

5.2.2 Consistent Initial Conditions

Before the integration process for problem (5.9) is activated, consistent initial conditions have to be determined. Suppose that the initial conditions for problem (4.1) are given by $\mathbf{x}(0) = \mathbf{x}_0$. The initial conditions for the phasor system (5.9) are complex values that can be expressed as $\underline{\mathbf{X}}(0) = \mathbf{A}(0) + j\mathbf{B}(0) = \mathbf{A_0} + j\mathbf{B_0}$. In this section, we discuss how the vectors $\mathbf{A_0}$ and $\mathbf{B_0}$ can be obtained.

To determine $\mathbf{A_0}$ we notice that

$$\mathbf{x}(0) = \Re\{\underline{\mathbf{X}}(0)e^{j\omega 0}\} = \mathbf{A_0}. \tag{5.10}$$

which means that the real parts of the complex initial conditions are equal to the values of the initial conditions specified for problem (4.1).

Further, using (5.7) we obtain:

$$\begin{aligned} \frac{\mathrm{d}}{\mathrm{d}t}\mathbf{x}(t)|_{t=0} &= \Re\{\frac{\mathrm{d}\underline{\mathbf{X}}}{\mathrm{d}t}|_{t=0} + \underline{\mathbf{X}}(0)j\omega\} \\ &= \Re\{\mathbf{A}'(0) + j\mathbf{B}'(0) + j\omega(\mathbf{A_0} + j\mathbf{B_0})\} \\ &= \mathbf{A}'(0) - \omega\mathbf{B}(0) \end{aligned} \tag{5.11}$$

which gives:

$$\mathbf{B}(0) = \mathbf{B_0} = \frac{\mathbf{A}'(0) - \mathbf{x}'(0)}{\omega}. \tag{5.12}$$

In general the values of $\mathbf{A}'(0)$ and $\mathbf{x}'(0)$ are not known and suitable approximations should be used. In case of the invertible $\mathbf{M}$ matrix, $\mathbf{x}'(0)$ can be computed as $\mathbf{M}^{-1}(\mathbf{r}(0) - \mathbf{K}\mathbf{x}(0))$.

For problems where it is a priory known that $\mathbf{A}(t) = \mathbf{A_0}e^{-\alpha t}$, where α is a decay time constant, a following formula for $\mathbf{B_0}$ can be deduced:

$$\mathbf{B_0} = -\frac{\mathbf{x}'(0) + \alpha\mathbf{A_0}}{\omega}. \tag{5.13}$$

In the general case, one can start the time integration from a time-harmonic steady-state situation, computed by solving $(\mathbf{K} + j\omega\mathbf{M})\underline{\mathbf{X}}(0) = \underline{\mathbf{R}}(0)$. Then, however, the behavior of the complex-valued time dependent problem at $t = 0$ is similar to a parabolic system, where a step function is applied. Hence, the large initial error may result in a large number of small time steps at the beginning of the time integration procedure. Then, the clear distinction between slow and fast dynamics may get lost.

5.2.3 Numerical Example

Consider a series RLC circuit depicted in Fig. 5.7a in which $L = 1$ H, $R = 2\ \Omega$, $C = 1/401$ F, $i_L(0) = 2$ A and $u_C(0) = -2$ V. The parameters of the circuit elements are selected in a way to ensure a damped response.

For this circuit, the phasor system (5.9) is constructed. The phasor unknowns are $\underline{U}_R(t)$, $\underline{U}_C(t)$ and $\underline{I}_L(t)$ and matrices $\mathbf{M}$ and $\mathbf{K}$ read:

$$\mathbf{M} = \begin{bmatrix} 0 & 0 & 0 \\ 0 & C & 0 \\ 0 & 0 & -L \end{bmatrix}, \quad \mathbf{K} = \begin{bmatrix} 1/R & 0 & 1 \\ 0 & 0 & -1 \\ 1 & -1 & 0 \end{bmatrix}. \tag{5.14}$$

The damped response for a current in a series RLC circuit is given by

$$i(t) = e^{-\alpha t}(B_1 \cos(\omega t) + B_2 \sin(\omega t)) \tag{5.15}$$

where the parameters α and ω are obtained from the circuit parameters:

$$\begin{aligned} \alpha &= R/2L = 1 \quad 1/\text{s} \\ \omega_0 &= 1/\sqrt{LC} = 20.02 \quad 1/\text{s} \\ \omega &= \sqrt{\omega_0^2 - \alpha^2} = 20 \quad 1/\text{s}. \end{aligned}$$

Thus, the values of α and ω are determined and can be used to compute consistent initial conditions for the phasor vector. The application of the formulas (5.10) and (5.13) gives $\underline{U}_R(0) = -4$ V, $\underline{U}_C(0) = (-2 - j40)$ V and $\underline{I}_L(0) = 2$ A.

The phasor system (5.9) with the matrices $\mathbf{M}$ and $\mathbf{K}$ given by (5.14) is adaptively integrated with the SDIRK 3(2) method. The envelope of the transient current response for the circuit, i.e., $|\underline{I}_L(t)|$, obtained by numerical time integration as well as the current response reconstructed from (5.5) afterwards, are illustrated in Fig. 5.7b.

The application of the error norm (4.44) with $\epsilon_{\text{tol}} = 10^{-3}$ results in 16 simulation time steps. No rejected time steps are observed. The black markers in Fig. 5.7b on the envelope curve of the solution show the time steps accepted by the adaptive time stepping procedure. The second curve showing the current in the circuit is also supplied with these time markers to demonstrate the effectiveness of the separation into slow and fast varying components.

To make a full comparison, the circuit model is simulated again on the same time interval without a separation into slow and fast varying components, i.e., using a real-valued system (4.1). The integration schemes SDIRK 3(2) and SDIRK 3(1) are applied. To estimate the local error, estimate (4.44) with $\epsilon_{\text{tol}} = 10^{-3}$ is employed. The statistic data on the number of the total/accepted/rejected number of the time steps are summarized in Tab. 5.2.

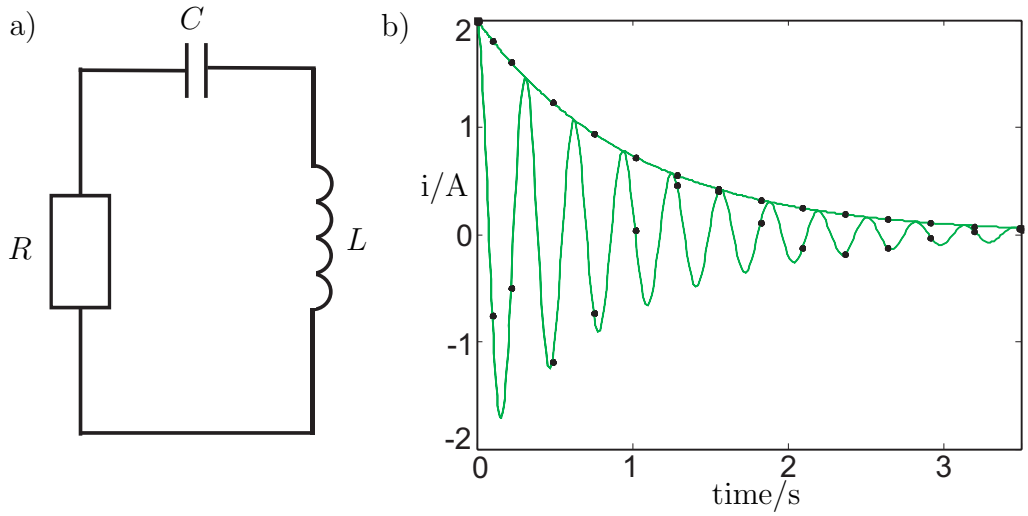

Figure 5.7: Test example: a) a damped series RLC circuit; b) the envelope of the current response obtained by numerical time integration and the current response reconstructed using (5.5) afterwards.

Number of Steps	Envelope Methods SDIRK 3(2)	Real-Valued System SDIRK 3(2)	Real-Valued System SDIRK 3(1)
Total	16	501	687
Accepted	16	396	682
Rejected	0	105	5

Table 5.2: Number of total/accepted/rejected time steps for the envelope and the real system integration methods.

The data in Tab. 5.2 demonstrate a dramatic increase in the computational costs in case if the separation of slow and fast varying components is not implemented. An adaptive integration of the real-valued system with SDIRK 3(2) method requires additional 485 time steps. Since each integration step requires the solution of four systems, additional 1940 systems have to be computed. However, according to the previous section and due to the purely sinusoidal dynamics of the solution, an adequate integration is achieved when specialized adaptive schemes such as SDIRK 3(1) are used. In this case the computational costs are even more higher: additional 2684 systems have to be solved. The magnitudes of the absolute error calculated during the time integration of the real-valued system with the SDIRK 3(2) and SDIRK 3(1) schemes are shown in Fig. 5.8.

To conclude we state that the envelope technique based on the separation of slow and fast varying components of a problem is an effective approach to significantly accelerate the process of the numerical time integration of electromagnetic problems achieving the same level of accuracy as one would obtain integrating real-valued systems without separation of dynamics.

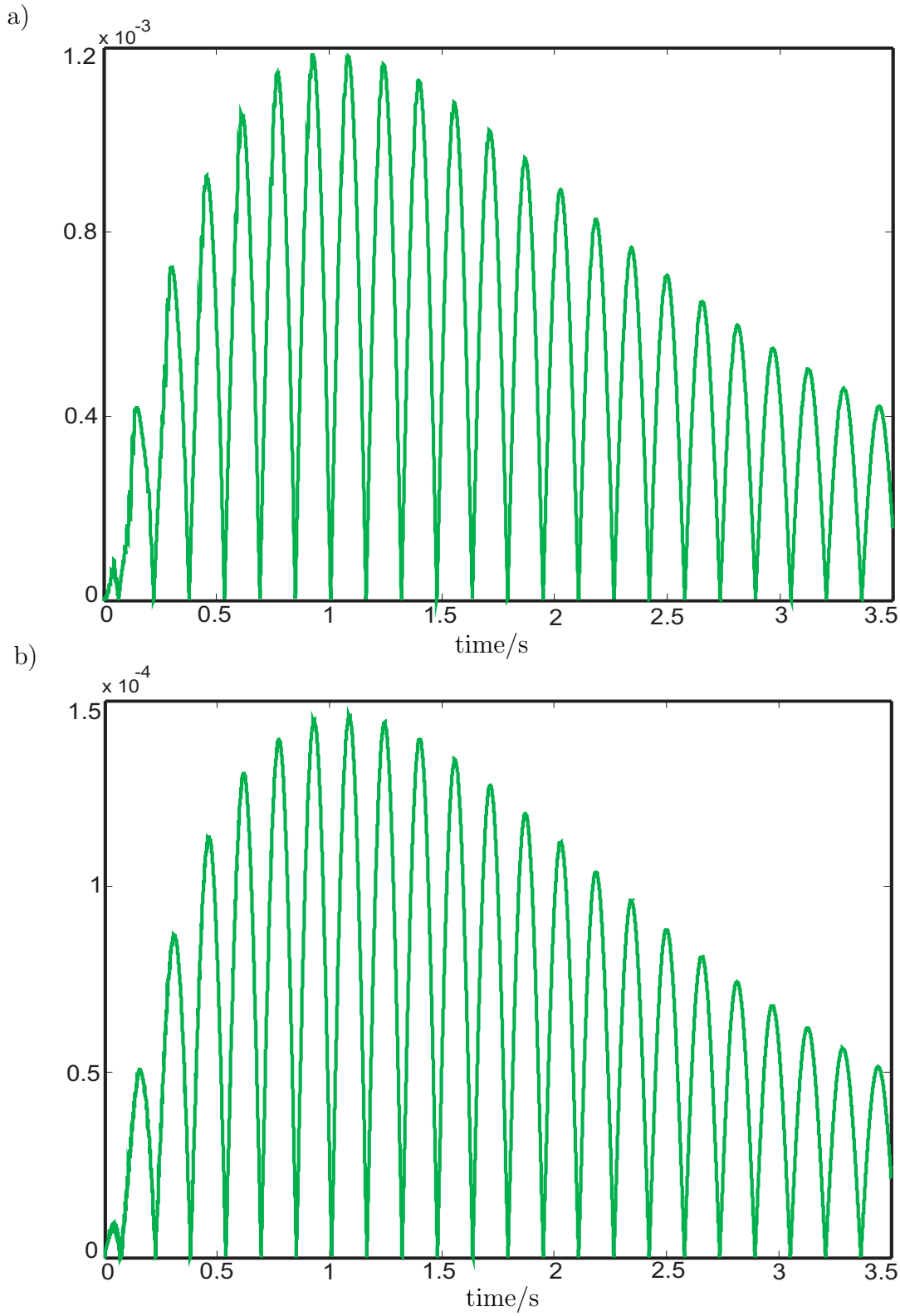

Figure 5.8: The magnitude of the absolute error calculated during the time integration of real-valued system (4.1) with the (a) SDIRK 3(2) method and (b) SDIRK 3(1) method.

Chapter 6

Field-Circuit Coupled Simulations with Switching Elements

In the final chapter of this thesis we develop general algorithms for the numerical simulation of field-circuit coupled problems with switching elements. In Section 6.1, relevant properties of switched networks are given and the reasons to use an ideal diode for modelling a true switching device are motivated. The topological changes arising in the numerical simulations due to switching elements are considered in Section 6.2. Section 6.3 starts with the derivation of the field-circuit transient coupled formulation with switching elements. To integrate the derived formulation in time, a three-step algorithm is proposed which is capable of handling the discontinuities effectively, thereby allowing the application of standard time-continuous integrators to the DAEs describing the switched systems.

6.1 Switched Networks

The theory of the nonswitched networks represents a well established research area. However, analysis methods for switched networks progress at a much slower rate. For analysis purposes, two categories of switched networks are distinguished [60]:

1. *Periodically switched linear networks* consisting of linear circuit elements and switches which change their states at predetermined and externally specified time instants. Examples include switched-capacitor filters and modulators. Such networks can be effectively analyzed by decomposing the original circuit into a sequence of linear circuit topologies that can be analyzed successively.[1]

2. *Switched nonlinear networks* consisting of linear circuit elements and switches changing their state at time instants that can be determined only during the time integration process. Such switches are called *internally controlled switches*. Typical examples are power converters.

[1] In general, if there are k switching elements, there will be 2^k different topologies.

There exist two approaches to simulate circuits with switching elements: either nonideal or ideal switch models are used. An ideal switch model has a zero resistance when it is in the conducting state, a zero admittance when it is in the blocking state, and a zero switching time between both states [60]. The ideal switch model introduces problems that are not encountered in the analysis of nonswitching analog networks. Models where switches are represented by the ideal switch model can no longer be treated by common circuit analyses because a discontinuous behavior may occur at switching time instants. These problems are usually avoided if nonideal switch models are used. However, there are several reasons to keep ideal switch models. Firstly, a nonideal switch is usually considered as a resistor with a very small resistance $R_{\text{conducting}}$ when the switch is in conducting state and a very large resistance $R_{\text{blocking}} = R_{\text{conducting}}^{-1}$ when the switch is in blocking state [61]. A typical value for $R_{\text{conducting}}$ chosen in circuit simulation with double precision arithmetic is 10^{-12} [62]. When a closing switch modeled as a nonlinear resistor causes a short-circuit of voltage sources and capacitor elements, its small resistance prevents an instantaneous redistribution of charge. Similarly, when an opening switch interrupts the current of a cutset of current sources and inductive elements, its representation by a large resistance allows for a non-instantaneous decay of the inductive current. The time constants $\tau_{\text{loop}} = R_{\text{conducting}} C_{\text{loop}}$ and $\tau_{\text{cutset}} = L_{\text{cutset}}/R_{\text{blocking}}$ with which these highly transient phenomena occur, depend on the capacitance C_{loop} of the short-circuited loop, the inductance L_{cutset} of the interrupted cutset and the small and large resistance values, $R_{\text{conducting}}$ and R_{blocking}, modeling the switch. The time integrator has to resolve these transients. Fast switches feature and a very small $R_{\text{conducting}}$ and a very large R_{blocking} will cause large differences in the relevant time constants in the system, leading to a large number of time steps. This problem can only be resolved efficiently by employing multi-rate time integration technique [63]. However, it is very expensive to step through such fast phenomena for a large field-circuit coupled model. The second numerical problem associated with this approach is due to the fact that the large and small limit resistances for the switches badly influence the condition number of the system matrices. It has been shown that not only the numerical condition but also the obtained results may depend on the chosen value for $R_{\text{conducting}}$ [60]. To tackle this problem, appropriate preconditioning techniques are mandatory.

The second motivation to use ideal switches is due to the fact that the response of the circuit usually does not change considerably if ideal or nonideal switches are used, but the simulation times may be affected considerably [60]. It is often the case for electrical devices operated at the low frequencies where the relative differences in time constants becomes prohibitive. In that case, a circuit simulator carrying out the switching events instantaneously is preferable.

Also when ideal switch models are used, the complicated behavior of semiconductor devices can be modeled. The typical 0.7 V voltage drop can be modeled by an independent voltage source. The parasitic resistances, capacitances, and inductances can be modeled by linear or nonlinear resistors, capacitors, and inductors, respectively. Because the discontinuous nature of the switch is represented by the ideal switch model, the additional circuit elements modeling the true semiconductor

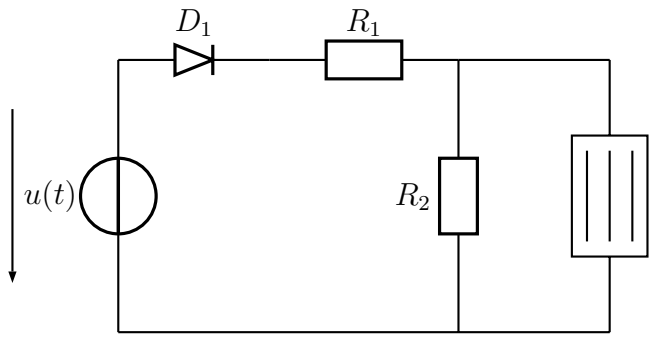

Figure 6.1: A stranded conductor connected to the external circuit containing a diode.

devices will not significantly influence the time constants and the system condition number.

In this work, the ideal switch model is employed to simulate the switches. Consequently, we need to treat the following items:

1. Changes in the topology of the circuit due to the switching events.

2. Integration over discontinuities arising due to switchings.

These issues are addressed in the following sections.

6.2 Topological Changes

For an ideal diode, we choose the model illustrated in Fig. 2.18a. An ideal diode is in the conducting state if i_D is positive and in the blocking state if v_D is negative. A conducting switch is equivalent to a zero-voltage source and it is therefore selected as a tree branch, whereas a blocking switch operates as a zero-current source and consequently appears in the cotree. Hence, the topological changes of the circuit are explicitly considered.

Fig. 6.1 represents a scheme where a conductor represented by a coil is connected to an external circuit consisting of a diode, two resistors and a voltage source. Since only one switching element is used, two different topologies are possible. They are illustrated in Fig. 6.2 where the tree branches are drawn with the solid lines and the cotree branches with the dashed lines. For the first topology, the circuit state variables are u_{R_1}, i_{R_2} and i_{coil}, whereas for the second topology, the circuit state variables are u_{R_1}, u_{R_2} and i_{coil}.

In the implementation, the tree tracing procedure is repeated after each switching event. This is acceptable for the relatively small circuits considered here.

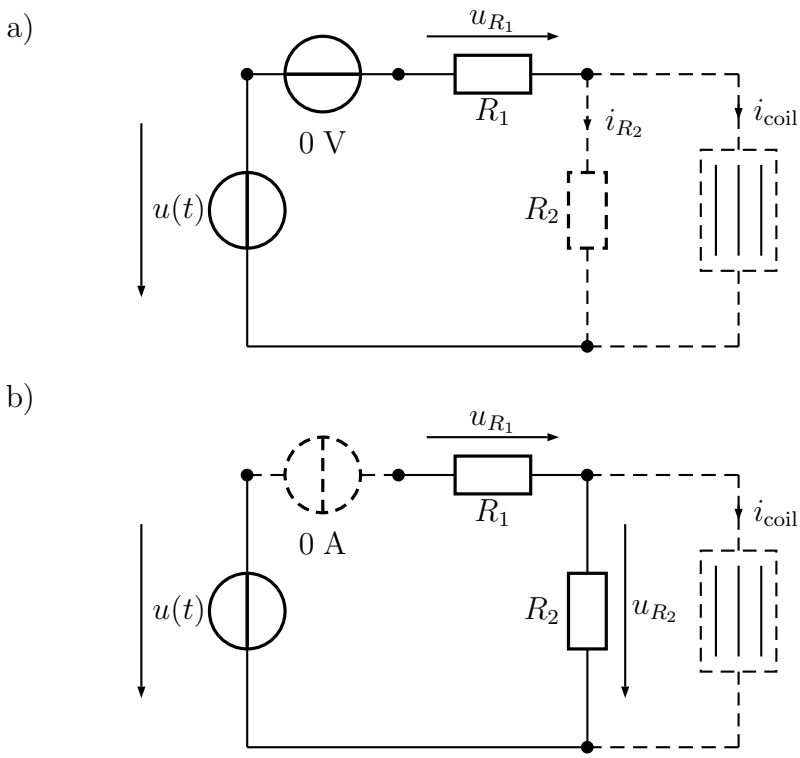

Figure 6.2: Tree/cotree partitioning of the model of Fig. 6.1 depending on the state of the diode. The tree branches are drawn with the solid lines and the cotree branches with the dashed lines: (a) when the diode is conducting, the circuit unknowns are u_{R_1}, i_{R_2} and i_{coil}; (b) when the diode is blocking, the circuit unknowns are u_{R_1}, u_{R_2} and i_{coil}.

6.3 Integration over Discontinuities

Standard numerical integration algorithms for DAE systems assume that the variables being integrated as well as their derivatives are continuous during the whole simulation time [64], [65]. The continuous problem is expressed mathematically by a set of DAEs represented by system (3.64). Due to the presence of switching elements in the circuit part of the problem, system (3.64) exhibits hybrid (continuous/discrete) behavior. Discontinuities occur, e.g., when the current in the conducting diode or the voltage drop over the blocking diode passes through zero. In 1994, Barton and Pantelides [66] developed a mathematical formulation for this problem as a sequence of initial value problems interspersed by instantaneous *events*[2] that may cause some form of discrete change to the initial value problem currently being solved. Very important is that these changes involve a manipulation of the functional form of the continuous mathematical model described by system (3.64) for

[2]In the literature, the same phenomenon is also alternatively termed *discontinuity*, *switch* or *guard*.

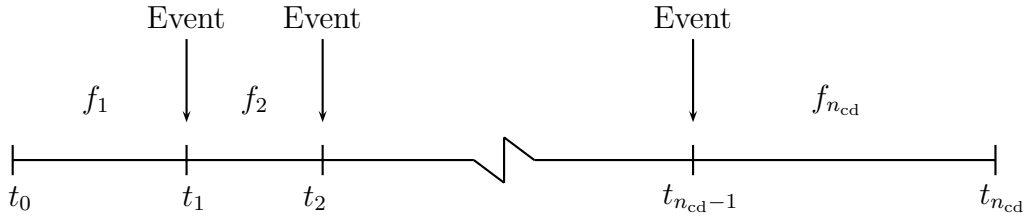

Figure 6.3: Time domain partitioning in combined discrete/continuous simulation. Functions $f_1, f_2, \ldots, f_{n_{\mathrm{cd}}}$ illustrate schematically one of the possible states of the hybrid system [66].

the currently treated state [66]. It means that in the case when a switching event is detected, the integration has to be stopped and system (3.64) has to be reformulated according to the new topology and to the new set of state variables. After that, a new time integration process is started. As a consequence, the time domain of interest $[t_0, t_{\mathrm{end}}]$ is partitioned into n_{cd} continuous subdomains $[t_{k-1}, t_k],\ k = 1, \ldots, n_{\mathrm{cd}}$ [66]. The value n_{cd} may be unknown a priory. The end of each continuous subinterval is determined by the occurrence of a switching event within the simulation process. This approach is illustrated schematically by Fig. 6.3 where the functions $f_1, f_2, \ldots, f_{n_{\mathrm{cd}}}$ represent schematically one of the possible states of the hybrid system. The initial time instant t_0 is assumed to be given whereas the final time instant t_{end} may be either given or specified implicitly through the termination conditions. The subdomains boundaries $t_k,\ k = 1, \ldots, n_{\mathrm{cd}} - 1$ are specified explicitly in case of periodically switched linear networks or determined implicitly during the simulation process if nonlinear switched networks are analyzed [66].

The set of equations and initial conditions of the first subdomain are specified by an individual simulation description and are usually known. The set of equations and initial conditions for the succeeding subdomains are determined from a combination of the final state of the system in the preceding subdomain and the consequences of the corresponding switch events [66].

The typical problems arising in the simulation of hybrid system are [67]:

1. Switching events may remain undetected.
2. The reliable localization of the events may require a large amount of computation time.
3. The time integrator may repeatedly signal the same switching event leading to an effect known as *discontinuity sticking*.

The main objective of the present chapter is to present a reliable numerical algorithm for the accurate time integration of the field-circuit coupled systems with switching elements that does not encounter the typical problems listed above. Here, we propose an algorithm consisting of three stages. Firstly, an event or discontinuity detection technique is discussed. As a second step of the algorithm, an event localization is implemented that accurately locates the events detected earlier. Finally, a set

of the consistent initial conditions featuring the new state of the hybrid system is determined. These three issues are elaborated in the following subsections.

6.3.1 Field-Circuit Coupled Formulation with Switching Elements

The mathematical mechanism for deriving a transient field-circuit coupled formulation with switching elements is identical to the one described in Section 3.4. The only difference is that those system matrix blocks that may be affected by topological changes due to switching events are supplied with the superscript (s). The state of the coupled system, here represented by (s), is determined by the states of all switching elements. Thus, hybrid transient field-circuit coupled formulation that also incorporates partial cutset/loop transformations, is defined by the following sequence of DAE sets:

$$\begin{bmatrix} \mathbf{M}_\sigma & \mathbf{0} & \mathbf{0} \\ -\mathbf{Q}^{(s)T}\mathbf{M}_\sigma & \mathbf{N}_C^{(s)} & \mathbf{0} \\ -\mathbf{P}^{(s)T} & \mathbf{0} & -\mathbf{N}_L^{(s)} \end{bmatrix} \frac{\mathrm{d}}{\mathrm{d}t} \begin{bmatrix} \widehat{\mathbf{a}} \\ \mathbf{u}_{\mathrm{twu}}^{(s)} \\ \mathbf{i}_{\mathrm{lnu}}^{(s)} \end{bmatrix} + \begin{bmatrix} \widetilde{\mathbf{C}}\mathbf{M}_{\mu^{-1}}\mathbf{C} & -\mathbf{M}_\sigma\mathbf{Q}^{(s)} & -\mathbf{P}^{(s)} \\ \mathbf{0} & \mathbf{N}_G^{(s)} & \mathbf{D}_{\mathrm{twu,lnu}}^{(s)} \\ \mathbf{0} & \mathbf{D}_{\mathrm{twu,lnu}}^{(s)T} & -\mathbf{N}_R^{(s)} \end{bmatrix} \begin{bmatrix} \widehat{\mathbf{a}} \\ \mathbf{u}_{\mathrm{twu}}^{(s)} \\ \mathbf{i}_{\mathrm{lnu}}^{(s)} \end{bmatrix} =$$

$$= \begin{bmatrix} \mathbf{0} \\ -\mathbf{D}_{\mathrm{twu,lni}}^{(s)}\mathbf{i}_{\mathrm{lni}}^{(s)}(t) + \mathbf{D}_{\mathrm{twu,lne}}^{(s)}\mathbf{G}_{\mathrm{lne}}^{(s)}\mathbf{B}_{\mathrm{lne,twi}}^{(s)}\mathbf{u}_{\mathrm{twi}}^{(s)}(t) + \mathbf{D}_{\mathrm{twu,lne}}^{(s)}\mathbf{C}_{\mathrm{lne}}^{(s)}\mathbf{B}_{\mathrm{lne,twi}}^{(s)}\frac{\mathrm{d}\mathbf{u}_{\mathrm{twi}}^{(s)}(t)}{\mathrm{d}t} \\ \mathbf{B}_{\mathrm{lnu,twi}}^{(s)}\mathbf{u}_{\mathrm{twi}}^{(s)}(t) - \mathbf{B}_{\mathrm{lnu,twe}}^{(s)}\mathbf{R}_{\mathrm{twe}}\mathbf{D}_{\mathrm{twe,lni}}^{(s)}\mathbf{i}_{\mathrm{lni}}^{(s)}(t) - \mathbf{B}_{\mathrm{lnu,twe}}^{(s)}\mathbf{L}_{\mathrm{twe}}^{(s)}\mathbf{D}_{\mathrm{twe,lni}}^{(s)}\frac{\mathrm{d}\mathbf{i}_{\mathrm{lni}}^{(s)}(t)}{\mathrm{d}t} \end{bmatrix} \quad (6.1)$$

where $t \in [t_k, t_{k+1}],\ k = 0, \ldots, n_{\mathrm{cd}} - 1$. Formulation (6.1) makes it possible for both the set of variables and the set of equations to vary from subdomain to subdomain. When one or multiple state changes take place, the circuit has to be reformulated according to the new topology and the integration process is processed with a set of consistent initial conditions featuring this new circuit topology. Since the considered electrical circuits are relatively small compared to the field part of the problem, the computational costs of this procedure are negligible [85].

6.3.2 Discontinuity Detection

In this stage, the algorithm determines whether at least one event function (e.g., the current in a conduction diode or the voltage in a blocking diode) becomes zero within the previous step.

Sign Check. A commonly used technique for event detection is to check for sign changes of the voltages and the currents in the branches containing switching elements at the beginning and at the end of the integration step. Discontinuities are then detected if the sign changes [62] [68], [69]. This method is simple, fast and reliable when the currents and voltages are piecewise linear in time, as is the case for commonly applied θ-type time integrators. Here, however, higher-order time integrators are employed. In this case, this discontinuity detection approach will detect only odd numbers of roots, while double, quadruple, etc. roots stay undetected. In

order to ensure a reliable event detection also for the higher-order time integration schemes, sign checks have to be implemented at very small time intervals leading to a computational overhead. Additionally, since in the general case the time intervals within which multiple roots may occur are not known a priory, it becomes arbitrary whether the correct checking interval is chosen. Thus, event detection by sign checks is unreliable and inefficient when higher-order time integration schemes are used, the number of switch events increases and the time intervals to be checked become extremely small in comparison with the overall simulation time [67], [70].

Sturm Sequence. In case of a higher-order time integration scheme, a reliable event detection is implemented using Sturm sequences [67], [71], [72]. For a polynomial $f_0(x)$, the Sturm sequence $f_0(x), f_1(x), \ldots, f_m(x)$ is given by

$$\begin{aligned} f_1(x) &= \frac{\mathrm{d}}{\mathrm{d}x} f_0(x), \\ f_2(x) &= -\mathrm{rem}\left(\frac{f_0(x)}{f_1(x)}\right), \\ &\vdots \\ f_m(x) &= -\mathrm{rem}\left(\frac{f_{m-2}(x)}{f_{m-1}(x)}\right) \end{aligned} \tag{6.2}$$

where the operator $\mathrm{rem}\left(\frac{\alpha}{\beta}\right)$ denotes the polynomial remainder of the division of α by β. The number of zeroes in the interval $(a, b]$ is equal to the number of sign variations in $\{f_0(a), f_1(a), \ldots, f_m(a)\}$ and $\{f_0(b), f_1(b), \ldots, f_m(b)\}$.

A straightforward question arises how one can obtain a polynomial $f_0(x)$ for any arbitrary time integration method and to derive from it a whole Sturm polynomial sequence. In case of higher-order Runge-Kutta time integration schemes, the interpolation formula (4.46) (see Chapter 4, Section 4.5) delivers a polynomial allowing to construct a Sturm sequence for use in the event detection step.

Discontinuity Locking. If an integration step tries to jump across a discontinuity, this usually results in repeated step failures and a significant reduction of the integration step [73]. This problem is avoided by applying the *locking* technique for the system of equations for each time step. This technique implies that during the time step the system of equations cannot change even if one or more switching events could take place. The state conditions are checked only at the end of each integration step with either the sign checking method (in case of θ-type time integration schemes) or by building the Sturm sequence (in case of higher-order Runge-Kutta time integrators). The main advantage of this technique is that the solution and its derivatives are continuous functions within the whole integration step [64], [66]. This approach eliminates the difficulties of integration over discontinuities and makes it possible to construct an interpolation polynomial of the form (4.46). The discontinuity locking technique, also used in this work, is well known and is throughout presented in literature [64], [68], [74].

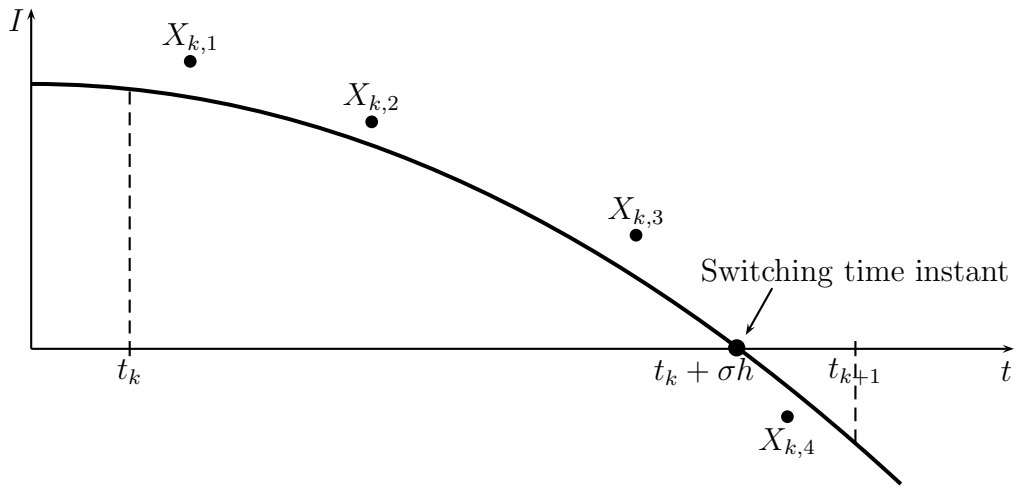

Figure 6.4: Localization of the switching event for a conducting diode: the calculated stage values $X_{k,i}, i = 1, \ldots, 4$ of the four stage Runge-Kutta time integrator are used to construct an interpolated dense-output polynomial with its root approximating the switching time instant $t_k + \sigma h$ of the diode.

6.3.3 Discontinuity Localization

If in the previous step of the algorithm one or more switching events are found to take place in the current integration step, the next task is to locate the earliest time instant in this interval. In [62] this was carried out using the bisection method. However, since the system has to be integrated several times until the switching time instant is determined within the prescribed accuracy, this approach may become time consuming.

An alternative technique becomes feasible thanks to the application of a higher-order time integration scheme. Namely, we can again employ a dense-output polynomial given by formula (4.46). Fig. 6.4 illustrates this idea for an arbitrary four-stage integration method: $\mathbf{X}_{k,i}, i = 1, \ldots, 4$ represent the calculated stage values at the time instants $t_i = t_k + c_i h, i = 1, \ldots, 4$. The stage derivatives are used to build an interpolation polynomial using formula (4.46). The roots $\sigma_1, \sigma_2, \ldots, \sigma_n$ of the polynomial (4.46) deliver the local time coordinates of the switching time instants and the real time instants for the switching events that have taken place between t_k and t_{k+1} are $t_k + \sigma_1 h, t_k + \sigma_2 h, \ldots, t_k + \sigma_n h$.

6.3.4 Consistent Initial Conditions

Because switching events change the circuit topology, the nature and even the number of circuit equations in (6.1) may change. Hence, at switching time instant, an adapted vector of initial conditions has to be computed [91]. The quantities that are directly associated with stored fractions of energy in the model, such as e.g., voltage drops over capacitors or currents in inductors, deserve special attention.

Topological problems arise when loops of current sources and inductive elements or cutsets of voltage sources and capacitive elements occur [75]. In circuits without switching elements, such situations are commonly alleviated on beforehand by the user. In the switched circuits, it is almost impossible to prevent such situations on beforehand, especially when the number of switching elements is very large. Hence, a suitable algorithm is due. After switching, a new tree is traced through the circuit accounting for the new topology. In loops that only consist of voltage-driven components, an instantaneous redistribution of charge is carried out. In cutsets that only contain current-driven components, an instantaneous redistribution of fluxes is carried out. In practical applications, every loop has at least a small parasitic series resistance and every cutset has a parallel parasitic resistance. The neglection of these resistances corresponds to the most difficult case where zero time constants reflecting instantaneous redistribution of charge and flux occur. Also in the practical case, it is recommended to either resolve very small time constants due to parasitic effects by a multi-rate time integration technique putting small intermediate time steps only for the circuit part, or to approximate highly transient parasite effects by instantaneous redistribution. In both cases, superfluous and expensive solutions of the field model part are avoided.

Instantaneous charge and flux distributions are considered by a procedure invoked before restarting the time integrator with the new topology. The proposed procedure consists of two independent parts that are separately considered below.

Instantaneous redistribution of charge. The instantaneous redistribution of charge in capacitive parts of the circuit is computed by integrating the expression

$$\mathbf{i} = \mathbf{C}\,\frac{\mathrm{d}\mathbf{u}}{\mathrm{d}t}$$

over an infinitesimal time step $[t^-, t^+]$, $t^+ = t^- + \Delta t$ with $\Delta t \to 0$ at the switching time instant, yielding

$$\mathbf{q}_{\mathrm{redistr}} = \int_{t^-}^{t^+} \mathbf{i}\,\mathrm{d}t = \int_{t^-}^{t^+} \mathbf{C}\,\frac{\mathrm{d}\mathbf{u}}{\mathrm{d}t}\,\mathrm{d}t = \mathbf{C}\,(\mathbf{u}^+ - \mathbf{u}^-) \tag{6.3}$$

where the voltages with superscript "-" are obtained by the last time step and the voltages with superscript "+" are the new consistent initial values.

Only conducting switches, voltage sources and capacitors are considered. All other branches operate as open circuit for charge redistribution. Hence, the original circuit is possibly splitted in several parts. A tree is traced through these circuit parts ensuring that all capacitors are in the co-tree yielding the fundamental cutset and loop matrices $\mathbf{D}^{(\mathrm{cap})}_{\mathrm{twu,lne}}$ and $\mathbf{B}^{(\mathrm{cap})}_{\mathrm{lne,twu}}$. A set of consistent initial voltages for the capacitor follows from solving

$$\begin{aligned}\left(\mathbf{N}_{\mathrm{C,twu}} - \mathbf{D}^{(\mathrm{cap})}_{\mathrm{twu,lne}}\mathbf{N}_{\mathrm{C,lne}}\mathbf{B}^{(\mathrm{cap})}_{\mathrm{lne,twu}}\right)\left(\mathbf{u}^+_{\mathrm{twu}} - \mathbf{u}^-_{\mathrm{twu}}\right) = \\ \mathbf{D}^{(\mathrm{cap})}_{\mathrm{twu,lne}}\mathbf{N}_{\mathrm{C,lne}}\mathbf{B}^{(\mathrm{cap})}_{\mathrm{lne,twi}}\left(\mathbf{u}^+_{\mathrm{twi}} - \mathbf{u}^-_{\mathrm{twi}}\right)\end{aligned} \tag{6.4}$$

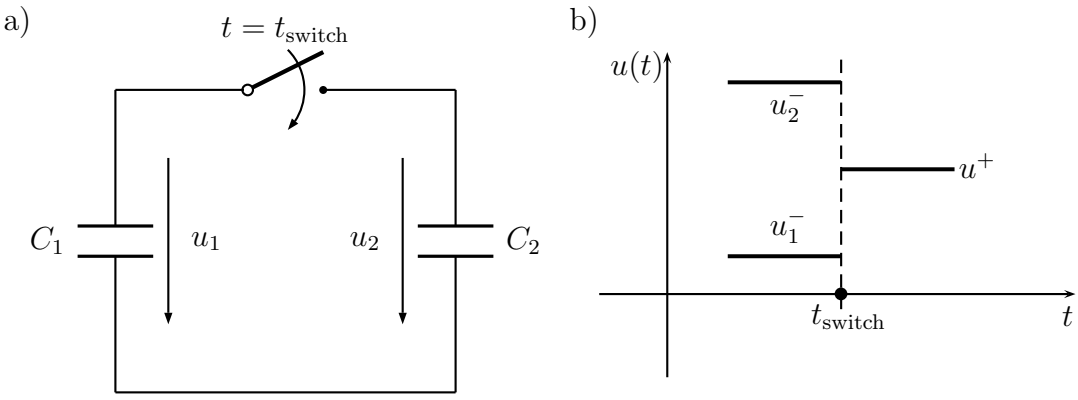

Figure 6.5: Determination of the consistent initial conditions for the capacitors / voltage source loops: a redistribution of charge is considered: (a) for $t < t_{\text{switch}}$ the switch is opened; after closing the switch at $t = t_{\text{switch}}$ the circuit has inconsistent initial conditions and momentarily violates the KVL, $C_1 = C_2 = 1$ F, $u_1 = 1$ V, $u_2 = 5$ V; (b) the voltage drop across the capacitors before and after switching.

where "(cap)" indicates the capacitive part of the circuit, "twu" and "lne" indicate the capacitors in the tree and co-tree, respectively. For voltage sources with a continuous output signal, $\mathbf{u}^+_{\text{twi}} - \mathbf{u}^-_{\text{twi}}$ is zero. For conducting switches $\mathbf{u}^+_{\text{twi}}$ is zero.

The graphical representation of this technique is illustrated by the example given in Fig. 6.5. The capacitors $C_1 = C_2 = 1$ F (Fig. 6.5a) have initial voltages $u_1(t^-_{\text{switch}}) = 1$ V and $u_2(t^-_{\text{switch}}) = 5$ V, respectively. When the switch is closed, the circuit is inconsistent and momentarily violates the KVL. Using (6.4) and knowing that $u_1(t^+_{\text{switch}}) = u_2(t^+_{\text{switch}})$ the consistent solution is obtained:

$$u_1(t^+_{\text{switch}}) = u_2(t^+_{\text{switch}}) = \frac{C_1 u_1(t^-_{\text{switch}}) + C_2 u_2(t^-_{\text{switch}})}{C_1 + C_2} \tag{6.5}$$

where $u(t^+_{\text{switch}})$ is the voltage drop across the capacitors after switching. Since there is no independent voltage supply, the voltages on the capacitors remain constant once the equilibrium condition has been reached and hence:

$$u_1(t) = u_2(t) = u_1(t^+_{\text{switch}}) = u_2(t^+_{\text{switch}}) = u(t^+_{\text{switch}}),\ t > t_{\text{switch.}} \tag{6.6}$$

as illustrated in Fig. 6.5b.

Instantaneous redistribution of flux. The instantaneous redistribution of flux in the inductive parts of the circuit is computed by integrating

$$\mathbf{u} = \mathbf{L}\,\frac{\mathrm{d}\mathbf{i}}{\mathrm{d}t}$$

over $[t^-, t^+]$, yielding

$$\psi_{\text{redistr}} = \int_{t^-}^{t^+} \mathbf{u}\,\mathrm{d}t = \int_{t^-}^{t^+} \mathbf{L}\,\frac{\mathrm{d}\mathbf{i}}{\mathrm{d}t}\,\mathrm{d}t = \mathbf{L}\,(\mathbf{i}^+ - \mathbf{i}^-). \tag{6.7}$$

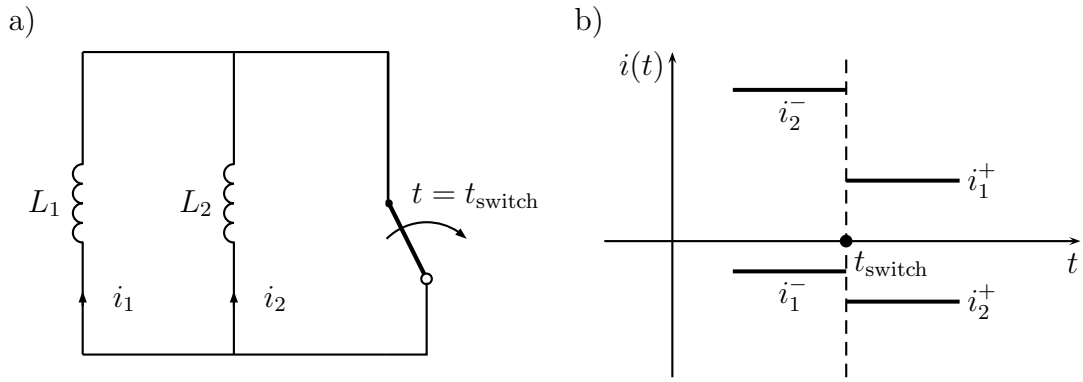

Figure 6.6: Determination of the consistent initial conditions for the inductors: a redistribution of flux is considered: (a) for $t < t_{\text{switch}}$ the switch is closed; after opening the switch at $t = t_{\text{switch}}$ the circuit has inconsistent initial conditions and momentarily violates the KCL, $L_1 = L_2 = 1$ H, $i_1 = -1$ A, $i_2 = 5$ A; (b) the currents through the inductors before and after switching.

Only blocking switches, current sources and inductors are considered. All other branches are short-circuited. A tree which only contains inductors is constructed leading to the fundamental cutset and loop matrices $\mathbf{D}^{(\text{ind})}_{\text{twe,lnu}}$ and $\mathbf{B}^{(\text{ind})}_{\text{lnu,twe}}$. A set of consistent initial currents for the inductors follows from solving

$$\left(\mathbf{N}_{\text{L,lnu}} - \mathbf{B}^{(\text{ind})}_{\text{lnu,twe}}\mathbf{N}_{\text{L,twe}}\mathbf{D}^{(\text{ind})}_{\text{twe,lnu}}\right)\left(\mathbf{i}^+_{\text{lnu}} - \mathbf{i}^-_{\text{lnu}}\right) = \mathbf{B}^{(\text{ind})}_{\text{lnu,twe}}\mathbf{N}_{\text{L,twe}}\mathbf{D}^{(\text{ind})}_{\text{twe,lni}}\left(\mathbf{i}^+_{\text{lni}} - \mathbf{i}^-_{\text{lni}}\right) \tag{6.8}$$

where "ind" indicates the inductive part of the circuit, "lnu" and "twe" indicate the inductors in the cotree and tree, respectively. For current sources with a continuous output signal $\mathbf{i}^+_{\text{lni}} - \mathbf{i}^-_{\text{lni}}$ is zero, whereas for blocking switches $\mathbf{i}^+_{\text{lni}}$ is zero.

The graphical representation of this technique is illustrated in Fig. 6.6. The inductors $L_1 = L_2 = 1$ H (Fig. 6.6a) have initial conditions $i_1(t^-_{\text{switch}}) = -1$ A and $i_2(t^-_{\text{switch}}) = 5$ A, respectively. When the switch is opened, the circuit momentarily violates the KCL. Using (6.8) the consistent solution is obtained:

$$i_2(t^+_{\text{switch}}) = -i_i(t^+_{\text{switch}}) = \frac{L_1 i_1(t^-_{\text{switch}}) + L_2 i_2(t^-_{\text{switch}})}{L_1 + L_2} \tag{6.9}$$

where $i_1(t^+_{\text{switch}})$ and $i_2(t^+_{\text{switch}})$ are the currents through the first and second inductor, respectively, after switching (see Fig. 6.6b).

After this two-step procedure, the voltage drops over the capacitive elements and the currents through the inductive elements are consistent with the new circuit topology. This property guarantees that the further time integration only has to resolve the relevant time constants in the field-circuit coupled system and not the rise times of the individual switches and the possible highly transient redistributions of charge and flux.

6.4 Numerical Examples

We conclude this chapter with two numerical examples which are studied focusing on the following aspects:

1. Spatial discretization of the field part of the problem by means of the FIT.
2. Tree/cotree partitioning of the networks.
3. Construction of the transient field-circuit coupled formulation accounting for switching elements.
4. Application of the higher order error controlled implicit Runge-Kutta time integration schemes for the numerical treatment of the coupled formulation.
5. Topological changes in the circuit part of the model due to switching events.
6. Efficient and reliable integration over discontinuities caused by the switching events.

The field parts of both test problems are discretized in space by means of the FIT. After a tree/cotree partitioning of the network is carried out, field-circuit coupled formulation (6.1) is set up. The obtained coupled formulation is integrated in time using the higher order error controlled implicit integration scheme SDIRK 3(2) characterized in Appendix A. To estimate the local error during the computation, error norm (4.44) with $\epsilon_{\text{tol}} = 10^{-3}$ is used.

Since the diodes are internally controlled switching devices, i.e., the time instants where they experience the state changes are not defined a priori, a three-step discontinuity-handling algorithm proposed in the work, is employed. The discontinuity detection procedure by means of the Sturm sequence is activated after each completed time step. In case that one or multiply state changes are reported, the time integration process is stopped. In the second step of the proposed algorithm, the local time coordinate σ of the leftmost switching event is calculated by finding the roots of the corresponding dense-output polynomials. For the SDIRK 3(2) integration scheme employed here, the dense-output polynomial is of degree three. The polynomial roots can be therefore calculated analytically. The obtained value of the local time coordinate σ is used to calculate the real leftmost switching time instant. When the switching event is localized, a final step of the algorithm is activated and the consistent initial conditions are calculated using formulas (6.4) and (6.8). Finally, the topology of the circuit is changed and the integration process is continued from the switching time time instant $t_n + \sigma h$ with modified system (6.1) and with the new consistent start values adopted to the new circuit topology.

Test problem 1. A first test problem is a step-up converter where the inductor loaded by the voltage source during the idle period is represented by a field model discretized by the FIT (Fig. 6.7a). The input voltage value is $U = 48$ V, the load is $R = 20\ \Omega$ and the capacitance is $C = 1.2\ \mu$F. Since the circuit part of the model contains two switching elements, four different network topologies are possible.

The described model is integrated numerically in the time period from 0 s until 20 ms using SDIRK 3(2) integration scheme. For this simulation, the numbers of accepted

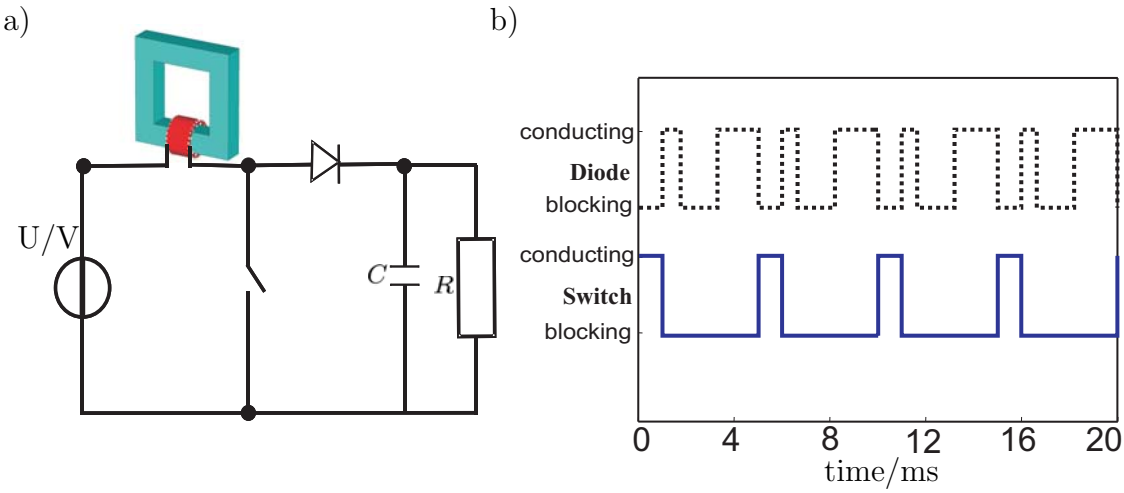

Figure 6.7: Test problem 1: (a) step-up converter with a conducting coil; (b) state changes of the switching elements.

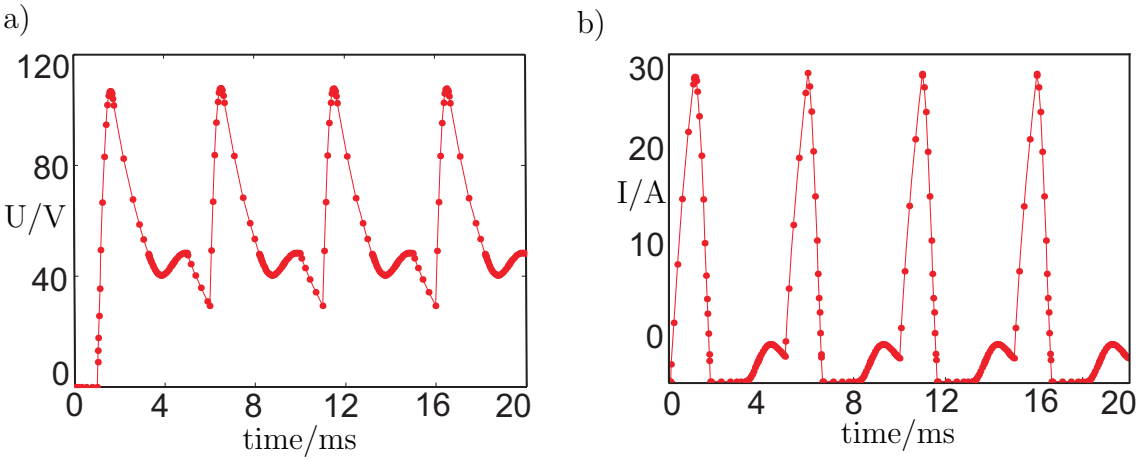

Figure 6.8: Test problem 1: calculated voltage in the capacitor (a) and current in the conducting coil (b).

and rejected time steps are 260 and 97, respectively. The prescribed conducting and blocking time periods for the switch (solid line) and the calculated switching stages of the diode (dashed line) are shown in Fig. 6.7b. The calculated voltage drop in the capacitor and current in the coil are presented in Fig. 6.8. The marks indicate the time instants selected by the adaptive time-step procedure.

Test problem 2. For the simulation of a three-phase transformer (Fig. 6.9) the primary side of which is connected to the power grid and the secondary side to a diode rectifier with an inductive load (Fig. 6.10), the derived field-circuit coupled transient formulation (6.1) is applied.

The following values for the circuit elements of the load are used: $L_{\text{load}} = 1$ mH and $R_{\text{load}} = 10$ mΩ. The model is excited by a three-phase sinusoidal voltage source with the frequency of 50 Hz. The power grid, the rectifier and the load are modeled

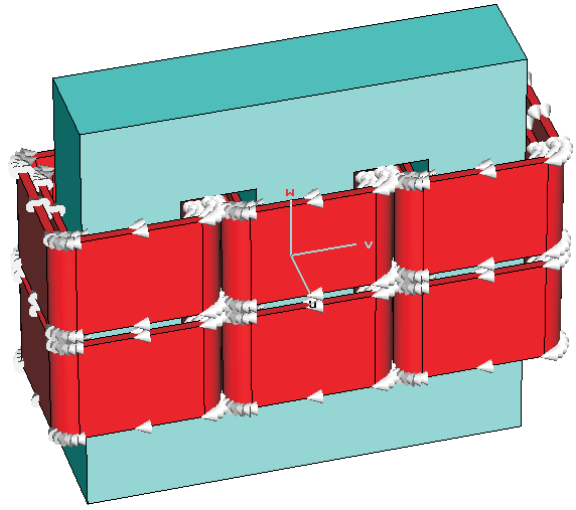

Figure 6.9: The 3D model of the three-phase transformer.

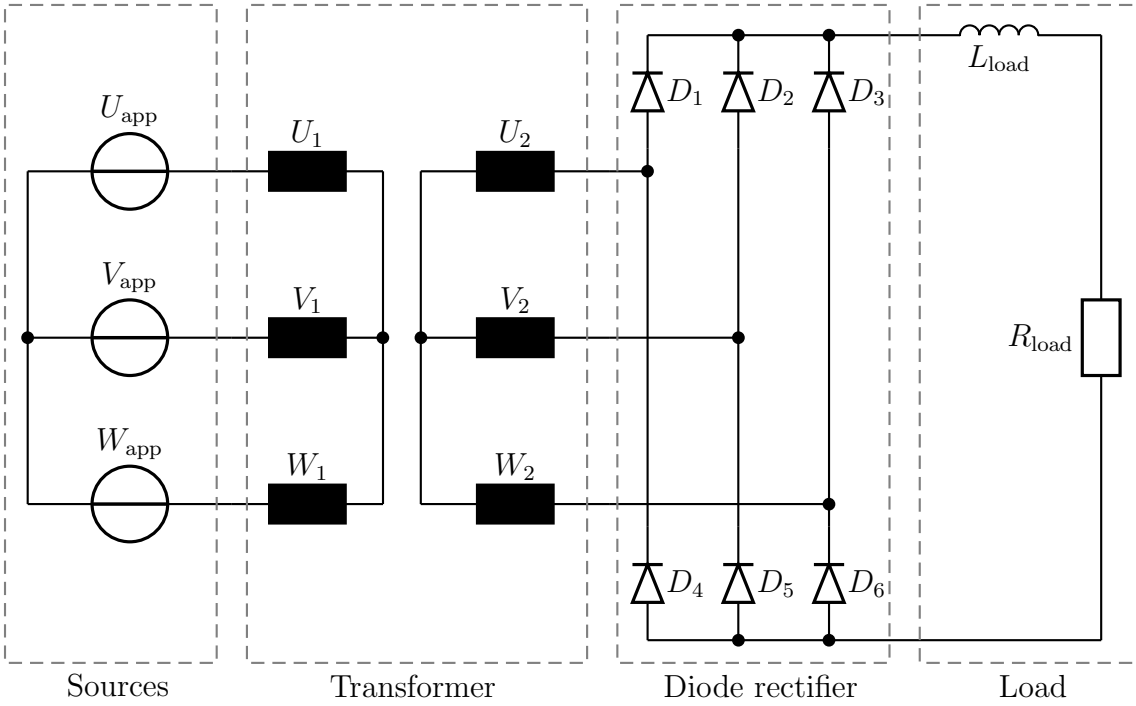

Figure 6.10: Three-phase transformer the primary side of which is connected to the power grid and the secondary side to a diode rectifier with an inductive load.

by equivalent circuit parameters whereas the three-phase transformer is represented by a field model in order to account for eddy currents. Since the circuit part of the model contains six diodes, 64 different network topologies are possible.

The described model is integrated numerically in the time period from 0 s until 0.3 s. In the performed simulation, the total number of time steps is equal to 476, 18 time steps are rejected. Fig. 6.11 shows the calculated current in the inductive load of

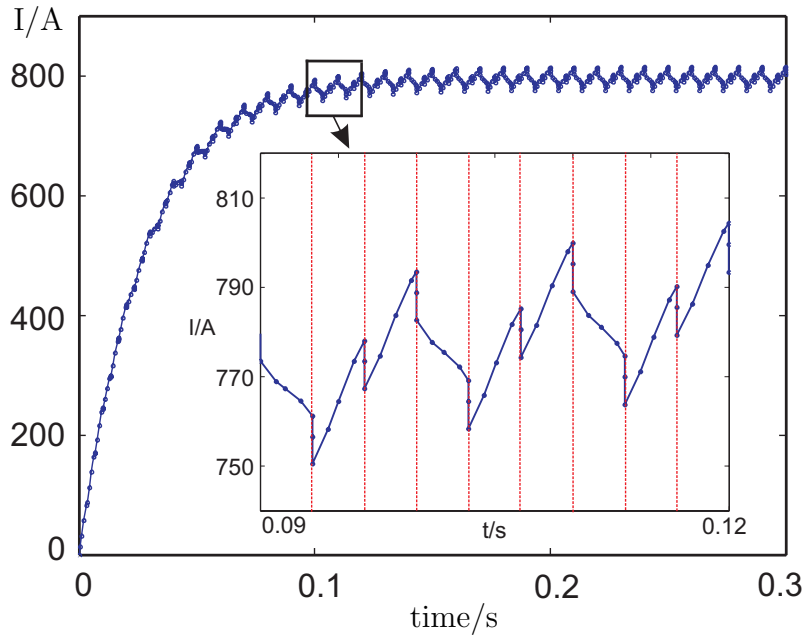

Figure 6.11: Current in the inductive load of the three-phase transformer.

the model. The vertical bars indicate the time instants at which one or more diodes switch. The marks indicate the time instants selected by the adaptive time-step procedure. Fig. 6.12 represents the behavior of all six diodes of the rectifier.

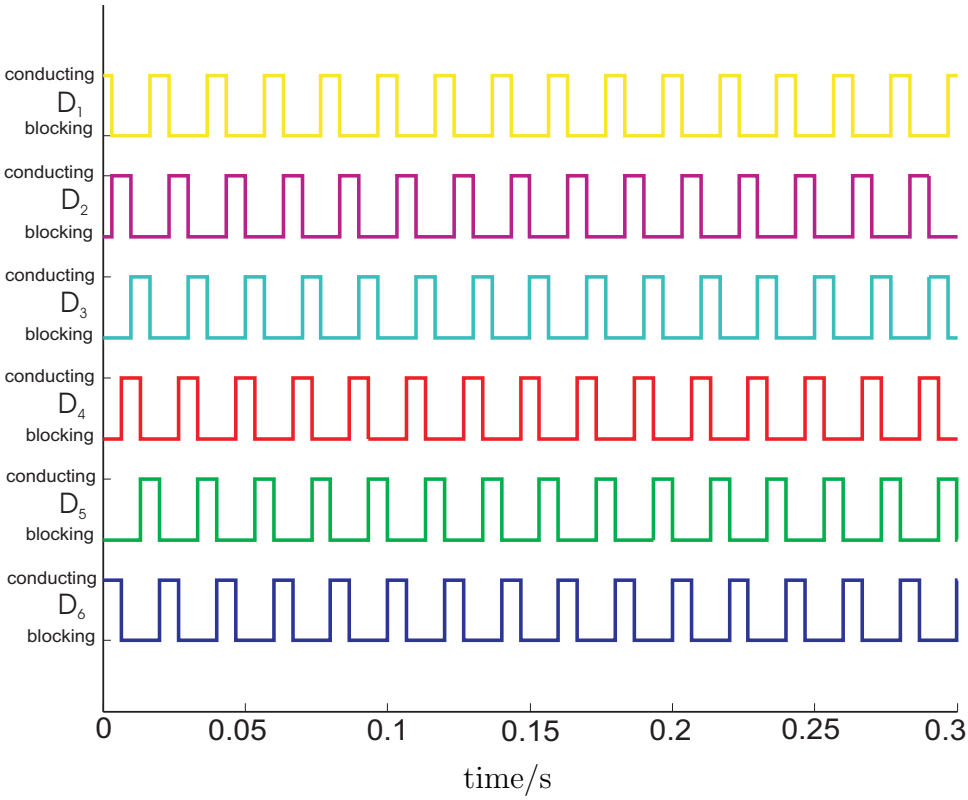

Figure 6.12: State changes in the diode rectifier.

Chapter 7

Conclusion

In the scope of this thesis, the derivation of a transient field-circuit coupled formulation is presented. In the field-circuit model, the field part is discretized by the Finite Integration Technique which allows to consider complicated geometries and local saturation or eddy current effects, whereas the other parts such as external sources and loads are treated by lumped parameters within a separate circuit model. A strong coupling is implemented: the field and the circuit models are coupled on the algebraic level and solved as a whole.

The Finite Integration Technique discretization of the magnetodynamic part of the model and its coupling with external circuits lead to a large system of differential-algebraic equations that cannot be treated numerically like regular ordinary differential equations. Since they are index 1 problems, they are treated by the implicit Runge-Kutta-type methods. The realization of these methods makes it possible to implement adaptive time stepping within the integration process thus effectively optimizing the central processing unit time as demonstrated by numerical examples.

For the field-circuit coupled models with switching elements, a special algorithm is elaborated which allows the application of the standard continuous time integrators to the differential-algebraic system of equations including discontinuities. The proposed algorithm consists of three steps: discontinuity detection, discontinuity localization and determination of consistent initial conditions.

The first step of the algorithm is realized through the construction of Sturm sequence that starts from the dense-output polynomial supplied by the Runge-Kutta time integrator. The second step of the algorithm is activated if one or multiple state changes are reported in the first step. The topology of the circuit part of the coupled model is changed according to the new states of the switching elements. Finally, a set of consistent initial conditions corresponding to the new circuit topology is determined and the integration process is continued. The last step of the proposed algorithm is challenging because the field part causes the major computational cost, and, as a consequence, a lot of computation time. Therefore, an efficient technique is proposed in the thesis by which highly transient phenomena in the circuit part are only resolved within the circuit model by considering instantaneous charge and flux redistribution inside the circuit thus avoiding a time-consuming evaluation of

the field problem. Two test problems illustrate the effectiveness of the proposed algorithm.

The numerical examples in the thesis show that standard error-controlled Runge-Kutta time integration methods fail for electromagnetic problems with sinusoidal excitation when the adaptive time step selection relies upon the comparison of a main solution and an embedded solution where the difference of orders is one. This problem is overcome by using an embedded solution that differs by two orders of approximations. Such an embedded solution is efficiently constructed by putting appropriate order conditions on the coefficients of the Butcher table as demonstrated in the work. Numerical examples illustrate the performance of the proposed numerical schemes.

For electromagnetic problems exhibiting sinusoidal functional behavior with a known angular frequency, a separation of variables into slow and fast varying components is implemented. Pure transient analysis is inefficient when it is necessary to resolve low frequencies in the presence of a high frequency components because the high-frequency dynamics forces a small time step whereas the low-frequency dynamics forces a long simulation time interval. In the thesis, a transient time-harmonic approach is proposed which is able to tackle problems mixing fast and slow dynamics. This approach can be considered as a bridge between the pure transient method and the steady-state simulation regime. In the frame of this approach, only the slow varying transients represented by an unknown amplitude and a phase of a full transient solution have to be integrated which leads to significant central processing unit time savings. Transient complex-valued systems arising from this approach are integrated adaptively with the implicit Runge-Kutta methods.

Appendix A

Coefficients of SDIRK Method

The Butcher table for the SDIRK method [56] defines a main solution of order three and two embedded solutions of second and first order, respectively:

$1-\sqrt{2}/2$	$1-\sqrt{2}/2$	0	0	0
1	$\sqrt{2}/2$	$1-\sqrt{2}/2$	0	0
$\sqrt{2}/2$	$5-3\sqrt{2}$	$2\sqrt{2}-6$	$1-\sqrt{2}/2$	0
1	$\sqrt{2}/3+1/6$	$\sqrt{2}/6-1/3$	$1/6$	$1-\sqrt{2}/2$
order 3	$\sqrt{2}/3+1/6$	$\sqrt{2}/6-1/3$	$1/6$	$1-\sqrt{2}/2$
order 2	$\sqrt{2}/2$	$1-\sqrt{2}/2$	0	0
order 1	$1/2$	$1/8$	$1/4$	$1/8$

.

According to (4.46), the dense-output interpolator corresponding to the solution of order three of this method reads [56]:

$$\bar{b}^T(\sigma) = \frac{1}{30}[1 \quad \sigma \quad \sigma^2] \begin{bmatrix} 22\sqrt{2}/2+15 & 236-150\sqrt{2} & 1-7\sqrt{2} & 135\sqrt{2}-222 \\ -14\sqrt{2}-15 & 135\sqrt{2}-262 & 13+14\sqrt{2} & 264-135\sqrt{2} \\ 2\sqrt{2} & 16+20\sqrt{2} & -9-7\sqrt{2} & -12-15\sqrt{2} \end{bmatrix}.$$

List of Notations

General Mathematical Expressions

$\mathbb{C}$	set of complex numbers
$\mathbb{N}$	set of natural numbers
$\mathbb{R}$	set of real numbers

Universal Constants

$c_0 = 2.99792458 \cdot 10^8$ m/s	velocity of electromagnetic wave in free space
$\epsilon_0 = 8.854 \cdot 10^{-12}$ F/m	permittivity of free space
$\mu_0 = 4\pi \cdot 10^{-7}$ H/m	permeability of free space
$\pi = 3.14159265$	in Euclidean geometry, the ratio of a circle circumference to its diameter

Classical Electrodynamics

$\vec{\mathrm{E}}$	electric field strength
$\vec{\mathrm{D}}$	electric flux density
$\vec{\mathrm{H}}$	magnetic field strength
$\vec{\mathrm{B}}$	magnetic flux density
$\vec{\mathrm{J}}$	electric current density
ρ	electric charge density
$\vec{\mathrm{P}}$	polarization of the medium
$\vec{\mathrm{M}}$	magnetization of the medium
χ_e	dielectric susceptibility
χ_m	magnetic susceptibility
ε_r	relative permittivity
ε	scalar absolute permittivity
μ_r	relative permeability

μ	scalar absolute permeability
$\vec{\mathrm{J}}_{\mathrm{cond}}$	conduction current density
σ	scalar conductivity
$\vec{\mathrm{J}}_{\mathrm{s}}$	source current density
$\vec{\mathrm{J}}_{\mathrm{conv}}$	convection current density
δ	diffusion constant
q	charge
$\vec{\mathrm{v}}$	speed of a moving charge q
A	two-dimensional domain
∂A	contour of the two-dimensional domain A
V	three-dimensional domain
∂V	boundary of the three-dimensional domain V
$\vec{\mathrm{a}}_{\mathrm{n}}$	normal vector
t	subscript to denote a tangential component of the field
n	subscript to denote a normal component of the field
ρ_s	surface charge density
φ	scalar potential
$\vec{\mathrm{A}}$	vector potential
ξ	scalar function
t	time
ℓ	length scale
τ	characteristic time of an excitation
τ_{em}	propagation time for an electromagnetic wave
τ_{e}	electroquasistatic charge relaxation time
τ_{m}	magnetoquasistatic current diffusion time
ℓ^*	characteristic length
η	intrinsic impedance of a medium

Finite Integration Technique

Ω	finite space region in $\mathbb{R}^3$
G, $\tilde{G}$	primary and dual space grids in Cartesian coordinates
N_p, I, J, K	total number of grid points and the numbers of grid lines in x, y, and z directions; $N_p = I \cdot J \cdot K$
i, j, k	space indices
$P(n)$, $\tilde{P}(n)$	points of the primary and dual grids
$L(n)$, $\tilde{L}(n)$	edges of the primary and dual grids

$A(n)$, $\tilde{A}(n)$	facets of the primary and dual grids
V, $\tilde{V}$	primary and dual grid volumes
$\widehat{\mathbf{e}}$, $\widehat{\mathrm{e}}$	vector of electrical grid voltages, component of the vector of electrical grid voltages
$\widehat{\widehat{\mathbf{b}}}$, $\widehat{\widehat{\mathrm{b}}}$	vector of magnetic grid fluxes, component of the vector of magnetic grid fluxes
$\mathbf{C}$, $\mathbf{S}$	discrete curl and divergence operators of the primary grid G
P_x, P_y, P_z	discretized partial differential operators
$\widehat{\mathbf{h}}$, $\widehat{\mathrm{h}}$	vector of magnetic grid voltages, component of the vector of magnetic grid voltages
$\widehat{\widehat{\mathbf{d}}}$, $\widehat{\widehat{\mathrm{d}}}$	vector of electric grid fluxes, component of the vector of electric grid fluxes
$\widehat{\widehat{\mathbf{j}}}$, $\widehat{\widehat{\mathrm{j}}}$	vector of the electrical grid currents, component of the vector of the electrical grid currents
$\widetilde{\mathbf{C}}$, $\widetilde{\mathbf{S}}$	discrete curl and divergence operator of the dual grid $\tilde{G}$
$\mathbf{q}$	vector of discrete electrical charges
ϕ	vector of the grid scalar electric potentials
$\widehat{\mathbf{a}}$	vector of the grid magnetic vector potentials
$\mathbf{G}$	discrete gradient matrix
$\mathbf{M}_{\varepsilon}$	discrete permittivity matrix
$\mathbf{M}_{\sigma}$	discrete conductivity matrix
$\mathbf{M}_{\mu^{-1}}$	discrete inverse permeability matrix
$\mathbf{D}_S$, $\tilde{\mathbf{D}}_S$	diagonal matrices of the primary and dual edge lengths
$\mathbf{D}_A$, $\tilde{\mathbf{D}}_A$	diagonal matrices of the cross-sections of primary and dual facets

Electrical Circuits

$p(t)$	electrical power
$u(t)$	voltage drop
$i(t)$	current
$q(t)$	electrical charge
W	energy
R	resistance
L	inductance
C	capacitance

Transient Field-Circuit Coupled Formulation

G_d	directed graph of a network
G_n	nonoriented graph of a network
$b_1, b_2, \ldots, b_n$	a set of branches in a network
$V_1, V_2, \ldots, V_k$	nodes of a graph
G_s	a subgraph of a graph G_n
T	a tree in a graph G_n
T_c	a cotree in a graph G_n
$\mathbf{A}$	incidence matrix of a directed graph G_d
$\mathbf{B}_a$	loop matrix of a directed graph G_d
$\mathbf{B}_b$	basic loop matrix
$\mathbf{B}$	fundamental loop matrix
$\mathbf{D}_a$	cutset matrix of a directed graph G_d
$\mathbf{D}_b$	basic cutset matrix
$\mathbf{D}$	fundamental cutset matrix
$\mathbf{u}$	vector of the branch voltage drops in a network
$\mathbf{i}$	vector of the branch currents in a network
Y_{br}	branch admittance
$f_{\mathrm{br,coup}}$	coupling term
Z_{br}	branch impedance
twi	index for the independent-voltage-source twigs
twu	index for the unknown voltage-driven twigs
twe	index for the eliminated current-driven twigs
lne	index for the eliminated voltage-driven links
lnu	index for the unknown current-driven links
lni	index for the independent-current-source links
δ	skin depth
f	frequency of a time-varying magnetic field
ℓ_{sol}, ℓ_{str}	lengths of the solid and stranded conductor, respectively
I_{sol}, I_{str}	total currents through the solid and stranded conductor, respectively
S_{sol}, S_{str}	cross-sections of the solid and stranded conductor, respectively
N_t	the number of strands of the stranded conductor
U_{sol}, U_{str}	voltage drops along the solid and stranded conductor, respectively

S_w	cross-section of a single strand of a stranded conductor
Ω_FIT	FIT domain
$\vec{\mathrm{J}}_\mathrm{sol}$	conduction current density in a solid conductor
$\vec{\mathrm{J}}_\mathrm{e}$, $\vec{\mathrm{J}}_\mathrm{s}$	eddy current and source current densities in a solid conductor
$\widehat{\widehat{\mathbf{j}}}_\mathrm{sol}$	vector of the grid conduction current densities in a solid conductor
$\widehat{\widehat{\mathbf{j}}}_\mathrm{e}$	vector of the grid eddy current densities in a solid conductor
$\widehat{\widehat{\mathbf{j}}}_\mathrm{s}$	vector of the grid source current densities
$\widehat{\mathbf{e}}_\mathrm{app}$	electric field distribution
$\tilde{\mathbf{Q}}$	2D incidence matrix for the coupling of the circuit to a solid conductor
$\tilde{G}_\mathrm{sol}$	dc conductance of the reference layer
ϕ_s	unknown vector of a grid scalar electric potentials
$\mathbf{N}_{\widehat{\mathbf{e}}}$	projection operator
G_sol	dc conductance of the solid conductor
$\mathbf{Q}$	coupling term for the coupling of the circuit to a solid conductor
$\widehat{\widehat{\mathbf{j}}}_\mathrm{app}$	vector of grid average current densities for a stranded conductor
$\tilde{\mathbf{P}}$	2D incidence matrix for the coupling of the circuit to a stranded conductor
$\mathbf{M}_{\sigma,\mathrm{aniso}}$	anisotropic conductivity matrix
$\mathbf{P}$	coupling term for the coupling of the circuit to a stranded conductor
$\mathbf{N}_{\widehat{\mathbf{j}}}$	projection operator
$\tilde{R}_\mathrm{str}$	dc resistance of the reference layer
R_str	dc resistance of the winding
L_str	inductance of the winding
$\mathbf{C}_\mathrm{twu}$, $\mathbf{C}_\mathrm{lne}$	capacitance matrices for the capacitive elements in a tree and in a cotree, respectively
$\mathbf{G}_\mathrm{twu}$, $\mathbf{G}_\mathrm{lne}$	conductance matrices for the conductive elements in a tree and in a cotree, respectively
$\mathbf{L}_\mathrm{lnu}$, $\mathbf{L}_\mathrm{twe}$	inductance matrices for the inductive elements in a cotree and in a tree, respectively
$\mathbf{R}_\mathrm{lnu}$, $\mathbf{R}_\mathrm{twe}$	resistance matrices for the resistor elements in a cotree and in a tree, respectively

$\mathbf{N}_\mathrm{G}$	admittance matrix after partial cutset/loop transformations
$\mathbf{N}_\mathrm{C}$	capacitance matrix after partial cutset/loop transformations
$\mathbf{N}_\mathrm{R}$	resistance matrix after partial cutset/loop transformations
$\mathbf{N}_\mathrm{L}$	inductance matrix after partial cutset/loop transformations

Numerical Integration

$\mathbf{M}$, $\mathbf{K}$	system matrices of the differential system
$\mathbf{x}(t)$, $x(t)$	vector of unknowns, one of its components
$\mathbf{r}(t)$	right-hand side of the differential system
λ	matrix pencil
$f(t, x)$	right-hand side of initial value problem
$x(t_{n+1})$	exact solution at t_{n+1}
x_{n+1}	approximate solution at t_{n+1}
h	time step
Φ	continuous evolution operator
Ψ	discrete evolution operator
$\psi(t_n, x_n, h)$	increment function of the one-step explicit integration method
$\psi(t_{n+1}, x_{n+1}, h)$	increment function of the one-step implicit integration method
$\epsilon_l(t, x, h)$	local (consistency) discretization error
$\epsilon_g(t_n)$	global discretization error
p	consistency order
L	Lipschitz constant
$\mathbf{A}$	system matrix of a test linear initial value problem
$\sigma(\mathbf{A})$	spectral radius of matrix $\mathbf{A}$
$\Re\{z\}$	real part of the complex value z
ρ	spectral radius of the increment operator
$R(h\lambda)$	stability function of the integration method
S	region of absolute stability of the integration method
θ	integration scheme parameter
$\mathbf{M}^*$, $\mathbf{K}^*$	modified $\mathbf{M}$ and $\mathbf{K}$ matrices
$\mathbf{I}$	unit matrix
$\mathbf{W}$	regular square matrix
$\mathbf{J}$	nilpotent Jordan block matrix
$\mathbf{b}$, $\hat{\mathbf{b}}$	weight and an embedded weight vectors of a Runge-Kutta method, respectively

$\mathbf{c}$	abscissa vector of a Runge-Kutta method
$\mathbf{A}$	coefficient matrix of a Runge-Kutta method
s	number of stages in a Runge-Kutta method
$\mathbf{X}_{n,i}$, $\mathbf{X}'_{n,i}$	vectors of stage values or stage derivatives, respectively
$\mathbf{y}$	error vector for a Runge-Kutta method
$\mathbf{x}^{(p)}$, $\mathbf{x}^{(\hat{p})}$	solution obtained with a main and with an embedded method, respectively
$\|\mathbf{y}\|_{\mathrm{err}}$	norm of the error vector $\mathbf{y}$
$\epsilon^{(p)}$	absolute error tolerance for the solution of order p
ν	numerical parameter of the adaptive integration scheme
$\epsilon_{x,i}^{(p)}$	absolute error tolerance for the component $x_i^{(p)}$
$a_{\mathrm{tol,i}}$, $r_{\mathrm{tol,i}}$	absolute and relative error tolerances
ϵ_{tol}	user-specified tolerance used to set up an upper bound for an absolute error of the time integration
μ	accelerating parameter of an adaptive integration scheme
ρ	safety factor
σ	local coordinate in a dense-output formula
β_{ij}^{ex}	extrapolator parameters

Efficiency Improvements in Adaptive Numerical Techniques

ω	angular frequency
$R_{(n+1)}(\omega t)$	reminder in a Taylor expansion formula
α, β, γ	numerical parameters do specify a weight vector
τ	excitation time constant
$\underline{\mathbf{X}}(t)$	phasor solution describing the slow dynamic phenomenon
$\underline{\mathbf{R}}(t)$	phasor representation of the low frequency excitation components
$\mathbf{A_0}$, $\mathbf{B_0}$	initial conditions for the phasor system

Field-Circuit Coupled Simulations with Switching Elements

(s)	a superscript used to show the state of the circuit
n_{cd}	number of continuous domains
$f_0(x), \ldots, f_m(x)$	Sturm polynomial sequence
$\mathrm{rem}\left(\frac{\alpha}{\beta}\right)$	polynomial reminder of the division of α by β

Abbreviations

ME	Maxwell's equations
EQS	Electroquasistatic (formulation)
MQS	Magnetoquasistatic (formulation)
KCL	Kirchhoff's current law
KVL	Kirchhoff's voltage law
SDIRK	Singly diagonally implicit Runge-Kutta method

List of Figures

List of Tables

Bibliography

Introduction

[1] R. Oestreich, E. Gjonaj, C. U. Scholler, M. Schäfer, T. Weiland. *Coupled Simulation using an Electromagnetic and a Fluid Flow Software Package and Applications*. Proceedings of the 7th International Symposium on Electric and Magnetic Fields, Aussois, France, June 20-22, 2006, pp. 215–216.

[2] J. H. Prevost. *Partitioned Solution Procedure for Simultaneous Integration of Coupled-Field Problems*. Communications in Numerical Methods in Engineering, vol. 13, pp. 239–247, 1997.

[3] D. K. Cheng. *Field and Wave Electromagnetics*. Addison-Wesley Publishing Company, USA, 1992.

[4] A. Y. Hannalla and D. C. Macdonald. *Numerical Analysis of Transient Field Problems in Electrical Machines*. IEE Proceedings, 123(9), pp. 893–898, 1976.

[5] A. Konrad. *The Numerical Solution of Steady-State Skin Effect Problems - an Integrodifferential Approach*. IEEE Transactions on Magnetics, vol. 17, no. 1, pp. 1148–1152, 1981.

[6] T. Nakata and N. Takahashi. *Direct Finite Element Analysis of Flux and Current Distributions under Specified Conditions*. IEEE Transactions on Magnetics, vol. 18, no. 2, pp. 325–330, 1982.

[7] J. Weiss and V. K. Garg. *Steady State Eddy Current Analysis in Multiply-Excited Magnetic Systems with Arbitrary Terminal Conditions*. IEEE Transactions on Magnetics, vol. 24, no. 6, pp. 2676–2678, 1988.

[8] I. A. Tsukerman, A. Konrad and J. D. Lavers. *A Method for Circuit Connections in Time-Dependent Eddy Current Problems*. IEEE Transactions on Magnetics, vol. 28, no. 2, pp. 1299–1302, 1992.

[9] P. Lombard and G. Meunier. *A General Purpose Method for Electric and Magnetic Combined Problems for 2D, Axisymmetric and Transient Systems*. IEEE Transactions on Magnetics, vol. 29, no. 2, pp. 1737–1740, 1993.

[10] G. Bedrosian. *A New Method for Coupling Finite Element Field Solutions with External Circuits and Kinematics*. IEEE Transactions on Magnetics, vol. 29, no. 2, pp. 1664–1668, 1993.

[11] H. De Gersem. *Simulation of Field-Circuit Coupled Motional Eddy Current Problems by Krylov Subspace Methods and Multilevel Techniques*. PhD Thesis, Katholieke Universiteit Leuven, 2001.

[12] I. A. Tsukerman, A. Konrad, G. Bedrosian and M. V. K. Chari. *A Survey of Numerical Methods for Transient Eddy Current Problems*. IEEE Transactions on Magnetics, vol. 29, no. 2, pp.1711–1716, 1993.

[13] I. Tsukerman. *A Stability Paradox for Time-Stepping Schemes in Coupled Field-Circuit Problems*. IEEE Transactions on Magnetics, vol. 31, no. 3, pp. 1857–1860, 1995.

[14] J. Gyselinck and J. Melkebeek. *Numerical Methods for Time Stepping Coupled Field-Circuit Systems*. In Proceedings of the International Conference on Modelling and Simulation of Electrical Machines, Converters and Systems (ELECTRIMACS 96), Saint-Nazaire, France, Sept. 1996, vol. 1, pp. 227–234.

Classical Electrodynamics

[15] U. van Rienen. *Numerical Methods in Computational Electrodynamics*. Springer, Berlin, 2001.

[16] M. N. O. Sadiku. *Numerical Techniques in Electromagnetics*. CRC Press, 2000.

[17] H. K. Dirks. *Quasi-Stationary Fields for Microelectronic Apllications*. Electrical Engineering 79, pp. 145–155, 1996.

[18] H. A. Haus and J. R. Melcher. *Electromagnetic Fields and Energy*. Prentice Hall, Englewood Cliffs, 1989.

[19] M. Wilke. *Zur numerischen Berechnung Quasistationärer elektromagnetischer Felder im Zeitbereich*. PhD Thesis, Cuvillier Verlag Göttingen, Germany, 2005.

Finite Integration Technique

[20] T. Weiland. *A Discretization Method for the Solution of Maxwell's Equations for Six-Component Fields*. International Journal of Electronics and Communication (AEÜ), vol. 31, pp. 116 – 120, 1977.

[21] R. Schuhmann and T. Weiland. *A Stable Interpolation Technique for FDTD on Nonorthogonal Grids*. International Journal on Numerical Modelling, vol. 11, pp. 299–306, 1998.

[22] R. Schuhmann. *Die nichtorthogonale Finite-Integrations-Methode zur Simulation elektromagnetischer Felder*. PhD Thesis, Darmstädter Dissertation D17, Technische Universität Darmstadt, 1999.

[23] P. Thoma and T. Weiland. *A Consistent Subgridding Scheme for the Finite Difference Time Domain Method*. International Journal on Numerical Modelling, vol. 9, pp. 359–374, 1996.

[24] M. Clemens and T. Weiland. *Discrete Electromagnetism with the Finite Integration Technique*. Progress in Electromagnetic Research (PIER) Monograph Series, PIER 32, pp. 65–87, 2001. Special Issue on "Geometrical Methods in Computational Electromagnetics".

[25] W.-K. Chen. *Graph Theory and its Engineering Applications*. Advanced Series in Electrical and Computer Engineering, vol. 5, World Scientific, Singapore, 1996.

[26] M. Clemens, R. Schumann and T. Weiland. *Algebraic Properties and Conservation Laws in the Disrete Electromagnetism*. FREQUENZ, Band 53, Ausgabe 11-12, pp. 219–225, 1999.

[27] M. Clemens, P. Thoma, T. Weiland and U. van Rienen. *A Survey on the Computational Electromagntic Field Calculation with the FI-Method*. Surveys on Mathematics in Industry, vol. 8, no. 3–4, pp. 213–232, 1998.

[28] M. Clemens and T. Weiland. *Maxwell's Equations Tailored to Numerical Simulations*. International Compumag Society Newsletter, vol. 8, no. 2, pp. 13–20, 2001.

[29] H. Krüger. *Zur numerischen Berechnung transienter elektromagnetischer Felder in gyrotropen Materialen*. Dissertation D17, Technische Universität Darmstadt, 2000.

[30] S. Gutschling. *Zeitbereichsverfahren zur Simulation elektromagnetischer Felder in dispersiven Materialien*. Dissertation D17, Technische Universität Darmstadt, 1998.

[31] M. Clemens and T. Weiland. *Numerical Algorithms for the FDiTD and FDFD Simulation of Slowly Varying Electromagnetic Fields*. International Journal of Numerical Modelling: Electronic Networks, Devices and Fields, vol. 12, pp. 3–22, 1999.

[32] H. De Gersem, M. Wilke, M. Clemens and T. Weiland. *Efficient Modelling Technique for Complicated Boundary Conditions Applied to Structured Grids*. COMPEL - the Intrenational Journal for Computation and Mathematics in Electrical and Electronic Engineering, vol. 23, no. 4, pp. 904–912, October 2004.

Linear Circuit Analysis and Network Topology

[33] W. H. Hayt and J. E. Kemmerly. *Engineering Circuit Analysis*. International Student Edition, McGrave-Hill Book Compony, Inc., 1962.

[34] R. A. DeCarlo and P.-M. Lin. *Linear Circuit Analysis*. Prentice Hall, Englewood Cliffs, New Jersey, 1995.

[35] J. A. Edminister. *Theory and Problems of Electric Circuits*. Schaum's Outline Series, Schaum Publishing Co., 1965.

[36] J. Vlach and K. Singhal. *Computer Methods for Circuit Analysis and Design*. Van Nostrand Reinhold, New Your, 1993.

Field-Circuit Coupled Formulation

[37] L. O. Chua and P. M. Lin. *Computer Aided Analysis of Electronic Circuits - Algorithms and Computational Techniques*. Prentice-Hall, New Jersey, 1975.

[38] H. De Gersem, K. Hameyer and T. Weiland. *Field-Circuit Coupled Models in Electromagnetic Simulation*. Journal of Computational and Applied Mathematics, vol. 168, no. 1–2, pp. 125 – 133, July 2004.

[39] H. De Gersem and T. Weiland. *Field-Circuit Coupling for Time-Harmonic Models Discretized by the Finite Integration Technique*. IEEE Transactions on Magnetics, vol. 40, no. 2, pp. 1334–1337, 2004.

[40] L. Kettunen. *Fields and Circuits in Computational Electromagnetism*. IEEE Transactions on Magnetics, vol. 37, no. 5, pp. 3393–3396, 2001.

[41] P. Dular, N. Sadowski, J. P. A. Bastos and W. Legros. *Dual Complete Procedures to Take Stranded Inductors into Account in Magnetic Vector Potential Formulations*. IEEE Transactions on Magnetics, vol. 36, no. 4, pp. 1600–1605, 2000.

[42] H. De Gersem, R. Mertens, U. Pahner, R. Belmans, and K. Hameyer. *A Topological Method Used for Field-Circuit Coupling*. IEEE Transactions on Magnetics, vol. 34, no. 5, pp. 3190–3193, 1998.

Time Integration of the Field-Circuit Coupled Problems

[43] E. Hairer and G. Wanner. *Solving Ordinary Differential Equations. Stiff and Differential-Algebraic Problems*. Springer-Verlag, Berlin, 2nd edition, 1996.

[44] K. E. Brenan, S. L. Campbell and L. R. Petzold. *Numerical Solution of Initial-Value Problems on Differential-Algebraic Equations*. SIAM, 1996.

[45] U. M. Ascher and L. R. Petzold. *Computer Methods for Ordinary Differential Equations and Differential-Algebraic Equations*. SIAM, 1998.

[46] P. Deuflhard and F. Bornemann. *Scientific Computing with Ordinary Differential Equations*. Springer-Verlag, New York, 2002.

[47] E. Hairer, S. P.Nørsett and G. Wanner. *Solving ordinary differential equations I. Nonstiff Problems*. Springer-Verlag, Berlin, 2nd edition, 1996.

[48] A. Prothero and A. Robinson. *On the Stability and Accuracy of One-Step Methods for Solving Stiff Systems of Ordinary Differential Equations*. Mathematics of Computation, vol. 28, pp. 145–162, 1974.

[49] A. Kværnø. *Singly Diagonally Implicit Runge-Kutta Methods with an Explicit First Stage*. BIT Numerical Mathematics, vol. 44, pp. 489–502, 2004.

[50] W. Hundsdorfer and J. Verwer. *Numerical Solution of Time-Dependent Advection-Diffusion-Reaction Equations*. Springer-Verlag, Berlin, 2003.

[51] A. Nicolet and F. Delincé. *Implicit Runge-Kutta Methods for Transient Magnetic Field Computation*. IEEE Transactions on Magnetics, vol. 32, pp. 1405–1408, 1996.

[52] J. de Swat and G. Söderlind. *On the Construction of Error Estimators for Implicit Runge-Kutta Methods*. Journal of Computational and Applied Mathematics, vol. 86, pp. 347–358, 1997.

[53] H. Wang, S. Taylor, J. Simkin, C. Biddlecombe and B. Trowbridge. *An Adaptive-Step Time Integration Method Applied to Transient Magnetic Field Problems*. IEEE Transactions on Magnetics, vol. 37, no. 5, pp. 3478–3481, 2001.

[54] K. Gustafsson. *Control-Theoretic Techniques for Stepsize Selection in Implicit Runge-Kutta Methods*. ACM Transactions on Mathematical Software, vol. 20, no. 4, pp. 496–517, 1994.

[55] J. Lang. *Two-Dimensional Fully-Adaptive Solutions of Reaction-Diffusion Equations*. Appl. Numer. Math., vol. 18, p. 223, 1995.

[56] F. Cameron. *Low-Order Runge-Kutta Methods for Differential-Algebraic Equations*. PhD Thesis, Tampere University of Technology, Finland, 1999.

[57] J. Driesen and K. Hameyer. *The Simulation of Magnetic Problems with Combined Fast and Slow Dynamics Using a Transient Time-Harmonic Method*. The European Physical Journal - Applied Physics, vol. 14, no. 3, pp. 165–169, 2001.

[58] K. Kundert. *Simulation Methods for RF Integrated Circuits*. Proceedings of ICCAD'97, November 9-13, 1997, San Jose, California.

[59] J. Driesen, R. Belmans and K.Hameyer. *Computation Algorithms for Efficient Coupled Electromagnetic-Thermal Device Simulation*. IEE Proceedings - Science, Measurement and Technology, vol. 149, no. 2, pp.67–72, 2002.

Field-Circuit Coupled Simulations with Switching Elements

[60] D. Bedrosian and J. Vlach. *Time-Domain Analysis of Networks with Internally Controlled Switches*. IEEE Transactions on Circuits and Systems - I: Fundamental Theory and Applications, vol. 39, no. 3, pp. 199–212, 1992.

[61] T. L. Quarles. *SPICE3 Version 3CI Users Guide*. Memorandum no. UCB/ERL M89/46, University of California, Berkeley, April 1989.

[62] P. Dular and P. Kuo-Peng. *An Efficient Time Discretization Procedure for Finite Element-Electronic Circuit Equation Coupling*. COMPEL - the Intrenational Journal for Computation and Mathematics in Electrical and Electronic Engineering, vol. 21, no. 2, pp. 274–285, 2002.

[63] M. Günther and P. Rentrop. *Multirate ROW Methods and Latency of Electrical Circuits*. Applied Numerical Mathematics, North-Holland, no. 13, pp. 83–102, 1993.

[64] M. B. Carver. *Efficient Integration over Discontinuities in Ordinary Differential Equation Simulations*. Mathematics and Computers in Simulation, North Holland Publishing Company, vol. XX, pp. 190–196, 1978.

[65] G. Mao and L. R. Petzold. *Efficient Integration over Discontinuities for Differential-Algebraic Systems*. Computers and Mathematics with Applications, vol. 43, pp. 65–79, 2002.

[66] P. Barton and C. Pantelides. *Modeling of Combined Discrete/Continuous Processes*. Journal of the American Institute of Chemical Engineers (AIChE Journal), vol. 40, no. 6, pp. 966–979, 1994.

[67] G. Grabner, R. Kittinger and A. Kecskeméthy. *An Integrated Runge-Kutta and Polynomial Root Finding Method for Reliable Event-Driven Multibody Simulation*. In Proceedings of the IFAC Workshop on Lagrangian and Hamiltonian Methods for Nonlinear Control, pp. 281–286, Seville, April 3–5, 2003.

[68] G. S. Joglekar and G. V. Reklatis. *A Simulator for Batch and Semi-Continuous Processes*. Computers and Chemical Engineering, vol. 8, no. 6, pp. 315–327, 1984.

[69] A. J. Preston and M. Berzins. *Algorithms for the Location of Discontinuities in Dynamic Simulation Problems*. Computers and Chemical Engineering, vol. 15, no. 10, pp. 701–713, 1991.

[70] G. Grabner and A. Kecskeméthy. *An Integrated Runge-Kutta Root Finding Method for Reliable Collision Detection in Multibody Systems*. Multibody System Dynamics, vol. 14, pp. 301–316, 2005.

[71] E. Isaacson and H. B. Keller. *Analysis of Numerical Methods*. Wiley, New-York, 1966.

[72] L. F. Shampine, I. Gladwell, and R. W. Brankin. *Reliable Solution of Special Event Localisation Problems for ODEs*. ACM Transactions on Mathematical Software, vol. 17, no. 1, pp. 11–25, 1991.

[73] F. E. Cellier. *Combined Continuous/Discrete System Simulation by Use of Digital Computers*. Ph.D. dissertation. Swiss Federal Institute of Technology. ETH, Zurich.

[74] C. C. Pantelides. *SpeedUp-Recent Advances in Process Simulation*. Computers and Chemical Engineering, vol. 12, no. 7, pp. 745–755, 1988.

[75] J. Vlach, J. M. Wojciechowski and A. Opal. *Analysis of Nonlinear Networks with Inconsistent Initial Conditions*. IEEE Transactions on Circuits and Systems - I: Fundamental Theory and Applications, vol. 42, no. 4, pp. 195–200, 1995.

Publications in Internatonal Journals and Conference Proceedings

[76] G. Benderskaya, H. De Gersem, M. Clemens and T. Weiland. *Transient Field-Circuit Coupled Formulation Based on the Finite Integration Technique and a Mixed Circuit Formulation*. Proceedings of the Sixth International Symposium on Electric and Magnetic Fields - EMF 2003, Aachen, Germany, October 6–9, 2003, pp. 369–372.

[77] G. Benderskaya, M. Clemens, H. De Gersem and T. Weiland. *Adaptive Transient Simulation of Field-Circuit Coupled Problems Including Switching Circuit Elements*. Proceedings of the International Conference PIERS 2004 - Progress in Electromagnetics Research Simposium 2004, Pisa, Italy, March 28–31, 2004, pp. 489–492.

[78] G. Benderskaya, M. Clemens, H. De Gersem and T. Weiland. *Embedded Runge-Kutta Methods for Field-Circuit Coupled Problems with Switching Elements*. Proceedings of the Eleventh Biennial IEEE Conference on Electromagnetic Field Computation - CEFC 2004, Seoul, Korea, June 6–9, 2004, p. 163.

[79] M. Clemens, G. Benderskaya, H. De Gersem, S. Feigh, M. Wilke, J. Yuan and T. Weiland. *Formulations and Efficient Numerical Solution Techniques for Transient 3D Magneto- and Electro-Quasistatic Field Problems*. Report No. 11/2004, Workshop on Computational Electromagnetism, Mathematisches Forschungsinstitut Oberwolfach, February 22–28, 2004, pp. 21–22.

[80] G. Benderskaya, M. Clemens, H. De Gersem and T. Weiland *Interpolation Technique for Effective Determination of Switching Time Instants for Field-Circuit Coupled Problems with Switching Elements*. Proceedings of the XVIII Symposium Electromagnetic Phenomena in Nonlinear Circuits - EPNC 2004, Poznań, Poland, June 28–30, 2004, pp. 17–18.

[81] G. Benderskaya, M. Clemens, H. De Gersem and T. Weiland. *Numerische Magnetfeld-Simulationen Gekoppelt an Elektrische Netzwerke unter Berücksichtigung Schaltender Bauelemente*. Kleinheubacher Tagung 2004, Programm und Abstracts (KHB 2004), 27. September–01. Oktober 2004, pp. 31–32.

[82] M. Clemens, M. Wilke, G. Benderskaya, H. De Gersem, W. Koch and T. Weiland. *Transient Electro-Quasistatic Adaptive Simulation Schemes*. IEEE Transactions on Magnetics, vol. 40, no. 2, pp. 1294–1297, 2004.

[83] G. Benderskaya, H. De Gersem, T. Weiland and M. Clemens. *Transient Field-Circuit Coupled Formulation Based on the Finite Integration Technique and a Mixed Circuit Formulation*. COMPEL - the International Journal for Computation and Mathematics in Electrical and Electronic Engineering, vol. 23, no. 4, pp. 968–976, 2004.

[84] G. Benderskaya, H. De Gersem and T. Weiland. *Integration over Discontinuities in Field-Circuit Coupled Simulations with Switching Elements* Proceedings of the 15th Conference on the Computation of Electromagnetic Fields - COMPUMAG 2005, Shenyang, China, June 26–30, 2005, vol. III, pp. 158–159.

[85] G. Benderskaya, M. Clemens, H. De Gersem and T. Weiland. *Embedded Runge-Kutta Methods for Field-Circuit Coupled Problems with Switching Elements.* IEEE Transactions on Magnetics, vol. 41, no. 5, pp. 1612–1615, 2005.

[86] G. Benderskaya, H. De Gersem and T. Weiland. *Adaptive Time Integration for Electromagnetic Models with Sinusoidal Excitation.* Proceedings of the 7th International Symposium on Electric and Magnetic Fields, Aussois, France, June 20-22, 2006, pp. 107–108.

[87] H. De Gersem, G. Benderskaya and T. Weiland. *Transient Field-Circuit Coupled Models of Electrical Actuators.* Proceedings of the 12th International Power Electronics and Motion Control Conference - EPE-PEMC 2006, Portoroz, Slovenia, August 30–September 01, 2006, pp. 1919–1924.

[88] G. Benderskaya, H. De Gersem and T. Weiland. *Numerical Integration of Field-Circuit Coupled Magnetoquasistatic Simulation with Switching Elements.* Proceedings of the 11th Seminar "NUMDIFF" on Numerical Solution of Differential and Differential-Algebraic Equations, University of Halle, Halle, Germany, September 4–8, 2006, p. 22.

[89] G. Benderskaya, H. De Gersem and T. Weiland. *Adaptive Envelope Integration of Electromagnetic Problems.* Proceedings of the 12th International IGTE Symposium on Numerical Field Calculation in Electrical Engineering, Graz University of Technology, Graz, Austria, September 17–20, 2006, pp. 37.

[90] G. Benderskaya, H. De Gersem, T. Weiland and M. Clemens. *Interpolation Technique for Effective Determination of Switching Time Instants for Field-Circuit Coupled Problems with Switching Elements.* COMPEL - the International Journal for Computation and Mathematics in Electrical and Electronic Engineering, vol. 25, no. 1, pp. 64–70, 2006.

[91] G. Benderskaya, H. De Gersem and T. Weiland. *Integration over Discontinuities in Field-Circuit Coupled Simulations with Switching Elements.* IEEE Transactions on Magnetics, vol. 42, no. 4, pp. 1031–1034, 2006.

[92] G. Benderskaya, H. De Gersem and T. Weiland. *Adaptive Time Integration for Electromagnetic Models with Sinusoidal Excitation.* Proceedings of the 7th International Symposium on Electric and Magnetic Fields, Aussois, France, June 20-22, 2006. Conference CD.

[93] G. Benderskaya, H. De Gersem and T. Weiland. *Adaptive Envelope Integration of Electromagnetic Problems.* Proceedings of the 12th International IGTE Symposium on Numerical Field Calculation in Electrical Engineering, Graz University of Technology, Graz, Austria, September 17–20, 2006, pp. 155–160. Conference CD.

Acknowledgements

Completing the thesis, I would like to thank all the people who helped me during the whole time of my work on this PhD project.

First of all, I thank Prof. Dr.-Ing. Thomas Weiland for the scientific supervision and the possibility to work in the research group for quasistatic modeling at TEMF. Due to his scientific and financial support, I got the opportunity to report the results of my research at several international conferences and to successfully complete this PhD project.

I would like to thank Prof. Dr. Jens Lang for the careful reading, reviewing and correcting the thesis as the second reviewer.

I thank Prof. Dr. Dr. h. c. mult. Manfred Glesner and Prof. Dr.-Ing. Abdelhak Zoubir for their willingness to act as the examiners during the PhD defence. My thank also goes to Prof. Dr.-Ing. Peter Meißner for taking the chair at the PhD defence.

Special thanks to Prof. Dr. Ir. Herbert De Gersem for his constant scientific guidance and careful reading and correcting this PhD thesis.

I am obliged to Dr.-Ing. Wolfgang Ackermann for his very kind, diligent and overall support and help in all aspects of scientific and human life.

I would like to thank Univ.-Prof. Dr. rer. nat. habil. Markus Clemens for his scientific guidance during the first two years of my work in Darmstadt.

Special thanks to Marlis Gorecki who gave me a lot of help in working and living!

I also thank Tuulikki and Joachim Lublinski for being all the time here like a mother and a father for me.

I thank all my TEMF colleagues, present and former, for providing a pleasant and friendly working atmosphere.

Another special thanks goes to our technical and administrative staff - Marianne Dorn, Dragos Munteanu, Heike Seiler, Hava Selmanaj, Dagmar Stenger and Achim Veuskens for their constant kind care and help!

Finally, I thank my parents - Olga Benderskaya and Victor Kuprienko and my grandmother Nina Chaikina for giving me all their love and support throughout my life. Without them it would be impossible to complete this PhD project!

Thank you all of you!

Curriculum Vitae

Galina Benderskaya

born on February 07, 1976, in Dimitrovgrad (Russia)

1983-1993	Secondary school No. 5 in Dimitrovgrad
1993-1998	Study of applied mathematics at the Department of Mathematics and Mechanics of Ulyanovsk State University, Russia, graduation with a diploma in applied mathematics
1993-1998	Study of English language and English linguistics at the Department of English Linguistics of Ulyanovsk State University, graduation with a diploma in English linguistics
1998-2002	Research assistant at the Department of Mathematics and Mechanics of Ulyanovsk State University
since 2002	Research assistant at the Institut für Theorie Elektromagnetischer Felder at the Technische Universität Darmstadt